Hybrid Modelling of a Traveling Wave Piezoelectric Motor

El, Ghouti N.

Publication date:
2000

Document Version
Også kaldet Forlagets PDF

Hybrid Modeling of a Traveling Wave Piezoelectric Motor

PhD Thesis

Norddin El Ghouti

Department of Control Engineering
Aalborg University
Fredrik Bajers Vej 7, DK-9220 Aalborg Ø, Denmark.

ISBN 87-90664-09-4
Doc. no. D-00-4383
May 2000

This thesis was typeset using LaTeX2$_\varepsilon$ in `report` document class.

The drawings were made in CorelDraw™ from Corel Corporation.
The graphs were generated in MatLab™ from MathWorks Inc.

Preface and Acknowledgments

This thesis is submitted in partial fulfillment of the requirements for the Doctor of Philosophy at the Department of Control Engineering, Aalborg University, Denmark. The work has been carried out in the period from July 1997 to May 2000 under the supervision of Associate Professor Jan Helbo.

I am gratefully indebted to my supervisor, Associate Professor Jan Helbo, for his guidance and encouragement throughout the project. Special thanks go to my co-supervisor, Associate Professor Rafael Wisniewski, for his help and advice during the project.

My sincere thanks go to Professor Bertrand Nogarede for having permitted me to stay at his laboratory at the LEEI, ENSEEIHT, Toulouse in France, for a period of four months, during the spring of 1999, and continue my research under his supervision. Furthermore, I greatly acknowledge the assistance from my colleagues within the research group dealing with piezoelectric transducers at the LEEI, and I am indebted for their kindness of allowing me to use their operational test bench.

Special thanks go to Professor Ramutis Bansevicius from Kaunas University of Technology, Lithuania, for his introductory course in the piezoelectric field and its many applications, and also for interesting and inspiring discussions during his one week stay at Aalborg University in November 1997. I am thankful to professor Anatoly Yerofeyev and his son Sergy from St. Petersburg State University, Russia, for their willingness to share their extensive knowledge in the field of modeling and control of piezoelectric transducers. I greatly acknowledge their courses, assistance and the many fruitful discussions during their one month stay at the Control Department in October 1998.

I am most thankful to the staff of the Control Department for their assistance and support.

I am foremost indebted to my parents, without them I would not be around, and also to my family for their unconditional support and trust.

May 2000, Aalborg, Denmark

Norddin El Ghouti

Summary

This thesis considers the modeling of the traveling wave piezoelectric motor. The main objective of this PhD project is to derive a suitable model for investigating some nonlinear control strategies in a simulated environment. Most of the existing modeling approaches are inappropriate for the control community due to their many drawbacks. The established analytical methods have high computational demands, whereas the equivalent circuit method lacks the ability to capture some of the important dynamics such as the frictional behavior of the contact mechanism driving this type of motors.

In order to overcome some of the drawbacks of the existing methods, and thereby meet the needs of the control community, three main approaches are considered in this modeling task.

First, the equivalent circuit method is investigated in order to derive a lumped model of an ultrasonic traveling wave rotary piezoelectric motor. This approach is carried out on the basis of the experimental investigation combined with the electrical network method. Consequently, an insight in the analysis of the electromechanical coupling force factor, which is responsible for the electrical to mechanical energy conversion, is obtained. Thereby, the difference between the effective force factor and the modal force factor is highlighted, and how these parameters should be integrated in the equivalent circuit model is emphasized. Furthermore, the effect of temperature on the mechanical resonance frequency is considered and thereby integrated in the final equivalent circuit model for long term operations.

Second, the laws of physics based on the energy balance method are used for the purpose of predicting, a priori, the performance of the motor as a function of the design parameters and thereby a theoretical model is derived. Since the dynamic characteristics of the real motor are difficult to capture in an analytical model, and the parameters of the motor are time varying and highly nonlinear, then some assumptions are required in order to simplify the modeling task and thus provide a suitable model for control purposes. Consequently, a general state space model is derived on the basis of the special design of the motor of interest, which is a two phase symmetrical system. Furthermore, a simplified model is derived within the framework of various assumptions on the be-

havior of the stator, which makes it possible to decouple the assumed excited modes and thereby predict the performance of the stator by a single second order system. The frictional behavior at the interface contact between the stator and the rotor constitutes the main problem in the modeling approach and therefore its modeling is treated with care in order to avoid large discrepancies with the physical plant. Consequently, the stick-slip behavior of the driving mechanism is integrated in the time varying parameters of the model. This makes it possible to predict most of the behavior and performance characteristics of the motor as a function of the external loading parameters. The outcome of this modeling approach is a less computationally demanding model suitable for control investigation purposes.

Finally, a hybrid model which combines the strength of the equivalent circuit method and the analytical method is derived. The analogy between the equivalent circuit model and the analytically reduced model of the unforced stator, which models the behavior of one phase of the stator, is highlighted. This makes it possible to substitute the parameters of the equivalent circuit model in the framework of the simplified analytical model. Consequently, the large uncertainties on the values of the dielectrical and electromechanical constants are avoided. The simplified hybrid model of the complete motor is thereby derived in terms of the forced stator model, the spinning motion model and the vertical motion model. Finally the effect of temperature on the mechanical resonance frequency is considered and thereby integrated in the final hybrid model for long term operations. The validity of the model has been established by simulations and comparison to the performance characteristics of the real system.

The results achieved by the different approaches are compared and a final conclusion is drawn.

Synopsis

Denne afhandling omhandler modellering af en vandre-bølge piezoelektrisk motor. Hovedformålet med dette PhD arbejde er at lave en simplificeret model som er velegnet til ikke lineær kontrol undersøgelse i et simuleret miljø. De fleste af de eksisterende modeller er uegnede til reguleringsbrug på grund af deres mange ulemper. De etablerede analytiske metoder kræver mange beregninger, hvorimod ækvivalent kredsløbsmetoden har en manglende evne til at fange nogle vigtige dynamiske forhold, såsom friktionsopførsel i den kontakt mekanisme der driver motoren.

For at overvinde nogle ulemper ved disse eksisterende metoder, og derved opfylde behovene i reguleringsøjemed, bliver tre væsentlige fremgangsmåder betragtet i denne modelleringsopgave.

Først undersøges ækvivalent kredsløbsmetoden for at opstille/udlede en god model af en ultralyds vandre-bølge roterende piezoelektrisk motor. Denne fremgangsmåde er udført på basis af den eksperimentelle metode kombineret med den elektriske netværksmetode. Altså opnås et indblik i analysen af den elektromekaniske koblingskraftfaktor, som er ansvarlig for den elektromekaniske energiforvandling. Derved fremhæves forskellen mellem den effektive kraftfaktor og den modale kraftfaktor, og det understreges hvordan disse parametre skal integreres i den ækvivalente kredsløbsmodel. Endvidere undersøges temperaturens indvirkning på den mekaniske resonans frekvens. Herved bliver temperaturen integreret i den endelige ækvivalente kredsløbsmodel for langtidspåvirkning.

Dernæst anvendes de fysiske love baseret på energibalancemetoden med henblik på a priori at forudsige motorens præstation/ydeevne som funktion af designparametrene, og derved etableres den teoretiske model. Eftersom den virkelige motors dynamiske karakteristika er svære at fange i en analytisk model, og motorens parametre er tidsvarierende og stærkt ulineære, så er nogle antagelser nødvendige for at simplificere modelleringsopgaven og derved etablere en passende model for reguleringsformål. Altså udledes en generel tilstandsmodel på basis af motorens specifikke design, som er et to fase symmetrisk system. Endvidere etableres en simplificeret model på grundlag af en række antagelser, som gør det muligt at afkoble de antagne stimulerede modes og derved

forudsige statorens ydeevne med en enkelt anden orden model. Friktionsopførslen på kontakt grænsefladen mellem stator og rotor udgør et væsentligt problem i modelleringsfremgangsmåden, og derved bliver dens modellering behandlet med omhyggelighed for at undgå for stor afvigelser fra det fysiske system. Altså integreres den drivende mekanismes stick-slip opførsel i modellens tidsvarierende parametre. Dette gør det muligt at forudsige motorens ydeevne som funktion af de ydre belastningers parametre. Udfaldet af denne modellerings fremgangsmåde er en mindre beregningskrævende model som er passende for reguleringsformål.

Tilsidst etableres en hybrid model, som kombinerer styrken af den ækvivalente kredsløbsmetode med styrken af den analytiske metode. Analogien mellem den ækvivalente kredsløbsmodel og den simplificerede analytiske model, som modellerer en enkelt fase af den fri stator, fremhæves. Dette gør det muligt at substituere den ækvivalente kredsløbsmodels parametre ind i den simplificerede analytiske model. Altså undgås den store usikkerhed på de dielektriske og de eleKtromekaniske konstanter. En simplificeret hybrid model af den komplette motor er derved etableret i form af den belastede stators model, rotors omdrejningsmodel og rotors vertikale bevægelsesmodel. Tilsidst betragtes temperaturens indvirkning på den mekaniske resonans frekvens, som derved bliver integreret i den endelige hybride model for langtidsbetjening. Modellens gyldighed er blevet påvist med simulering og sammenligning med motorens virkelige karakteristika.

De resultater som opnås med de forskellige fremgangsmåder sammenlignes og derved udledes en endelig konklusion.

Contents

List of Figures **xiii**

List of Tables **xvii**

Nomenclature **xix**

1 Introduction **1**

1.1 Background and motivation 1

1.2 Previous work 3

1.2.1 Motor design 4

1.2.2 Control system design 5

1.2.3 Vibrations, elasticity, contact mechanics and materials 6

1.3 Objectives and contributions 8

1.4 Structure of the thesis 10

2 Piezo-Electricity and Applications **11**

2.1 Piezoelectric transducers 11

2.1.1 The state of the art 11

2.1.2 Limitations in piezoelectric materials 13

2.1.3 The trends in piezoelectric actuators 14

2.2 The fundamental piezoelectric relations 15

2.2.1 Constitutive relation of (Θ, T, E)-Type. 15

2.2.2 Tensor index abbreviations and matrix representations 18

2.2.3 Fundamental relations for various independent variable sets 21

2.2.4 Electromechanical coupling factor 22

3 Experimental Approach **25**

3.1 The objectives . . . 25

3.2 The ultrasonic motor . . . 25

3.3 The experimental characteristics . . . 29

3.3.1 Outline of the experimental investigation methodology . . . 29

3.3.2 Speed-phase characteristics at various frequencies . . . 31

3.3.3 Speed-frequency characteristics at various voltage amplitudes . . . 32

3.3.4 Speed-torque characteristics at various frequencies . . . 33

3.3.5 Feedback-frequency characteristics at various load torques . . . 34

3.3.6 Speed-feedback characteristics at various normal forcings . . . 35

3.3.7 Speed-feedback characteristics at various load torques . . . 36

3.3.8 The resonance frequency of the feedback signal at various temperatures of the motor . . . 37

3.3.9 The electrical admittance characteristic of the free stator . . . 38

3.3.10 The nonlinearities of the motor . . . 39

3.3.11 The electrical admittance of the loaded motor at various amplitudes of the voltage supply . . . 40

3.3.12 The electrical admittance of the loaded motor at various load torques . . . 42

4 Equivalent Circuit Model **43**

4.1 Background of the equivalent circuit method . . . 43

4.1.1 The ring type transducer . . . 43

4.1.2 The free stator around the fundamental resonance . . . 55

4.1.3 The complete motor around the fundamental resonance . . . 60

4.1.4 Speed and feedback signal relationship for the motor . . . 62

4.2 Equivalent circuit model derivation . . . 63

4.2.1 The free stator . . . 63

4.2.2 The unloaded motor . . . 74

4.2.3 The loaded motor . . . 78

4.2.4 Temperature integration in the final equivalent circuit model . . . 79

4.2.5 Simulation of the effect of varying temperature . . . 81

4.3 Simulation and model validation . . . 81

4.3.1 The effect of the driving frequency on the motor . . . 82

4.3.2 The effect of the varying torque on the loaded motor . . . 82

4.4 Conclusion and perspectives 84
4.4.1 Advantages and performances 85
4.4.2 Drawbacks and limitations 85
4.4.3 The alternatives 85

5 Analytical Model **87**
5.1 The general framework model of the traveling wave piezoelectric motor 87
5.1.1 The background of the general framework model derivation 87
5.1.2 The general compact model representation 100
5.2 The state space model 101
5.2.1 Assumptions 101
5.2.2 The applied voltage 103
5.2.3 Calculation and diagonalization of the modal mass matrix 104
5.2.4 Calculation and diagonalization of the modal stiffness matrix 105
5.2.5 Calculation and diagonalization of the electromechanical coupling matrix 108
5.2.6 The state space representation 109
5.3 The explicit state space model 110
5.3.1 The pressure distribution at the stator-rotor interface contact 111
5.3.2 The explicit normal modal forcing vector 113
5.3.3 The explicit tangential modal forcing vector 114
5.3.4 The explicit interface force 117
5.3.5 The explicit interface torque 117
5.3.6 The explicit state space representation 118
5.4 The simplified model 120
5.4.1 The simplified model of the stator 120
5.4.2 Vertical motion model 120
5.4.3 Spinning motion model 121
5.4.4 The complete simplified model 122
5.4.5 Prerequisites for simulation 122
5.5 Conclusion and perspectives 123
5.5.1 Advantages and performances 124
5.5.2 Drawbacks and limitations 124
5.5.3 The alternatives 124

6 Hybrid Model **125**
6.1 The general framework model of the forced stator . . . 125
6.1.1 The explicit general model of the forced stator . . . 126
6.1.2 The explicit actuator equation . . . 126
6.1.3 The explicit sensor equation . . . 128
6.1.4 The model representation of the forced stator . . . 130
6.2 Modeling of the free stator . . . 130
6.2.1 Identification of the parameters $M, \mathcal{D}_o, K_o$ and η . . . 131
6.3 The explicit model of the complete motor . . . 133
6.4 The complete hybrid model . . . 134
6.4.1 The simplified model . . . 134
6.4.2 Temperature integration in the hybrid model . . . 135
6.5 Summary of the complete hybrid model . . . 136
6.6 Simulation and model validation . . . 137
6.6.1 The effect of the driving frequency on the motor . . . 137
6.6.2 The effect of varying torque on the motor . . . 138
6.6.3 The effect of varying temperature on the motor . . . 139
6.7 Conclusion and Perspectives . . . 141
6.7.1 Advantages and performances . . . 141
6.7.2 Drawbacks and limitations . . . 142
6.7.3 Perspectives . . . 142

7 Conclusion and Perspectives **143**
7.1 Overview of the content of this thesis . . . 143
7.2 Final conclusion . . . 149
7.3 Perspectives and recommendations . . . 150

A Test Bench **157**
A.1 The experimental test bench . . . 157
A.1.1 The manual test setup . . . 157
A.1.2 The automatic test setup . . . 159

B Vibration of an Annular Plate **163**

C Motor Data **165**

List of Figures

1.1 The Shinsei motor. 1: Cover, 2: bearing, 3: spring, 4: stator, 5: piezoceramic, 6: friction material, 7: rotor. 4

2.1 The motion 19
2.2 The longitudinal mode of vibration 20
2.3 The transversal mode of vibration 21
2.4 The shear mode of vibration 21

3.1 The naked assembled motor and the piezoceramic ring 26
3.2 Exploded view of the complete stator 26
3.3 An exploded view of the annular stator and the annular rotor 27
3.4 The operating principle of the traveling wave motor 27
3.5 The exploded view of the complete motor 28
3.6 The rotary speed versus the phase shift at various frequencies 31
3.7 The rotary speed versus the excitation frequency at various voltage amplitudes . 32
3.8 The rotary speed versus the load torque at various frequencies 33
3.9 The amplitude of the feedback signal versus the excitation frequency at various load torques 34
3.10 The rotary speed versus the amplitude of the feedback signal at various normal forcings 35
3.11 The rotary speed versus the amplitude of the feedback signal at various load torques 36
3.12 The resonance frequency of the feedback signal versus temperature 37
3.13 The admittance of one phase of the RPEM over a large span of frequencies . . . 38
3.14 Nonlinearity of the free stator around the fundamental frequency 40
3.15 The admittance of the RPEM at various voltage amplitudes of the power supply 41

3.16 The admittance of the RPEM at various load torques 42

4.1 Admittance locus (Nyquist diagram) of a piezoelectric transducer 44
4.2 Frequency response (Bode magnitude diagram) of a piezoelectric transducer . 44
4.3 The stator of the traveling wave motor regarded as a straight beam 45
4.4 Elementary section of a piezoelectric beam subject to bending deformation of transverse type 45
4.5 Piezoelectric straight beam of lenght l subject to bending deformation of transverse type powered by an AC voltage 48
4.6 Mason's six input terminal ECM of the annular plate piezoelectric device 50
4.7 The electromechanical ECM for one phase of the ideal stator with no losses over a large span of frequencies 53
4.8 The electromechanical ECM for one phase of the ideal stator with no losses around the fundamental resonance frequency 55
4.9 The electromechanical ECM for one phase of the real stator integrating the losses around the fundamental resonance frequency 55
4.10 The ECM for one phase of the real stator integrating the losses, around the fundamental resonance frequency, and where the mechanical parameters are seen as their electrical equivalents 56
4.11 Nyquist diagram of the electromechanical transducer around its fundamental resonance and antiresonance frequencies 58
4.12 Bode magnitude diagram of the electromechanical transducer around its fundamental resonance and antiresonance frequencies 58
4.13 Bode magnitude diagram of the electromechanical transducer around its fundamental resonance frequency 60
4.14 The ECM of the two phase complete RPEM 61
4.15 The ECM of the complete RPEM 61
4.16 Comparison between the admittance of phase A and the admittance of phase B of the stator around the fundamental resonance frequency 63
4.17 The electrical equivalent circuit model of one phase of the free stator 64
4.18 Bode magnitude and phase diagram of the electrical admittance of the stator around the fundamental resonance frequency 64
4.19 Nyquist diagram of the electrical admittance of the stator around the fundamental resonance frequency 65
4.20 The electromechanical equivalent circuit model of the free stator 67
4.21 Bode and Nyquist diagrams of the EM vibrating gain admittance of the stator around the fundamental resonance frequency 68

4.22 Prediction of the electrical admittance of the stator around the fundamental resonance frequency 69
4.23 Prediction of the EM vibrating gain admittance of the stator around the fundamental resonance frequency 70
4.24 Prediction of the admittance of the stator over a large span of frequencies 71
4.25 Readjustment of the mechanical damping by simulation in terms of the admittance prediction of the RPEM 75
4.26 The ECM of the unloaded RPEM 77
4.27 The ECM of the loaded RPEM 79
4.28 The complete ECM of the RPEM integrating the effect of temperature changes . 79
4.29 Speed prediction under varying temperature of the RPEM 81
4.30 Comparison of speed-frequency characteristics for the unloaded RPEM: simulation, feedback prediction and measurement 82
4.31 Speed-frequency characteristics of the RPEM under different load torques: measurement and feedback prediction 83
4.32 Comparison of speed-frequency characteristics for the RPEM subject to different load torques: simulation, feedback prediction and measurement 84

5.1 The ring type stator 88
5.2 Section of the ring type stator undergoing bending deformations 88
5.3 Section of the loaded ring-type piezoelectric motor where the forced stator is undergoing bending deformations 94
5.4 The geometry of the stator 102
5.5 The nine wave piezoceramic ring 103
5.6 Section of the loaded stator undergoing bending deformations 111
5.7 Section of the loaded stator undergoing bending deformations in the moving coordinate system 112

6.1 Comparison of the speed-frequency characteristics for the unloaded motor: simulation and measurements 137
6.2 Prediction of the speed-frequency characteristics at various load torques 138
6.3 Comparison of the speed-frequency characteristics for the loaded motor: simulation and measurements, at load torques 0.1 Nm , 0.2 Nm and 0.3 Nm respectively 139
6.4 Prediction of the speed-frequency characteristics at various temperatures 140

A.1 The manual test setup 158
A.2 The automatic test setup 159

A.3 Operating principle of the Mach-Zehnder interferometer 160
A.4 The modified Mach-Zehnder interferometer for external measures 161
A.5 Operating principle of the Polytec laser interferometer 162

List of Tables

2.1 Different piezoelectric relation-types in matrix notation 22

3.1 Specification of the USR60 28
3.2 The geometrical data of the stator 39
3.3 The resonance frequencies for different modes of vibration: Comparison between the measurements and the theoretical predictions 39

4.1 Correlation between the electrical and the mechanical parameters 56
4.2 The characteristic parameters of the electrical network method 59
4.3 The identified parameters of the electrical admittance 65
4.4 The identified parameters of the electromechanical motional admittance 68

5.1 Summary of the explicit state space model and its parameters 119
5.2 Summary of the complete simplified analytical model 122
5.3 Summary of the parameters that constitute the prerequisites for simulation 123

6.1 Summary of the complete hybrid model 136

Nomenclature

Symbols

Tensor notations in piezoelectric relations

S_{ij}	Second-rank tensor mechanical strain
T_{ij}	Second-rank tensor mechanical stress
E_i	First-rank tensor electrical field
D_i	First-rank tensor electrical displacement
P_i	First-rank tensor electrical polarization
c_{ijkl}	Fourth-rank tensor elastic stiffness coefficient
s_{ijkl}	Fourth-rank tensor elastic compliance coefficient
ε_{ij}	Second-rank tensor dielectric permitivity constant
β_{ij}	Second-rank tensor dielectric permeability constant
d_{nij}	Third-rank tensor piezoelectric constant
α_{ij}	Second-rank tensor thermal expansion constant
p_n	First-rank tensor pyroelectric constant

Matrix notations in piezoelectric relations

$\mathbf{S}$, S_i	Mechanical strain vector and its components
$\mathbf{T}$, T_i	Mechanical stress vector and its components
$\mathbf{D}$, D_i	Electrical displacement vector and its components
$\mathbf{E}$, E_i	Electrical field vector and its components
$\mathbf{P}$, P_i	Electrical polarization vector and its components
$\mathbf{c}$, c_{ij}	Elastic stiffness matrix and its components
$\mathbf{s}$, s_{ij}	Elastic compliance matrix and its components
$\mathbf{d}$, d_{ij}	Piezoelectric constant matrix and its components
$\mathbf{e}$, e_{ij}	Dielectric constant matrix and its components
ε, ε_{ij}	Dielectric permitivity constant matrix and its components
$\mathbf{p}$, p_i	Pyroelectric constant vector and its components
α, α_i	Thermal expansion constant vector and its components

Remaining notations

Θ	Temperature of the system
Ξ	Entropy (per unit volume) of the system
$\mathcal{C}$	Specific heat per unit mass
ρ	Mass density
G	Gibbs free energy per unit volume
U	Internal energy of the system
U_{elas}	Elastic energy of the system
U_{elec}	Electric energy of the system
U_{int}	Interaction energy of the system
$\mathbb{k}$	Electromechanical coupling factor
I	Electric current
V	Electric voltage
q	Electric charge
$\dot{u}$	Displacement velocity
F	Force
W_d	Dissipated energy within the system
W_a	Applied energy to the system
Y	Total electrical admittance of the system
Y_d	Damping electrical admittance of the system
Y_m	Motional electrical admittance of the system
y_m	Motional electromechanical admittance of the system
u	Displacement
$\mathtt{a}$	Acceleration
m	Inertial vibrating mass of the beam
x, y, z	Cartizien coordinates
v_{ph}	Phase velocity of the plane wave
k	Wave number of the plane wave
λ	Wave length of the plane wave
ω	Angular frequency of the plane wave
$\underline{X} = Xe^{j\omega t}$	Complex notation
$\underline{Z}$, $\underline{Z_o}$	Elastic impedances of the system
Π	Electromechanical force factor of the system
(R_d, C_d, R, L, C)	Parameters of the electrical admittance of the system
(r, l, c)	Parameters of the electromechanical admittance of the system
f	Excitation frequency
f_s	Motional (series) resonance frequency
f_p	Parallel resonance frequency
f_r	Resonance frequency
f_a	Antiresonance frequency
f_h	Frequency at maximum admittance
f_l	Frequency at minimum admittance
Δf_{-3dB}	Pass band at $-3dB$ of the frequency response
Q	Mechanical quality factor

ϑ	Maximum tangential vibration velocity of the particles of the stator
R_o	Middle radius of the annular plate
η	Modal force factor of the system
η_x	Direct modal force factor of the feedback electrode
V_x	Developed voltage on the feedback electrode
I_x	Electrical current flowing out of the feedback electrode
C_x	Blocking capacitance of the feedback electrode
R_r	Radial shape constant of the traveling wave
$w(r, \theta, t)$	Traveling wave
$\cos k\theta$, $\sin k\theta$	Mechanical orthogonal modes
$\cos \omega t$, $\sin \omega t$	Temporal orthogonal modes
A, ω	Amplitude and angular frequency of the traveling wave respectively
ξ_i	Temporal amplitude of vibration
$\mathcal{P}$	Total power needed to supply the two phase motor
a	Inner radius of the stator
b	Outer radius of the stator
γ	Constant depending on the modal shape of the stator in radial direction
$\mathcal{P}_x$	Loss of power due to pressure
R_x	Resistance representing the loss of power due to pressure
Ω	Rotary speed of the motor
Ω_{id}	Ideal rotary speed of the motor
Ω_o	Measured rotary speed of the motor
$\Delta\Omega_f$	Speed drop due to normal forcing
$\Delta\Omega_\tau$	Speed drop due to load torque
I_m	Motional current
I_{id}	Ideal motional current image of the ideal rotary speed of the motor
I_{m_o}	Motional current image of the measured rotary speed of the motor
I_f	Motional current image of the speed drop due to normal forcing
I_τ	Motional current image of the speed drop due to load torque
$\aleph$	Proportionality factor of the speed-current relationship
α	Slope of the speed drop and the normal forcing characteristic
β	Slope of the speed drop and the load torque characteristic
R_f	Resistance representing the frictional losses due to normal forcing
C_f	Capacitance representing the resonance shift due to normal forcing
R_τ	Resistance representing the frictional losses due to load torque
C_τ	Capacitance representing the resonance shift due to load torque
$\mathcal{T}$	The torque
f_{r_o}, f_r	Resonance frequencies at the ambient and working temperature respectively
C_{T_o}	Total capacitance of the loaded motor at ambient temperature
C_T	Total capacitance of the loaded motor at working temperature
ℓ	Slope of the resonance-temperature characteristic
$\Delta\Theta$	Temperature gradient during operation of the motor

L	Lagrangian of the system
δ	Small variation
δL	Small variation of the Lagrangian
δW	Variational work done by the external forces
δW_n	Variational normal work of the external forces
δW_t	Variational tangential work of the external forces
δW_e	Variational electrical work energy of the system
E_k	Kinetic energy of the system
E_p	Potential energy of the system
E_e	Electrical energy of the system
r, θ, z	Polar coordinates
u, v, w	Wave coordinates
$\mathbf{u}_o$	Three dimensional centerline displacement in the r, θ and z directions
$\dot{\mathbf{u}}_o$	Three dimensional centerline velocity in the r, θ and z directions
$\mathbf{u}$	Displacement vector of the deformed surface in the r, θ and z directions
$\dot{\mathbf{u}}$	Displacement velocity vector of the deformed surface in the r, θ and z directions
ξ	Mechanical modal amplitude vector dependent only on time
Φ_m	Mechanical mode matrix (called deflection matrix) dependent only on r and θ
$\mathbf{L}_m$	Lazarus mapping operator
$\mathbf{N}_m$	Strain matrix function of the coordinates (r, θ, z)
Φ_u, Φ_v, Φ_w	n-dimensional row vector shape functions
φ	Shapes on the electric potential within the stator
Φ_e	Electrical shape matrix
$\mathbf{v}$	Voltage vector at the electrodes of the stator
$\mathbf{L}_e$, $\mathbf{N}_e$	Electrical mapping operator matrices
$\mathbf{q}$	Electrical charge vector on the electrodes of the stator
$\mathbf{I}$	Electrical current vector on the electrodes of the stator
σ	Electrical charge density vector on the surface of the piezoceramic
$\mathbf{F}_\mathbf{n}^*$	Normal modal forcing vector at the contact interface
$\mathbf{F}_\mathbf{t}^*$	Tangential modal forcing vector at the contact interface
$P(r, \theta, t)$	Pressure distribution at the interface contact between the stator and the rotor
$\zeta_v, sign(v_s, v_\theta)$	Sign function depending on the relative velocity between the rotor and the stator
v_s	Velocity of the particles of the stator
v_θ	Rotor tangential velocity in circumferential direction
$\dot{\theta}$	Angular velocity of the rotor
F_{app}	Applied axial load on the motor
F_{int}	Generated force at the interface contact
$\mathcal{T}_{app}$	Applied load torque on the motor
$\mathcal{T}_{int}$	Generated torque at the interface contact
$\mathbf{M}_s$	Modal mass matrix of the substrate
M_s	Modal mass of the substrate
$\mathbf{M}_p$	Modal mass matrix of the piezoelectric plate
M_p	Modal mass of the piezoelectric plate
$\mathbf{M}$	Total modal mass matrix of the stator
M	Total modal mass of the stator
$\mathbf{K}_s$	Modal stiffness matrix of the substrate

K_s	Modal stiffness of the substrate
$\mathbf{K}_p$	Modal stiffness matrix of the piezoelectric plate
K_p	Modal stiffness of the piezoelectric plate
$\mathbf{K}$	Total modal stiffness matrix of the stator
K_o	Total modal stiffness of the stator
II	Modal electromechanical coupling matrix
$\mathbf{C}_p$	Modal piezoelectric capacitance matrix
C_p	Modal piezoelectric capacitance of the stator
$\mathcal{D}$	Structural damping matrix assumed to be diagonal
$\mathcal{D}_o$	Modal structural damping of the stator
F_{n1}, F_{n2}	Components of the normal force vector
F_{t1}, F_{t2}	Components of the tangential force vector
A_*, B_*, $\mathtt{u}$	Transfer matrices and the control signal of the state space representation
$P(x)$	Pressure distribution at the interface contact in the moving coordinate frame
$w(x)$	Traveling wave in the moving coordinate frame
x_0	Slip point coordinate of the half width of the contact zone
x_s	Stick point coordinate of the contact zone
$\mathbf{c}_p$	Plane stress stiffness matrix of the piezoceramic
$\mathbf{c}_s$	Plane stress stiffness matrix of the substrate
$s_{11}^E, s_{12}^E, s_{66}^E$	Compliance components at constant electrical field
$c_{11}^E, c_{12}^E, c_{66}^E$	Stiffnesse components at constant electrical field
e_{31}	Dielectrical constant
d_{31}	Piezoectrical constant
ε_{33}^T , ε_{33}^S	Electrical permitivity at constant stress and constant strain respectively
ρ_s	Mass density of the substrate
ρ_p	Mass density of the piezo plate
V_s	Volume of the substrate
V_p	Volume of the piezo plate
V_t	Total volume of the considered system
J	Young's modulus of the substrate
ν	Poisson ratio of the substrate
$\mathtt{G}$	Shear modulus of the substrate
ϕ_{w_1}, ϕ_{w_2}	Orthogonal mechanical modes excited within the stator
ξ_1 , ξ_2	Temporal modal amplitudes of the excited modes
V_A, V_B	Applied voltage to phase *A* and phase *B* respectively
$\hat{V}$	Maximum amplitude of the applied voltage
ϕ_A, ϕ_B	Electrical shape functions of the nine wave motor
q_A, q_B	Electrical charge on phase *A* and phase *B* respectively
$\mathcal{D}_v$	Modal damping of the stator in forced conditions
K_v^o	Modal stiffness of the stator in forced conditions at the ambient temperature
K_v	Modal stiffness of the stator in forced conditions at the working temperature
$\mathtt{z}$	Relative displacement of the rotor in vertical direction
h	Half thickness of the stator
ι_p	Thickness of the piezoelectric plate
R_o	Middle radius at the contact surface
ϵ	Width of the contact surface

$\varkappa_r$	Rotor stiffness per unit area
M_r	Rotor mass
J_r	Rotor inertia
$\mathcal{D}_z$	Rotor damping in vertical direction
$\mathcal{D}_r$	Rotor damping in spinning direction
μ	Coulomb's friction coefficients

Abbreviations

USM	UltraSonic Motor
PEM	PiezoElectric Motor
RPEM	Rotary PiezoElectric Motor
ECM	Equivalent Circuit Model
EM	Electro-Mechanical
FEA	Finite element analysis
USR60	Shinsei ultraSonic motor type "R60"

Chapter 1

Introduction

This thesis considers the modeling of the rotary type piezoelectric motor driven by the dynamical friction mechanism at the rotor-stator interface contact (Sashida and Kenjo (1993)). The driving friction is generated by the excitation of a traveling wave within the body of the stator. This excitation is normally achieved through a proper power supply.

> *The general concept of all solid state motors is to generate gross mechanical motion through the amplification and repetition of micro-deformations of active materials, in this case piezoceramics. The key principles that govern this type of motors are first the orbital motion of the stator at the rotor contact points, which can be achieved through proper control of the active material, second the frictional interface between the rotor and the stator must rectify the micro-motion to produce macro-motion of the rotor.*

The thesis focuses on three main issues: 1) Improving the existing equivalent circuit modeling approaches (Nogarede and Piecourt (1994); Sashida and Kenjo (1993)) for better prediction of the performance characteristics of the motor. 2) Improving the existing theoretical modeling approaches (Hagood and Andrew (1995);Hagedorn *et al.* (1998)) by reducing the complexity of the model and thereby making it suitable for control purposes. 3) Making a comparison and thereafter fusion of the two derived models in order to overcome some of the drawbacks inherent in each model and thereby achieve a better performance objective.

1.1 Background and motivation

Industrial requirements have in the past focused mainly on improving the quality and quantity of electromagnetic motors. This has resulted in the huge amount of motors

found in almost all areas of applications. Recently, the advance in the field of smart structures and active materials has led to new kinds of motors. Consequently, there exist numerous examples from different area of application, where piezoelectric motors developed recently have shown to be superior to their electromagnetic counterparts. These new devices are already used in Aerospace, Aviation, Shipping, Cars and Camera.

For instance, the traveling wave Piezo Electric Motor (PEM) has excellent performance and many useful features such as high holding torque, high torque at low speed, quiet operation (ultrasonic), simple structure, compactness in size and no electromagnetic interferences. However, the mathematical model of the PEM is complex and difficult to derive due to its driving principle based on high-frequency mechanical vibrations and frictional force, (Sashida and Kenjo (1993)). Despite many attempts a lumped motor model of the PEM is unavailable so far. The dynamical characteristics of the PEM are complicated, highly nonlinear, and the motor parameters are time varying due to temperature rise and changes in motor drive operating conditions. Therefore it is difficult to predict the performance characteristics of the PEM under various working conditions.

Most of the existing work in the field of Piezoelectricity has been carried out by scientists in order to establish linear relationships between different parameters that describe piezoelectric phenomena (Ikeda (1996); Holland and EerNisse (1969) and Mason (1964)). The theoretical approach provides linear equations which describe the electromechanical behavior in any piezoelectric transducer by applying the basic laws of physics. The empirical approach is, however, based on the measurement of the electromechanical constants in terms of admittance and equivalent circuit information. This approach, which is referred to by Equivalent Circuit Modeling (ECM), is a powerful alternative to the theoretical approach (Ikeda (1996)) for solving the practical problems in question. Consequently, the complexity and the large discrepancy between linear theory and the real nonlinear physical piezoelectric transducer is avoided.

Equivalent circuit modeling of the traveling wave UltraSonic Motor (USM) "Shinsei type USR60" has been the subject of extensive research all over the world and important contributions have been established in (Sashida and Kenjo (1993)). In (Nogarede and Piecourt (1994)) a systematic modeling approach has been reported. The complexity of the conversion process of the electromechanical energy within this device is daunting. The increase of temperature during operation strongly affects the performance of the motor. Despite many reported attempts, the modeling of this device is still a challenging problem. Therefore, an insight is needed in order to understand how the electromechanical coupling factor, which guarantees the effective energy conversion, can be incorporated in the ECM in order for the simulated model to match the performance characteristics of the physical system in a better way.

Analytical modeling of the traveling wave piezoelectric motor has also been the subject of extensive research all over the world and important contribution has been reported in (Hagood and Andrew (1995)). Due to the complexity of the conversion process of the electromechanical energy within this type of motors and the increase of temperature

during operation an insight is needed in order to understand how to capture most features of the motor in a lower order analytical model. The symmetrical nature of the stator, decoupling the correlated excited modes, the effect of the stick-slip behavior of the driving mechanism on the mechanical resonance frequency of the motor: are the main topics considered for deriving a simple analytical model of the PEM presented in this thesis.

It has been observed in practice that the mechanical resonance frequency of the motor shifts towards lower frequencies during the operation of the motor due to the temperature increase within the body of the stator. In order to overcome this problem a tracking facility which will update the temperature sensitive parameters is integrated in the ECM and the hybrid analytical models presented in this thesis.

This thesis reports on the attempt to solve the highly demanding problem of performance prediction of the PEM. The rotary traveling wave ultrasonic motor "Shinsei type USR60" is the case study considered in this work. Consequently the objective is to derive a simple and a low computationally demanding model of the PEM providing the ability to predict most of the performance characteristics of the motor under various working conditions. The emphasis is on the combination of the electrical network method, the physics underlying piezoelectric phenomena, the variational work and elasticity theory (Hamilton's principle), besides contact mechanics (friction) and finally the basic laws of dynamics.

1.2 Previous work

Concerning piezoelectric motors, there is a substantial body of literature. This is a result of the past three decades significant but scattered activity in different research areas.

Most of the research activity has been concentrated on the design, modeling, power supply and control of these devices. Piezoelectric transducers are a fairly new field but with already several powerful quantitative and qualitative modeling methods and tools. Key references in this work can be found in (Uchino (1997); Ikeda (1996); Ragulskis *et al.* (1988); Holland and EerNisse (1969); Mason (1964)). A summary on different approaches for modeling and coping with these new kinds of devices can be found in (Ueha and Tomikawa (1993)) (see also Sashida and Kenjo (1993)). The existing modeling approaches are mainly based on the equivalent circuit method, the analytical method based on the variational work by applying Hamilton's principle and the finite element modeling (FEM) approach. Among other interesting approaches the fuzzy approach (Izuno and Nakaoka (1994)) can be mentioned.

Frequency control is the widely used technique for controlling these devices (Ueha and Tomikawa (1993)). Pioneering work in incorporating the findings of suitable power supply for these devices has been the forte of the Japanese. This extension of conventional control strategy has become known as *frequency control*.

1.2.1 Motor design

Toshi Sashida is regarded by many to be the inventor of the piezoelectric motor. He indirectly caused the development of the Shinsei motor shown in figure 1.1, which has spurred much interest all over the world ever since. Consequently, their simple mechan-

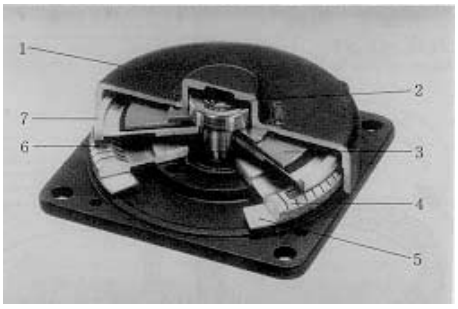

Figure 1.1: The Shinsei motor. 1: Cover, 2: bearing, 3: spring, 4: stator, 5: piezoceramic, 6: friction material, 7: rotor.

ical construction, efficiency, and high power density have encouraged the development of many different classes of piezoelectric motors. They typically use one or several piezoelectric ceramic crystals as the energy source. In Japan (Sashida (1985)), (Kumada (1987)), (Kumada *et al.* (1991)) and many other Japanese researchers have developed high performance piezoelectric motors for a variety of applications. In Europe and the USA a strong interest has been shown and considerable effort on development has been made in the last decade on PEM development, especially in the USA.

In order to establish the design method for a particular motor, a model is convenient for understanding the operational mechanism of the motor. The design of the motor is the specifications of the motor which are determined from the required characteristics of the motor, such as the maximum torque and the maximum speed of rotation. The approach adopted by researchers is to provide a general framework for modeling these motors as well as to provide design tool for optimizing prototypes with the added flexibility of allowing for a wide variety of geometries and materials. In particular, the design of dynamic systems for precise rotary and linear motion devices has been a significant research topic all over the world. In Japan, (Hirata and Ueha (1995)) proposed a method of design for a traveling wave type ultrasonic motor. This method is based on two models of the ultrasonic motor. A two dimensional elastic contact model is used for estimating the friction drive between the rotor and the stator of the motor. Moreover, an electrical equivalent circuit is used to estimate the interaction between the electrical and the mechanical parts of the motor. The proposed method is applied to the design of a prototype motor which was validated by the experiments. In Europe and the USA, more advanced methods for modeling and analyzing these devices in the design phase are used. In the

USA, (Hagood and Andrew (1995)) proposed a general framework analytical model of a piezoelectric rotary ultrasonic motor. This model is derived for the purpose of predicting, a priori, motor performance as a function of the design parameters. The model presented by Hagood lays the foundations of a general framework capable of representing numerous existing motors.

1.2.2 Control system design

While simpler in general, the complexity of piezoelectric motor controllers is still frightening. Contribution to literature in this area is dominated by the Japanese. Like the traditional electromagnetic motors, the control system of the piezoelectric motors is designed around a certain model of the motor, and in the model it controls values analogous to the velocity and torque of the motor. Thus, a simple model of the motor system would be useful for initial experiments in designing the motor and its control system. A small model of the ultrasonic motor can be found in (Sashida and Kenjo (1993)), where the author claims that the linear "equivalent circuit" model matches the actual response relatively well, making it useful for designing a control system without resorting to actual experimentation. Likewise, (Nogarede and Piecourt (1994)) proposed a systematic modeling approach by using the equivalent circuit method. By using this model the author designed a simplified power driving system. It must be emphasized that much of the literature covering new control designs of this kind of motors appears not only in academic journals but also in patents. In general these control systems are only designed as driving circuits for the motor, and therefore suffer from their inability to cope with the problems associated with the transient phases of the motor's operation. The most important control problem with the motor is the influence of temperature on the resonance frequency of the stator. Unfortunately, when the temperature of the motor changes, it may not be able to start or it may shut down if it is running. To address these problems associated with the unstable operation of piezoelectric motors during their operation, and thereby achieve the performance objective despite the influences of temperature fluctuations and changes in external loading on the motor, control systems are designed for the motor supplied with its electronic drive in the post phase of the motor design. Several innovative control systems for use with the piezoelectric motor are reported in the literature. Adaptive control systems have been implemented successfully for controlling both the position (Lin and Kuo (1997)) and the speed (Senjyu *et al.* (1997)) of the motor. In (Izuno and Nakaoka (1994)) the authors designed a fuzzy-logic controller for the piezoelectric motor. It is a simple approach but somewhat difficult to implement in hardware. However, the system maintains the commanded speed of the motor with little error despite large changes in torque or commanded speeds. The most important contribution to the literature on the model based control system of the piezoelectric motor is reported in a series of three articles in (Maas and Grotstollen (1996*a*)), (Mass and Grotstollen (1997)-Jun) and (Maas *et al.* (1997)-Oct). Despite the innovative results in these contributions, the implementation in hardware is an expensive and difficult task.

1.2.3 Vibrations, elasticity, contact mechanics and materials

The development of the piezoelectric motors has spurred an interest in the vibration characteristics of plates laminated with piezoelectric materials. In particular, the annular plate composed of one stainless steel lamina ("substrate") and either one or two piezoelectric laminas, a common configuration for piezoelectric motors. (Hagedorn and Wallashek (1992)) has demonstrated a simple model for the free vibration of the stator disk and (Hagedorn *et al.* (1993)) an improved model, using finite element analysis (FEA), for the free vibration of the disk with non uniform thickness. However, forcing due to the piezoelectric elements and the laminated nature of the stator is ignored in their studies. Including these factors into the model makes it more difficult to avoid finite element analysis, and, indeed, (Maeno *et al.* (1990)) studied a ring motor including two-body contact mechanics using finite element analysis program. (Maeno and Bogy (1992)) examined the motor again with contact mechanics and fluid interaction using a combination of analytical and finite element analysis techniques.

While finite element analysis (FEA) is indispensable for many applications, particularly with complex geometries, it is inconvenient for system design. Each design iteration requires a new finite element mesh to be generated and a new numerical solution to be obtained. This process, known as FEA parametric optimization, is computationally expensive, and it provides a compelling reason to seek analytical solutions. The ability to predict the motion of the stator is essential for subsequent modeling of the interaction between the stator and the rotor which is required to predict motor performance. Therefore research in the vibrations and elasticity has been concentrated on refining the modeling and the numerical methods, in order to develop better analytical tools for the design of new PEMs. This problem, as well as questions concerning the excitation mechanism and the contact between the stator and the rotor were addressed in order to provide motors of higher efficiency and power, and thereby explore their full potential.

The most important questions related to piezoelectric ultrasonic motors are how much force and power can be delivered and what form the torque-speed curve will take. Among other important questions the tribological issues like wear, lifetime or the effect of surface asperities must be considered. The friction mechanism in the motor is inefficient and not well understood. The type of energy transfer is believed to be a significant contributor to the energy wasted in the motor, and the components involved have largely been designed in an ad-hoc manner. These two problems are the primary motivators for the huge activity in the research community in improving the contact mechanism responsible for much of the motor performance.

In the research on piezoelectric ultrasonic motors the mathematical modeling of the contact mechanics and the optimization of lifetime and operational characteristics of the motors by a proper choice of contact materials and design parameters have been significant topics. Analytical, numerical and experimental methods have been employed in the investigation. A survey of the literature on the contact mechanics of ultrasonic

motors is given in (Wallaschek (1998)). The author claims that the survey is far from complete since it is difficult to identify and include all relevant papers. The author has, however, tried to give a comprehensive and representative survey. Furthermore, Wallaschek claims that a rigorous solution of the dynamic contact problem is very difficult and has, to the best of his knowledge, not been found yet, even for the special case of piezoelectric ultrasonic motors.

The contact mechanics of ultrasonic motors are rather complicated due to the fact that many parameters should be taken into account. The operational characteristics depend on the form, frequency and amplitude of the stator vibration, the stiffness and damping of the contact layer, the flexibility of the rotor, the normal preload force, the static deflection of the stator and rotor and the frictional characteristics of the contact materials as well as their surface topology and microstructure. Furthermore, most material properties strongly depend on temperature and manufacturing tolerance concerning flatness, and alignment of the contact surface plays an important role. Obviously it is rather difficult to include all these aspects in a single, general contact model. It is more promising instead to develop problem-oriented models for specific applications. Piezoelectric ultrasonic motors are usually analyzed in two steps. First, the vibrating structure is designed to achieve the the required vibration modes, operational frequency and the amplitude. Then the nonlinear contact mechanic is studied under the assumption that the vibration characteristics of the vibrating structure are not affected by the contact process. This assumption is not accurate due to the fact that the whole system, including the rotor and the vibrating structure, is a coupled dynamic system. However, the separation of the analysis process simplifies the investigations and often results in a good description of the motor's behavior.

Mathematical models of the contact mechanics of ultrasonic motors are useful for understanding the principles of energy transfer at the frictional interface, and they are also used for the a priori calculation of motor characteristics such as no-load speed, staal torque, efficiency or stationary torque-speed curves. They are needed for the simulation of the overall system behavior as well as for the optimization of design parameters or operational characteristics. The contact mechanics of piezoelectric ultrasonic motors determine the operational characteristics, like rotational speed and torque or transmitted mechanical power and efficiency. Wear properties and lifetime of piezoelectric ultrasonic motors are also determined by contact mechanics. A first attempt to classify models for the contact mechanics of traveling wave ultrasonic motors was made by (Flynn (1995)), who started with a very simple contact model and then analyzed a series of progressively more sofisticated contact mechanisms. A similar approach was chosen by (Wallaschek (1998)) who gave a detailed discussion on different contact models at various levels.

The selection of friction materials is a very important step in the design of ultrasonic motors. Good friction materials for traveling wave motors should have high wear resistance and stable mechanical properties with respect to temperature and other environmental

changes. Up to now, however, no general rules can be formulated for this process. Most of the knowledge obtained so far is based on experimental results and is empirical. In practice different polymer blends have been tested and the most detailed discussion of this subject is given by (Ueha and Tomikawa (1993)).

1.3 Objectives and contributions

The main objective of this work is the derivation of a simplified and low computationally demanding model of the rotary traveling wave piezoelectric motor. Many of the existing models are unsuitable for control design investigation purposes due to their huge complexity and high computational demands. Therefore, an insight in the modeling process is needed in order to meet the requirements of a flexible test bench suitable for the control community. The modeling approaches that are addressed in this work are the equivalent circuit modeling which uses the electrical network method, the analytical modeling which uses the energy method based on Hamilton's principle and finally the hybrid modeling which is the combination of the strength of the two previously stated modeling approaches.

The first contribution of this work is the derivation of an improved equivalent circuit model of a rotary traveling wave piezoelectric ultrasonic motor "Shinsei type USR60". The modeling is performed on the basis of an experimental approach combined with the electrical network method and some simplification assumptions about the physical behavior of the real system. The main contributions under this approach are that

- An insight in the analysis of the electromechanical coupling factor, which is responsible for the electrical to mechanical energy conversion, is obtained. Consequently, the difference between the effective coupling force factor and the modal coupling force factor is highlighted, and how these parameters can be integrated in the equivalent circuit model is emphasized.

- The effect of the temperature on the mechanical resonance frequency is considered and thereby integrated in the final model for long term operations.

The validity of the model has been established by comparing the performance characteristics of the simulated model to the real performance characteristics of the system.

The second contribution of this work is the derivation of a general framework simplified analytical model by using the energy method based on Hamilton's principle. Consequently, the state space model of the complete traveling wave type rotary piezoelectric motor is derived by applying the basic laws of variational work and elasticity theory (Hamilton's principle). The main contributions under this approach are that

- A reduced general state space model is derived on the basis of the special design of the motors of interest (i.e. two phase symmetrical systems).

- A further simplified model is given within the framework of various assumptions on the behavior of the stator. Consequently, the assumed excited modes are decoupled and thereby the performance characteristics of the stator are predicted by a single second order system.

- The stick-slip behavior of the driving mechanism is integrated in the time varying parameters of the model. This makes it possible to predict most of the behavior and performance characteristics of the motor as a function of the external loading parameters.

- The outcome of this modeling approach is a less computationally demanding model suitable for control investigation purposes.

The derived model does not integrate the effect of temperature. Consequently, the model is assumed to be valid only for short term operation.

The third contribution of this work is the derivation of a hybrid model for predicting the performance characteristics of an ultrasonic piezoelectric motor type USR60. In this work the general framework model of the traveling wave type annular forced stator is derived by applying the basic laws of variational work and elasticity theory (Hamilton's principle). The main contributions within the framework of the hybrid modeling approach are that

- A reduced model is derived on the basis of the special design of the stator of interest and various assumptions on its behavior.

- The analogy between the equivalent circuit model and the analytically reduced model of the free stator, which both model the behavior of one phase of the stator, is highlighted. This makes it possible to substitute the parameters of the equivalent circuit model in the simplified analytical model. Consequently, the large uncertainty on the dielectrical and electromechanical constants is avoided.

- The simplified hybrid model of the complete motor is thereby derived in terms of the forced stator model, the spinning motion model and the vertical motion model.

- Finally the effect of temperature on the mechanical resonance frequency is considered and thereby integrated in the final model for long term operations.

The validity of the model has been established by simulation and comparison to the performance characteristics of the real system.

1.4 Structure of the thesis

The thesis is organized as follows

- **Chapter 2** briefly outlines the piezoelectric transducers and their applications, and also introduces the general background of Piezoelectricity.
- **Chapter 3** presents the traveling wave motor USR60, which is used as a case study in this thesis, and the experimental investigation of the performance characteristics of this motor when operating under various working conditions.
- **Chapter 4** presents the background of the equivalent circuit method and the model derivation of the USR60 based on this method. The importance of the electromechanical force factor is emphasized and the effect of temperature is considered.
- **Chapter 5** is devoted to the analytical modeling of the motor based on the energy method which uses the variational work by applying Hamilton's principle. The complexity and the order of the model are addressed and the outcome is a simplified and low computationally demanding model.
- **Chapter 6** is devoted to the comparison and fusion of the equivalent circuit model and the analytical model in one simple and robust hybrid model. The hybrid model is mainly an improvement of the analytical model, where the parameters of the model representing the stator are provided by the equivalent circuit method and the remaining dynamics of the motor are modeled by the analytical method, and where the effect of temperature is integrated in the final hybrid model for long term operations.
- **Chapter 7** finalizes this thesis by providing an overview of its contents, concluding remarks, perspectives and recommendations for future use of this work.

Chapter 2

Piezo-Electricity and Applications

This chapter presents an overview of the piezoelectric transducers and their applications, and finally some of the theoretical background that lays the foundations of piezoelectricity.

2.1 Piezoelectric transducers

In this section an overview of the piezoelectric materials will be presented and thereafter their use as actuators for solving some engineering problems will be discussed together with their limitations and advantages compared to the traditional and well-established electromagnetic devices. Finally the trends of these new devices will be discussed in the framework of the more general class of smart structures.

2.1.1 The state of the art

Much of the revived interest in piezoceramic actuators comes from the trend towards smart materials and structures. The chronological evolutionary step taken in the development of such materials is going from trivial, to smart and finally to intelligent materials. In the area of electromechanical transducers/actuators, ferroelectrics are found to be superior to other solid state materials in many applications. It is therefore important to stress research and development which center on ferroelectrics in particular the piezoelectric materials.

In contrast to magnetostriction and thermal dilatation which in general present a small

induced strain, piezoelectric strain and electrostriction can be induced by an electrical field, and relatively large strain can be obtained in various materials. Hence they are considered most promising.

In the field of solid state motors where there is an increasing need for small scale motors, the conventional electromagnetic motor proves to be inadequate, it is rather difficult to produce a small size electromagnetic motor with sufficient energy-efficiency. On the other hand piezoelectric motors whose, efficiency is insensitive to size and presents the ability to cope with harsh environmental conditions, are superior in the mm-size motor area and therefore present an alternative solution. Besides motors there are two other categories of devices which need compact actuators such as positioners and vibration suppressors. For the positioners, to miniaturize the actuator size, electrically-controlled types are preferred in general and piezoelectric actuators in particular have proven to be superior. For the vibration suppressors, active and passive vibration suppression in space structures, military and commercial vehicles using piezoelectric micro-actuators, have also proven to be a promising technology.

Solid state motors based on piezoelectric materials are widely known as ultrasonic motors. The reason behind that is that they often use mechanical vibrations with frequencies above 20 kHz (which the human ears can't detect) as its drive source. The magnitude of these vibrating oscillations is very small not exceeding the μm range, that is why the resonance effect of the piezoceramic must be used in order to reach higher gain and thus obtain high speeds, owing to the high frequencies.

There is basically a large class of ultrasonic motors which constitutes a subclass of the even larger class of vibromotors (Ragulskis *et al.* (1988)). The invention by T. Sashida in 1982 of the first successful traveling wave ultrasonic motor has spurred many proposals, especially in Japan, on the use of various modes of vibrations, e.g. longitudinal, flexural or torsional, to obtain elliptical motion of the stator at the rotor contact points. The methods for obtaining elliptical motion can be roughly divided into those using a single vibration mode and those using multiple (two or more) vibration modes.

- *The single vibration mode type* can be classified into
  - *The standing wave type*
  - *The traveling wave type*
- *The multiple vibration modes type* can be divided into
  - *The modal conversion type*, in which two vibrational modes are obtained from a single source using modal conversion
  - *The multiple-mode type*, in which different vibrational modes (including coupled vibration) are produced, also using a single piezoelectric transducer

  - *The mode-rotation type*, in which the mode is rotated by driving the degenerate modes at different phases

  - *The hybrid transducer type*, in which different piezoelectric transducers with their respective power sources are used to produce different vibrational modes

Many different shapes, including rods, rings, disks, bars and cylinders, etc., were tried with the modes that were suitable for these shapes, and research was vigorously pursued on the characteristics and application of these motors. This research is still going on today. Theoretical evaluation of the conversion process, optimization of design, and assessment of the possibility of a more powerful ultrasonic motor are also undertaken. There are also studies on motors which have a gas or a liquid, for instance, interposed between the rotor and the stator.

2.1.2 Limitations in piezoelectric materials

There are many shortcomings of piezoelectric materials, for instance

- *Fatigue failure* resulting from the alternating stress in the ceramic elements

- *Looseness of the piezoelectric properties* in the neighborhood of the Curie temperature point ($> 300^{o}$C)

- *Weakening of the adhesive bond* occurring below the Curie point

- *Change in Young's modulus* with temperature causing a change in the resonant frequency and thereby resulting in lowering the performance of the device

- *Short life span* owing to rapid wear and tear

- *Large frictional losses* due to the complex nature of vibrations which together with other phenomena such as

  - *Sliding and deformation losses* lead to lower efficiencies, for example at most $\sim$50% in ultrasonic motor applications

In order to overcome these shortcomings and improve the efficiency, an in-depth study of dielectric properties of the piezoceramic and their vibrational behavior together with contact surface behavior has been undertaken.

2.1.3 The trends in piezoelectric actuators

In many special applications, where flexibility in the choice of the shape is required and the duration of operation is short, ultrasonic motors have proved to be more adequate than the traditional electromagnetic motors; for instance, the ultrasonic motors are suitable for the following applications

- *Actuators for robots*, where the requirement for a lightweight motor capable of producing high torque (tens of Nm) can be easily fulfilled by an ultrasonic motor
- *Actuators of devices for consumer goods*, successful applications which make full use of the flexibility of the shape, controllability and quiet operation of the motor, already exist in the car industry, in drive mechanisms for autofocus lenses in cameras etc.
- *Actuators for precise positioning devices*, rapid positioning devices with accuracies of the order of nanometer are being used in the production of semiconductors, moreover, linear and rotary ultrasonic motors and appropriate control methods are being developed for various applications in positioning devices
- *Actuators for miniaturized machines*, research into the use of static electrical motors and bio-actuators as drives for micro-mechanisms is also being conducted but has yet to produce some results
- *Actuators for machines used in space*, because ultrasonic motors do not require any lubrification and they present high torque at low speed, they are well-suited for operating in vacuum and in the absence of the gravity in space
- *Actuators for material conveyors*, because of their quiet operation ultrasonic motors are well-suited for the conveyance of parts

2.2 The fundamental piezoelectric relations

In a piezoelectric media interaction processes take place between the thermal, mechanical, and electrical systems. The variables in the piezoelectric system are mechanical strain S_{ij} and stress T_{ij} tensors, electrical field E_i and displacement D_i (or the polarization P_i) and finally the temperature Θ and entropy Ξ (per unit volume) of the system.

For the mechanical system the elastic relation between intensive and extensive variables is given by

$$T_{ij} = c_{ijkl} S_{kl} \quad \text{or} \quad S_{ij} = s_{ijkl} T_{kl}$$

For the electric system the constitutive relation is

$$D_i = \varepsilon_{ij} E_j \quad \text{or} \quad E_i = \beta_{ij} D_j$$

and for the thermal system the relation is expressed as

$$\delta \Xi = (\rho \mathcal{C} / \Theta) \delta \Theta$$

where the fourth-rank tensors c_{ijkl} and s_{ijkl} are the elastic stiffness and the elastic compliance coefficient respectively, the second-rank tensors ε_{ij} and β_{ij} are the dielectric constant and dielectric permeability respectively, $\mathcal{C}$ is the specific heat per unit mass and ρ is the density.

In the piezo-media intensive and extensive variables are not independent when interaction processes take place between thermal, mechanical and electrical systems (Ikeda (1996)). The possible interactions are electromechanical, thermomechanical and finally thermoelectrical. The derivation of the constitutive relation for the coupled piezoelectric systems is based on thermodynamic functions such as Helmholz free energy, Gigbbs free energy, Elastic Gibbs energy and Electric Gibbs energy. The choice of the thermodynamical function leads to different variable-type relations, thus for the electric displacement scheme (D-scheme) with isotherm or adiabatic assumption (Ikeda (1996)) four different constitutive relations are obtained, they are referred to by (S,D)-Extensive or h-form, (T,E)-Intensive or d-form, (T,D)-Mixed or g-form and (S,E)-Mixed or e-form. An alternative derivation of formulae is merely a transformation from one type of relation to another, but some care must be taken in rearranging the terms.

2.2.1 Constitutive relation of (Θ, T, E)-Type.

The relevant thermodynamic function is the Gibbs free energy $G(\Theta, T, E)$ per unit volume, and the variables $\delta\Theta$, $T$and E are assumed to be intensive variables (Ikeda (1996)). The Gibbs free energy is given by

$$G = U(\Xi, S, D) - \Theta\Xi - T_{ij}S_{ij} - E_n D_n \tag{2.1}$$

where $U(\Xi, S, D)$ is the internal energy of the system (constant) and the suffixes are

$$i, j, n = 1 \text{ to } 3$$

From the exact differential

$$dG = -\Xi d\Theta - S_{ij}dT_{ij} - D_n dE_n \tag{2.2}$$

we obtain

$$\begin{cases} \Xi = -\left[\frac{\partial G}{\partial \Theta}\right]_{T,E} \\ S_{ij} = -\left[\frac{\partial G}{\partial T_{ij}}\right]_{\Theta,E} \\ D_n = -\left[\frac{\partial G}{\partial E_n}\right]_{T,\Theta} \end{cases} \tag{2.3}$$

Taking the total derivative

$$dS_{ij} = \left[\frac{\partial S_{ij}}{\partial T_{ij}}\right]_{\Theta,E} dT_{ij} + \left[\frac{\partial S_{ij}}{\partial E_n}\right]_{T,\Theta} dE_n + \left[\frac{\partial S_{ij}}{\partial \theta}\right]_{T,E} d\Theta \tag{2.4}$$

Simularly

$$dD_n = \left[\frac{\partial D_n}{\partial T_{ij}}\right]_{\Theta,E} dT_{ij} + \left[\frac{\partial D_n}{\partial E_k}\right]_{T,\Theta} dE_k + \left[\frac{\partial D_n}{\partial \theta}\right]_{T,E} d\Theta \tag{2.5}$$

and

$$d\Xi = \left[\frac{\partial \Xi}{\partial T_{ij}}\right]_{\Theta,E} dT_{ij} + \left[\frac{\partial \Xi}{\partial E_n}\right]_{T,\Theta} dE_n + \left[\frac{\partial \Xi}{\partial \theta}\right]_{T,E} d\Theta \tag{2.6}$$

where the suffixes are

$$i, j, n, k = 1 \text{ to } 3$$

Since dG is a perfect differential, the relationships below follow from (2.3), with the partial derivatives identified as

- Elastic compliance

$$s_{ijkl}^{\Theta,E} = -\left[\frac{\partial^2 G}{\partial T_{ij}\partial T_{kl}}\right]_{\Theta,E} = \left[\frac{\partial S_{ij}}{\partial T_{kl}}\right]_{\Theta,E}$$

- Dielectric constant

$$\varepsilon_{nm}^{T,\Theta} = -\left[\frac{\partial^2 G}{\partial E_n \partial E_m}\right]_{T,\Theta} = \left[\frac{\partial D_n}{\partial E_m}\right]_{T,\Theta}$$

- Thermal constant

$$\frac{\rho \mathcal{C}^{T,E}}{\Theta} = -\left[\frac{\partial^2 G}{\partial \Theta^2}\right]_{T,E} = \left[\frac{\partial \Xi}{\partial E_m}\right]_{T,E}$$

- Piezoelectric constant

$$d_{nij}^{\Theta} = -\left[\frac{\partial^2 G}{\partial T_{ij} \partial E_n}\right]_{\Theta} = \left[\frac{\partial D_n}{\partial T_{ij}}\right]_{\Theta,E} = \left[\frac{\partial S_{ij}}{\partial E_n}\right]_{T,\Theta}$$

- Thermal expansion constant

$$\alpha_{ij}^{E} = -\left[\frac{\partial^2 G}{\partial T_{ij} \partial \Theta}\right]_{E} = \left[\frac{\partial S_{ij}}{\partial \Theta}\right]_{T,E} = \left[\frac{\partial \Xi}{\partial T_{ij}}\right]_{\Theta,E}$$

- Pyroelectric constant

$$p_n^T = -\left[\frac{\partial^2 G}{\partial \Theta \partial E_n}\right]_{T} = \left[\frac{\partial D_n}{\partial \Theta}\right]_{T,E} = \left[\frac{\partial \Xi}{\partial E_n}\right]_{T,\Theta}$$

When the function G is differentiated and the above constants are used a set of three equations is obtained

$$\begin{cases} S_{ij} = \alpha_{ij}^{E} \delta\Theta + s_{ijkl}^{\Theta,E} T_{kl} + d_{mij}^{\Theta} E_m \\ D_n = p_n^T \delta\Theta + d_{nkl}^{\Theta} T_{kl} + \varepsilon_{nm}^{T,\Theta} E_m \\ \delta\Xi = \frac{\rho \mathcal{C}^{T,E}}{\Theta} \delta\Theta + \alpha_{ij}^{E} T_{ij} + p_m^T E_m \end{cases} \tag{2.7}$$

where the suffixes are

$$i, j, k, l, m, n = 1 \text{ to } 3$$

and where according to custom, the differential symbols are removed from S, D, T and E (Mason (1964)) and the symbol δ is used to indicate a small variation of Θ and Ξ. This set of equations is the constitutive relation in the coupled system, here called the (Θ, T, E)-Type.

2.2.2 Tensor index abbreviations and matrix representations

As interchangeable indices can be treated as a set, the tensor notation is turned into simpler matrix expressions by index abbreviations (Ikeda (1996)). For instance, the (Θ, T, E)-Type constitutive relation is considered. When using matrix expressions, the following three equations are sufficient to give the constitutive relation

$$\begin{cases} \mathbf{S} = \alpha^E \delta\Theta + \mathbf{s}^{\Theta,E}\mathbf{T} + \mathbf{d}^{t\Theta}\mathbf{E} \\ \mathbf{D} = \mathbf{p}^T \delta\Theta + \mathbf{d}^{\Theta}\mathbf{T} + \varepsilon^{T,\Theta}\mathbf{E} \\ \delta\Xi = \frac{\rho \mathcal{C}^{T,E}}{\Theta}\delta\Theta + \alpha^{tE}\mathbf{T} + \mathbf{p}^{tT}\mathbf{E} \end{cases} \tag{2.8}$$

where

$$\mathbf{D} = \begin{bmatrix} D_1 \\ D_2 \\ D_3 \end{bmatrix}; \mathbf{E} = \begin{bmatrix} E_1 \\ E_2 \\ E_3 \end{bmatrix}; \mathbf{p} = \begin{bmatrix} p_1 \\ p_2 \\ p_3 \end{bmatrix}; \varepsilon = \begin{bmatrix} \varepsilon_{11} & \varepsilon_{12} & \varepsilon_{13} \\ \varepsilon_{21} & \varepsilon_{22} & \varepsilon_{23} \\ \varepsilon_{31} & \varepsilon_{32} & \varepsilon_{33} \end{bmatrix};$$

$$\mathbf{S} = \begin{bmatrix} S_1 \\ S_2 \\ S_3 \\ S_4 \\ S_5 \\ S_6 \end{bmatrix}; \mathbf{T} = \begin{bmatrix} T_1 \\ T_2 \\ T_3 \\ T_4 \\ T_5 \\ T_6 \end{bmatrix}; \alpha = \begin{bmatrix} \alpha_1 \\ \alpha_2 \\ \alpha_3 \\ \alpha_4 \\ \alpha_5 \\ \alpha_6 \end{bmatrix};$$

$$\mathbf{d} = \begin{bmatrix} d_{11} & d_{12} & d_{13} & d_{14} & d_{15} & d_{16} \\ d_{21} & d_{22} & d_{23} & d_{24} & d_{25} & d_{26} \\ d_{31} & d_{32} & d_{33} & d_{34} & d_{35} & d_{36} \end{bmatrix};$$

$$\mathbf{s} = \begin{bmatrix} s_{11} & s_{12} & s_{13} & s_{14} & s_{15} & s_{16} \\ s_{21} & s_{22} & s_{23} & s_{24} & s_{25} & s_{26} \\ s_{31} & s_{32} & s_{33} & s_{34} & s_{35} & s_{36} \\ s_{41} & s_{42} & s_{43} & s_{44} & s_{45} & s_{46} \\ s_{51} & s_{52} & s_{53} & s_{54} & s_{55} & s_{56} \\ s_{61} & s_{62} & s_{63} & s_{64} & s_{65} & s_{66} \end{bmatrix}$$

Superscript t indicates the mathematical transpose of the matrix. Thus, formulae and constants are easily transformed using matrix algebra.

In the case of an adiabatic and isotherm process the relation (2.8) reduces to the following (T,E) relation

$$\begin{cases} \mathbf{S} = \mathbf{s}^E\mathbf{T} + \mathbf{d}^t\mathbf{E} \\ \mathbf{D} = \mathbf{d}\mathbf{T} + \varepsilon^T\mathbf{E} \end{cases} \tag{2.9}$$

This relation refers to a certain identification of the directions in the considered media as shown in figure 2.1. For convenience, the depolarizing field is oriented parallel to the axis 3. The components S_1, S_2, S_3 and T_1, T_2, T_3 of **S** and **T** represent respectively tensile strains and stresses parallel to the axes 1, 2 and 3, whereas the components S_4, S_5, S_6 and T_4, T_5, T_6 respectively represent shear strains and stresses around these same axes (1, 2 and 3).

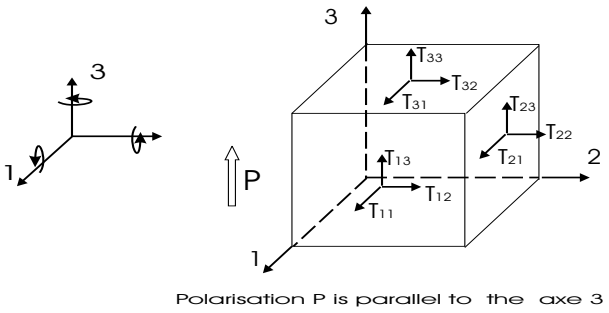

Figure 2.1: The motion

The subscript indices used for representing the stresses shown in figure 2.1 indicate axis directions for cause and effect. For instance T_{31} is the stress in the 1-direction caused by a pressure or electrical field in the 3-direction. Due to the symmetry involved in this interaction process the nine components of the stress tensor reduce to six components, and the double indices are replaced by one index as shown in the following

$$\begin{aligned} T_{11} &= T_1 \\ T_{22} &= T_2 \\ T_{33} &= T_3 \\ T_{23} &= T_{32} = T_4 \\ T_{31} &= T_{13} = T_5 \\ T_{12} &= T_{21} = T_6 \end{aligned} \tag{2.10}$$

In the particular case of the PZT ceramics used in piezomotors, the symmetrical nature of the crystal structure induces further simplification. Consequently, the PZT ceramics which belong to the crystal class "6mm" of the hexagonal system (Ikeda (1996)), have their matrices **s**, ε and **d** reduced to

$$\mathbf{s} = \begin{bmatrix} s_{11} & s_{12} & s_{13} & 0 & 0 & 0 \\ s_{12} & s_{11} & s_{13} & 0 & 0 & 0 \\ s_{13} & s_{13} & s_{33} & 0 & 0 & 0 \\ 0 & 0 & 0 & s_{44} & 0 & 0 \\ 0 & 0 & 0 & 0 & s_{44} & 0 \\ 0 & 0 & 0 & 0 & 0 & s_{66} \end{bmatrix} \tag{2.11}$$

$$\varepsilon = \begin{bmatrix} \varepsilon_{11} & 0 & 0 \\ 0 & \varepsilon_{11} & 0 \\ 0 & 0 & \varepsilon_{33} \end{bmatrix} \tag{2.12}$$

$$\mathbf{d} = \begin{bmatrix} 0 & 0 & 0 & 0 & d_{15} & 0 \\ 0 & 0 & 0 & d_{15} & 0 & 0 \\ d_{31} & d_{31} & d_{33} & 0 & 0 & 0 \end{bmatrix} \tag{2.13}$$

Due to the fact that the components of the matrix **d** are reduced to three non zero elements d_{33}, d_{31} and d_{15}, the electromechanical coupling in the piezoelectric ceramics is achieved through three principal modes of vibrations. These modes are the longitudinal mode (d_{33}), the transversal mode (d_{31}) and finally the shear mode (d_{15}).

- **Longitudinal mode (33)**: in the longitudinal effect the deformations take place parallel to the electric axis as shown in figure 2.2

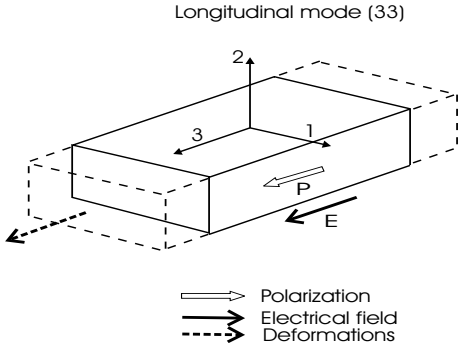

Figure 2.2: The longitudinal mode of vibration

- **Transversal mode (31)**: in the transverse effect the deformations take place perpendicular to the electric axis as shown in figure 2.3

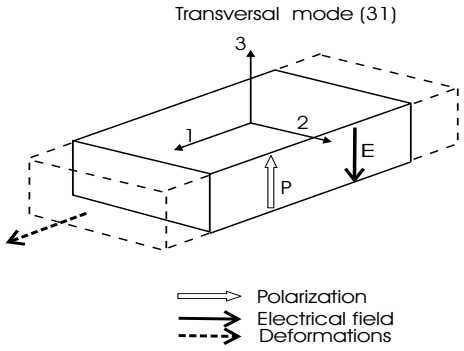

Figure 2.3: The transversal mode of vibration

- **Shear mode (15)**: in the shear effect the deformations take place around the axis perpendicular to the plan containing the electrical field vector and the polarization as shown in figure 2.4

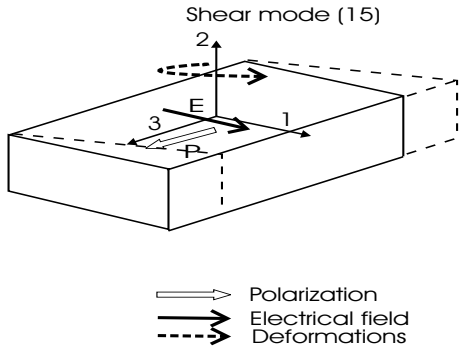

Figure 2.4: The shear mode of vibration

2.2.3 Fundamental relations for various independent variable sets

The following table 2.1 presents different piezoelectric relation forms related to independent variable types under the adiabatic and isotherm assumptions (Ikeda (1996)).

Independent Variable	Type	Piezo-electric relation	Form
S,D	Extensive	$\begin{cases} \mathbf{T} = \mathbf{c}^D\mathbf{S} - \mathbf{h}^t\mathbf{D} \\ \mathbf{E} = -\mathbf{h}\mathbf{S} + \beta^S\mathbf{D} \end{cases}$	h-form
T,E	Intensive	$\begin{cases} \mathbf{S} = \mathbf{s}^E T + \mathbf{d}^t\mathbf{E} \\ \mathbf{D} = \mathbf{d}T + \varepsilon^T\mathbf{E} \end{cases}$	d-form
T,D	Mixed	$\begin{cases} \mathbf{S} = \mathbf{s}^D\mathbf{T} + \mathbf{g}^t\mathbf{D} \\ \mathbf{E} = -\mathbf{g}\mathbf{T} + \beta^T\mathbf{D} \end{cases}$	g-form
S,E	Mixed	$\begin{cases} \mathbf{T} = \mathbf{c}^E\mathbf{S} - \mathbf{e}^t\mathbf{E} \\ \mathbf{D} = \mathbf{e}\mathbf{S} + \varepsilon^S\mathbf{E} \end{cases}$	e-form

Table 2.1: Different piezoelectric relation-types in matrix notation

2.2.4 Electromechanical coupling factor

The coupling factor is the parameter that guarantees the effective energy conversion in a linear interaction system. For the piezoelectric transducers this factor is defined for the respective mode of vibration at its static limit when $\omega \longrightarrow 0$. There are different ways of defining this coupling factor and in most cases this coefficient K is measured in percentages, however, it is more meaningful to deal with its square K^2 which corresponds to the energy ratio.

The following definition is provided by (Mason (1964))

$$\Bbbk^2 = \frac{\text{Stored electrical energy}}{\text{Supplied electrical energy}} \text{ or } \Bbbk^2 = \frac{\text{Stored mechanical energy}}{\text{Supplied mechanical energy}}$$

For the electromechanical interaction system this square factor is further defined by

$$\Bbbk^2 = \frac{U_{int}^2}{U_{elas}U_{elec}} \tag{2.14}$$

where U_{elas} , U_{elec} and $2U_{int}$ denote respectively the increments of elastic, electric and interaction energies, and where the total increment energy of the interaction system is given by $U = U_{elec} + 2U_{int} + U_{elas}$.

For the intensive type of the fundamental piezoelectric relation, the coupling factor, see (Ikeda (1996)), is defined by

$$\Bbbk^2 = \frac{\text{Coefficients square of the interaction term}}{\text{Coefficients product of the diagonal terms}} \tag{2.15}$$

However this simple method does not apply to the extensive type of the fundamental piezoelectric relation and therefore care should be taken in choosing the relevant fundamental relation.

For the piezoelectric transducer represented by a four terminal expression such that

$$\begin{cases} I = \varrho_{11}(\omega)V + \varrho_{12}(\omega)F \\ \dot{u} = \varrho_{21}(\omega)V + \varrho_{22}(\omega)F \end{cases} \tag{2.16}$$

where $\varrho_{12} = \varrho_{21}$, ω is the angular excitation frequency and $I, V, \dot{u}, F$ are the electric current, voltage, displacement velocity and force respectively, the coupling factor is given by the low frequency limit of

$$\Bbbk(\omega) = \frac{\varrho_{12}(\omega)}{\sqrt{\varrho_{11}(\omega)\varrho_{22}(\omega)}} \tag{2.17}$$

such that

$$\Bbbk = \lim_{\omega \longrightarrow 0} \Bbbk(\omega). \tag{2.18}$$

A more general definition of the square coupling factor is defined as the ratio between the dissipated energy W_d within the interaction system and the applied energy W_a to the system

$$\Bbbk^2 = \frac{W_d}{W_a} \tag{2.19}$$

Chapter 3

Experimental Approach

This chapter presents the Shinsei ultrasonic motor USR60 used as a case study in this thesis. Thereafter the results of the experimental investigation conducted on this motor when operating under various working condition are reported.

3.1 The objectives

The Rotary Piezo Electrical Motor (RPEM) investigated in this project is the Shinsei traveling wave motor type USR60. The objectives of the experimental investigation are, first to establish the physical understanding of the behavior of the motor when operating under various working conditions. The emphasis is put on the nonlinearities and various operating characteristics of the motor. Second the identification of the parameters and their respective ranges which are necessary for the modeling task.

3.2 The ultrasonic motor

The traveling wave piezoelectric motor considered in this thesis consists of two parts, the stator and the rotor. They are cylindrically shaped that mate together along their faces as shown in figure 3.1. The stator has seventy-two teeth cut into it in a circular pattern on one face on which the rotor rest upon. One thin cylindrical piezoceramic disk is bonded to the opposite face of the stator. Entirely electroded on one side with silver material and electroded on the opposite side in a pie-shaped pattern with eighteen slices as shown in figure 3.1. Each pie-shaped section is polarized in the opposite direction to the adjacent section except for the slice related to the ground and the slice used for sensing the feedback signal which remains neutral. By attaching wires to the electrodes, a voltage may

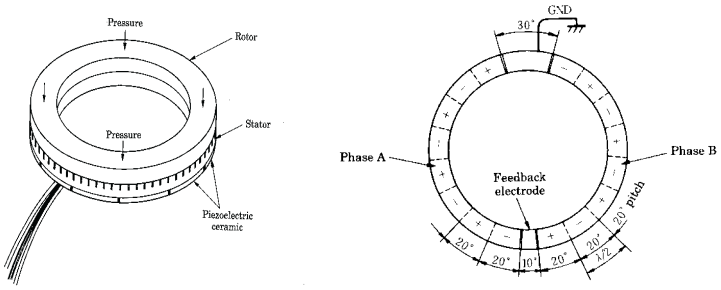

Figure 3.1: The naked assembled motor and the piezoceramic ring

be induced across the piezoceramic plate, causing it to flex due to the electromechanical coupling involved. The piezoceramic plate and its electrodes are thereafter bonded to the elastic stainless steel (substrate) plate with an adhesive material to form the stator. An exploded view of the parts that constitute the stator is shown in figure 3.2.

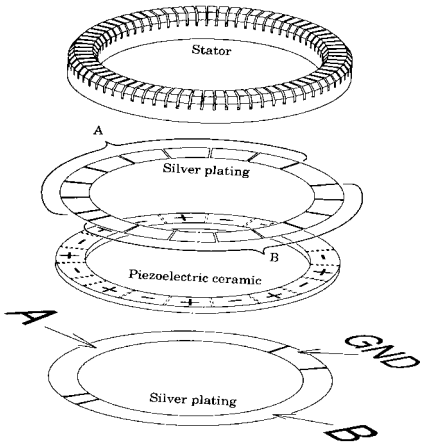

Figure 3.2: Exploded view of the complete stator

In the ultrasonic motor the oscillation energy generated at the surface of the stator must effectively be transmitted to the rotor to create unidirectional motion. The rotor has a structure consisting of a ring and a slider bonded to the ring as shown in figure 3.3. The rotor is placed upon the teeth of the stator and has a central shaft which goes through a hole in the stator which has a small bearing placed inside, see figure 3.5.

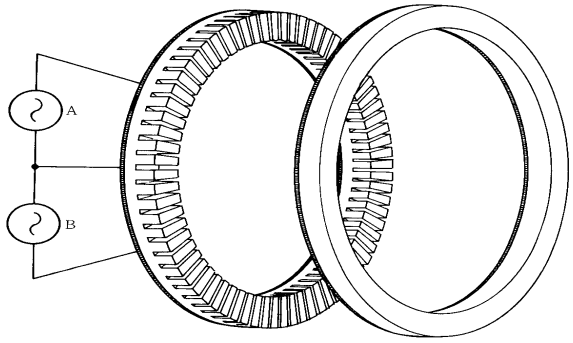

Figure 3.3: An exploded view of the annular stator and the annular rotor

With nine sectors in the stator, nine circumferential waves are generated. This waveform is a so called standing wave. Sector *A* is positionally shifted three quarters of wavelength out of to sector *B* as shown in figure 3.1. When two high frequency voltages 90^o out phase temporally are applied to sector *A* and *B* separately and simultaneously, standing waves generated by these two voltages are interfered mutually and results in a traveling wave at the surface of the stator as shown figure 3.4 which can be viewed as a section of the ring type rotary motor.

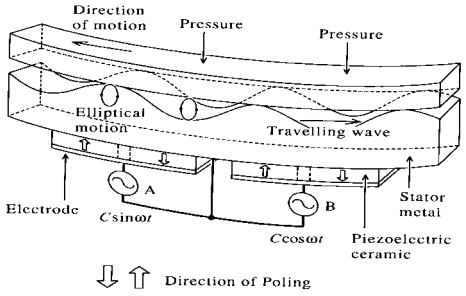

Figure 3.4: The operating principle of the traveling wave motor

The propagation of the acoustic traveling wave in the stator body makes the individual particles of the stator move in an elliptical fashion. Consequently, the rotor placed on the top of the vibrating stator would be rotated in a direction retrograde to the direction of the traveling wave as shown in figure 3.4.

The specification of the traveling wave piezoelectric motor USR60 reported in the manufacturer's user's manual (Shinsei Co.Ltd. USR60) are given in table 3.1.

Driving frequency	40 kHz
Rated voltage	100 Vrms
Rated Torque	0.32 N.m
Rated output	3 W
Rated speed	90 rpm
Rated current	53 mA X 2phase
Starting torque	3 Kg.cm
Holding torque	3.2 Kg.cm
Operating temperature	-10 ^oC to +50 ^oC
Weight	240 g

Table 3.1: Specification of the USR60

For the purpose of getting some knowledge of the complete hardware that constitutes the Shinsei motor and how it is assembled, an exploded view of the traveling wave motor is shown in figure 3.5.

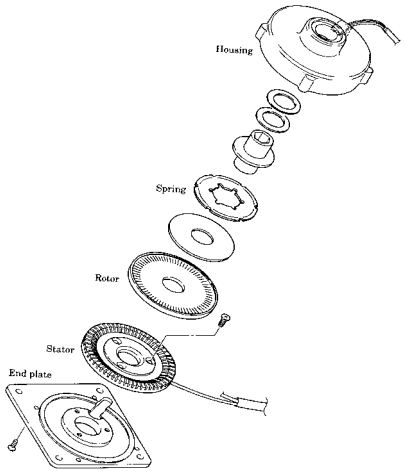

Figure 3.5: The exploded view of the complete motor

3.3 The experimental characteristics

The experimental investigation of the behavior of the motor is carried out by using the test bench presented in appendix A. The influence of the excitation and load parameters on the behavior of the motor is explored within the range of their limits. During the whole process of investigation these parameters have been kept at values not exceeding their nominal values, which are reported in the manufacturer's user's manual (Shinsei Co.Ltd. USR60).

3.3.1 Outline of the experimental investigation methodology

As in the case of the traditional electromagnetic motors, the experimental investigation, which will highlight the behavior of the piezoelectric motor considered in this thesis, consists of the establishment of the operating characteristics of the motor under various working conditions. However, the main objective of this thesis is the derivation of a simplified model for predicting the performance characteristics of the motor. This model is intended to fulfill the the needs of the control community in order to investigate a variety of control methods when applied to the motor in a simulated environment. Consequently, the interesting operating characteristics of the motor are those that are closely related to the performance of the motor in terms of speed prediction. The following items give an overview of the experiments to be carried out on the motor and their relevance for achieving the fixed objective.

- The traveling wave motor is a two phase symmetrical system powered by a two phase power supply. Therefore it is important to investigate the influence of the amplitude, frequency and phase of the power supply on the performance characteristics of the motor. Consequently, the following characteristics are of interest
  - The influence of the temporal phase shift on the rotary speed of the PEM at different excitation frequencies.
  - The influence of the excitation frequency and the amplitude voltage of the power supply on the rotary speed under nominal conditions.
  - The speed-torque characteristic of the motor under nominal conditions of operation, when working in the neighborhood of the fundamental resonance frequency

- The feedback electrode of the piezoelectric motor provides valuable information about the traveling wave characteristics within the stator due to the piezoelectric direct effect. Consequently, the following characteristics are of interest
  - The amplitude of the feedback signal as a function of the excitation frequency under various load torques

  - The speed of the motor as a function of the amplitude of the feedback signal at various normal forcings
  - The speed of the motor as a function of the amplitude of the feedback signal at various load torques

- The thermomechanical interaction within the PEM cannot be ignored due to the fast and huge heating process that takes place during the operation of the motor. Consequently, the influence of the temperature changes on the motor is investigated by monitoring the shift of the resonance frequency of the feedback signal versus the temperature under nominal conditions of operation.

- The electromechanical behavior of the motor can be obtained in terms of admittance measurements over a suitable span of frequencies. The objective is to highlight the behavior of the free stator by providing its electrical admittance over a large span of frequencies and thereby make some comparisons with other approaches which predict the behavior of the transducer by applying the basic laws of physics.

- The piezoelectric motor exhibits a strong nonlinear behavior around the resonance frequency. Consequently, the admittance measurement of the motor should be carried out in sweep up and sweep down frequency condition around the fundamental resonance in order to highlight this phenomenon.

- The admittance measurement of the motor is a constant voltage method, which means that the voltage must be maintained at its constant value during the admittance measurement. In contrast to the free stator, it is expected that the admittance of the forced stator is dependent on the external conditions. Consequently, the following characteristics are of interest
  - The influence of the amplitude voltage of the power supply on the admittance of the loaded motor
  - The influence of the load torque variation on the admittance of the loaded motor

It must be emphasized that when conducting the experiments on the free stator, lower voltages (≤ 50 Vpp) are used in order to avoid the possible damages to the piezoceramic of the stator.

3.3.2 Speed-phase characteristics at various frequencies

The traveling wave motor USR60 has a two phase construction where one electrode pattern provides the cosine spatial mode and the other pattern provides its orthogonal sine spatial mode. By driving these two modes out of phase temporally, a traveling wave is produced. Figure 3.6 shows the influence of the temporal phase shift on the rotary speed of the PEM at different excitation frequencies.

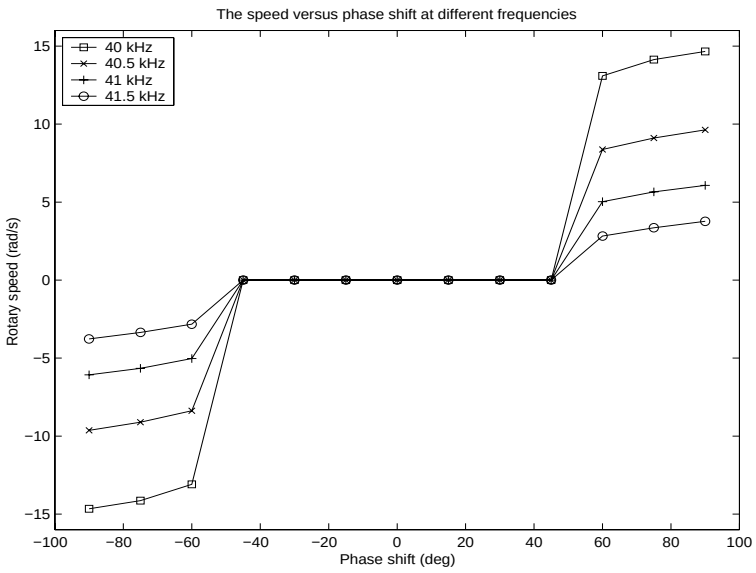

Figure 3.6: The rotary speed versus the phase shift at various frequencies

The results are obtained for the following nominal values of the remaining parameters

Amplitude voltage (Vrms)	100
Normal forcing (N)	160
Load torque (Nm)	0

From figure 3.6 it is clear that the highest speed is achieved for a temporal phase shift of $+90^o$ or -90^o, which indicates that the two phases fulfill the symmetry requirements for a perfect traveling wave generation. Furthermore the speed-phase characteristics indicate that the phase shift has the influence on the motor speed only in intervals $[+90^o - 30^o, +90^o]$ and $[-90^o, -90^o + 30^o]$, and that the characteristics in these intervals are almost straight lines, whereas in the interval $[-90^o + 30^o, +90^o - 30^o]$ the PEM is out of work. Moreover, it can be noticed, from figure 3.6, that the speed is slightly sensitive to the variation of the phase shift, in the working intervals, which suggests that the phase shift alone is not a convenient parameter for controlling the PEM.

3.3.3 Speed-frequency characteristics at various voltage amplitudes

The excitation of the PEM is normally carried out by a two phase power supply and due to the symmetrical nature of its design a common voltage amplitude is used in order to achieve high performance. Furthermore, the PEM is a piezo-electromechanical system which has several resonance frequencies, and the performance of the PEM depends highly on the excitation frequency of the power supply, and therefore there is a need to investigate the behavior and the performance of the motor around the fundamental resonance frequency. The influence of the excitation frequency and the amplitude voltage of the power supply on the rotary speed is investigated under nominal conditions.

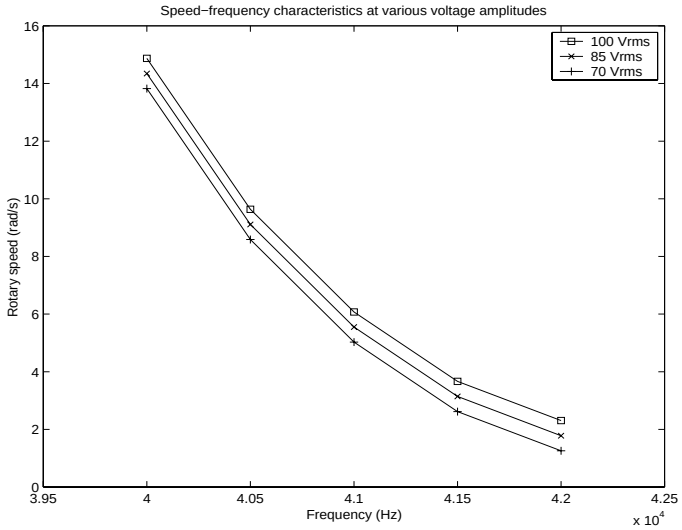

Figure 3.7: The rotary speed versus the excitation frequency at various voltage amplitudes

The results are obtained for the following nominal values of the remaining parameters

Phase shift (deg)	90^o
Normal forcing (N)	160
Load torque (Nm)	0

From figure 3.7 it can be noticed that the speed is slightly sensitive to the voltage amplitude variations, but highly sensitive to the excitation frequency in the interval $[40\ kHz\ ,\ 42\ kHz]$. This suggests that amplitude voltage alone is not a convenient parameter for controlling the PEM, whereas frequency alone can be a suitable parameter for controlling the PEM.

3.3.4 Speed-torque characteristics at various frequencies

The speed-torque characteristic is an important characteristic that measures the performance of any motor. The investigation of the speed drop versus load torque is carried out in the neighborhood of the fundamental resonance frequency where the efficiency of the PEM is the highest possible according to data sheet of the motor in the user's manual provided by the manufacturer.

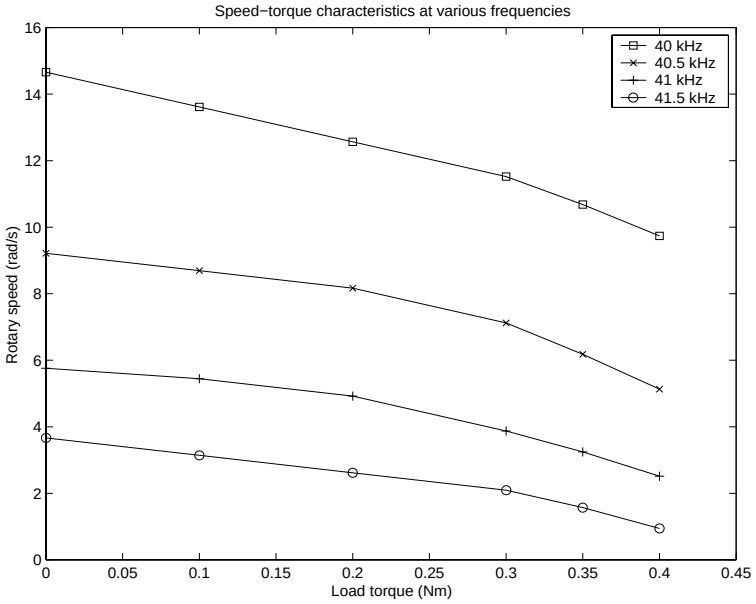

Figure 3.8: The rotary speed versus the load torque at various frequencies

The results are obtained for the following nominal values of the remaining parameters

Phase shift (deg)	90^o
Amplitude voltage (Vrms)	100
Normal forcing (N)	160

From figure 3.8 it can be noticed that the speed-torque characteristic is almost straight line for each excitation frequency and that these characteristics are almost parallel for the excitation frequencies in the interval $[40\ kHz\ ,\ 41.5\ kHz]$ and load torques not exceeding $0.3\ Nm$, which suggests that the effect of load torque can be accounted for by a constant speed drop factor proportional to the load torque for all operating frequencies in the range of $[40\ kHz\ ,\ 41.5\ kHz]$.

3.3.5 Feedback-frequency characteristics at various load torques

The traveling wave in the stator of USR60 is created by the superposition of two standing waves provided by each excited phase of the stator according to the piezoelectric converse effect (i.e. $voltage \rightarrow deformation$). The neutral part (i.e. feedback electrode) of the piezoceramic lying between the two excited phases provides a voltage signal according to the piezoelectric direct effect (i.e. $deformation \rightarrow voltage$). By sensing this neutral part valuable information about the traveling wave characteristics can be obtained. Consequently, an intuitive understanding of the behavior of the motor is possible.

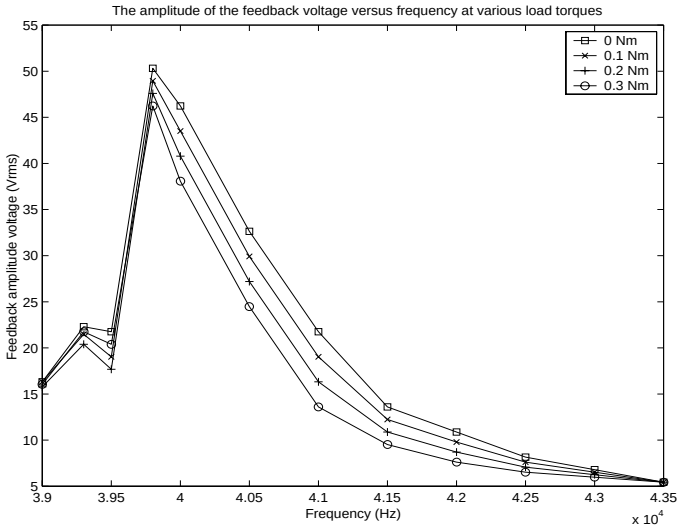

Figure 3.9: The amplitude of the feedback signal versus the excitation frequency at various load torques

The results are obtained for the following nominal values of the remaining parameters

Phase shift (deg)	90^o
Amplitude voltage (Vrms)	100
Normal forcing (N)	160

From figure 3.9 it can be noticed that the feedback-frequency characteristics exhibit a resonance behavior around the fundamental frequency $(40kHz)$ of the PEM, and that for frequencies in the interval $[40\ kHz\ ,\ 41.5\ kHz]$ these characteristics are almost linear for each load torque in the interval $[0\ Nm\ ,\ 0.3\ Nm]$, which suggests a constant drop in the amplitude voltage of the feedback signal proportional to the load torque for each frequency in this interval.

3.3.6 Speed-feedback characteristics at various normal forcings

The RPEM is a solid state motor driven by the dynamical friction at the interface contact between the stator and the rotor. The performance of the motor is a function of the nature of the contact layer and the intensity of pressure that maintains this contact under various working conditions. The investigation of the influence of the normal pressure on the performance of the PEM is carried out by monitoring the feedback signal and the rotary speed of the motor under various normal forcings

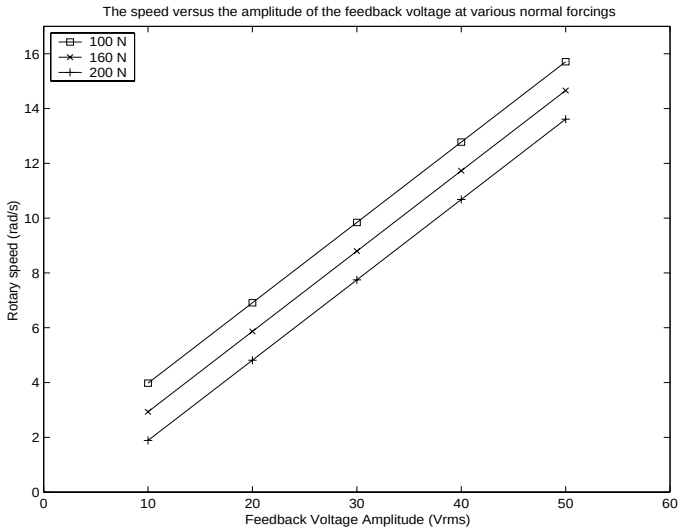

Figure 3.10: The rotary speed versus the amplitude of the feedback signal at various normal forcings

The results are obtained for the following nominal values of the remaining parameters

Phase shift (deg)	90^o
Amplitude voltage (Vrms)	≤ 100
Load torque (Nm)	0

From figure 3.10 it can be noticed that the speed-feedback characteristics are almost linear for each normal forcing. Furthermore, figure 3.10 suggests that there is a constant speed drop proportional to the variation of the normal forcing at each amplitude of the feedback voltage. However, it must be noticed that the resonance frequency of the feedback voltage varies during the changes of the normal forcing which suggests that the normal forcing must be maintained at its nominal value during the whole process of investigation.

3.3.7 Speed-feedback characteristics at various load torques

The investigation of the influence of the torque on the performance of the PEM can be carried out by monitoring the feedback signal and the rotary speed of the motor under various load torques

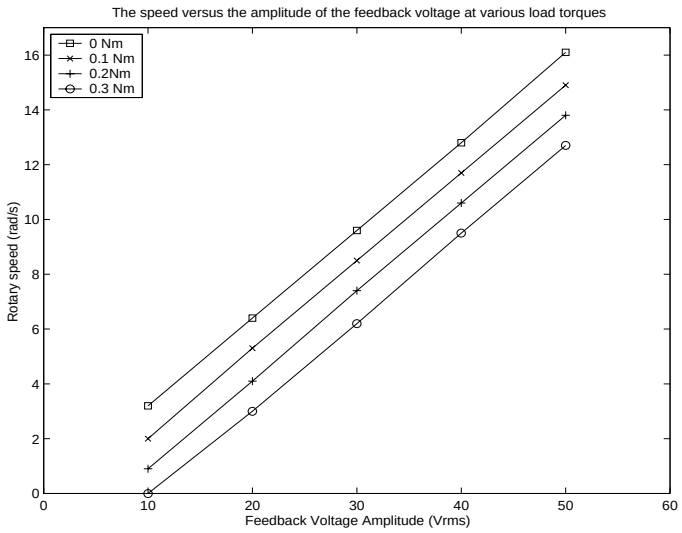

Figure 3.11: The rotary speed versus the amplitude of the feedback signal at various load torques

The results are obtained for the following nominal values of the remaining parameters

Excitation frequency (kHz)	$40\ kHz$
Phase shift (deg)	90^o
Amplitude voltage (Vrms)	≤ 100
Normal forcing (N)	160

From figure 3.11 it can be noticed that the speed-feedback characteristics are almost linear for each load torque. Moreover, figure 3.11 suggests that there is a constant speed drop proportional to the variation of the load torque at each amplitude of the feedback voltage. However, it must be noticed that, unfortunately, the frequency of the feedback voltage varies during the changes of the load torque, which suggests that a tracking facility of the resonance frequency of the feedback signal must be integrated in the control system design of the PEM.

3.3.8 The resonance frequency of the feedback signal at various temperatures of the motor

The PEM is a piezo-electromechanical system subject to at least three kinds of interaction phenomena. The interaction process can be electromechanical, thermoelectrical and thermomechanical. For the PEM under investigation it is assumed that the thermoelectrical interaction is negligible, but the thermomechanical interaction cannot be ignored due to the fast and huge heating process that takes place during the operation of the motor. The investigation of the influence of temperature on the performance of the motor is carried out by monitoring the shift of the resonance frequency of the feedback signal versus the temperature changes of the PEM during operation at its nominal values.

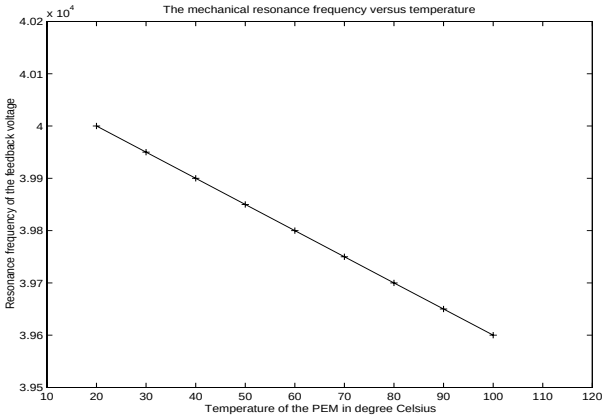

Figure 3.12: The resonance frequency of the feedback signal versus temperature

The results are obtained for the following nominal values of the parameters

Excitation frequency (kHz)	40 kHz
Phase shift (deg)	90^o
Amplitude voltage (Vrms)	100
Normal forcing (N)	160
Load torque (Nm)	0

From figure 3.12 it can be noticed that the frequency-temperature characteristic is almost linear, which suggests that the resonance frequency of the feedback signal shifts towards lower frequencies. Thus, it can be assumed that this shift is proportional to the temperature changes during the operation of the motor. This result is of crucial importance when designing the control system of the PEM in order to achieve the performance objectives despite the changes in temperature.

3.3.9 The electrical admittance characteristic of the free stator

The electromechanical behavior of any transducer can be obtained in terms of admittance measurements over a suitable span of frequencies. The span of frequencies that is of interest is usually around the fundamental resonance frequency of the transducer. However, it is important to explore a large span of frequencies in order to get a better understanding of the behavior of the transducer, and thereby make some comparisons with other approaches predicting the behavior of the transducer by applying the basic laws of physics.

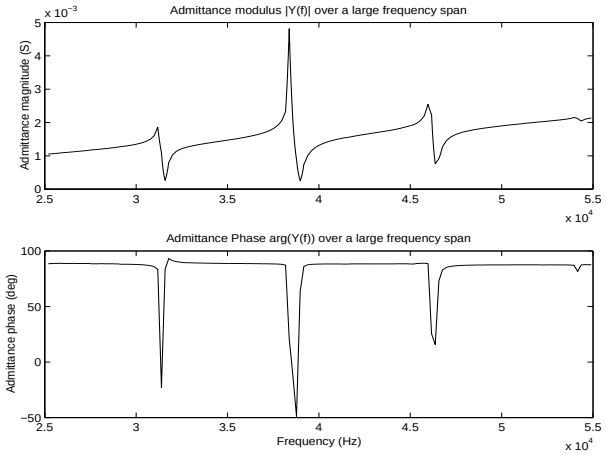

Figure 3.13: The admittance of one phase of the RPEM over a large span of frequencies

The results of the admittance measurement of the PEM shown in figure 3.13 are obtained for a free stator supplied by a constant voltage ($50\ Vpp$), figure 3.13 shows Bode magnitude and phase plots over a frequency span of $[25\ kHz\ ,\ 55\ kHz]$. It can be noticed that over the explored span of frequencies the stator exhibits three resonant frequencies, where the fundamental frequency lies in the middle due to the sharpness of the amplitude of the admittance at this point.

According to the elasticity theory of vibration applied to a free annular vibrating plate see appendix B, the resonant frequency f_{r_n} of the plate for the n 'th mode is given by (B.12) and reads

$$\begin{cases} f_{r_n} = \frac{\lambda_n^2}{2\pi}\sqrt{\frac{\mathcal{G}}{\rho \mathfrak{h}}} \\ \text{where } \lambda_n = \frac{n}{R_o} \text{ and } \mathcal{G} = \frac{J\mathfrak{h}^3}{12} \end{cases}$$

where the poisson ratio is neglected. By using the geometrical data of the investigated stator, which are given in table 3.2, the theoretical prediction of the resonance frequencies at different modes of vibration are reported in table 3.3.

h thickness of the bronze without teeth (m)	$2e^{-3}$
ρ bronze density (kg m^{-3})	8780
J young modulus of the bronze (N m^{-2})	$1.12e^{11}$
R_o middle radius of the annular stator (m)	$26.25e^{-3}$
n the mode's rank	8, 9, 10

Table 3.2: The geometrical data of the stator

mode n	measured resonance freq (Hz)	theoretical resonance freq (Hz)
8	31200	30480
9	38400	38580
10	46300	47690

Table 3.3: The resonance frequencies for different modes of vibration: Comparison between the measurements and the theoretical predictions

From table 3.3 it can be noticed that there is almost an agreement between theoretical and practical results. From figure 3.13 it can be noticed that the mode 9 exhibits the sharpest magnitude around its resonance. The other two modes (8 and 10) exhibit a damped magnitude compared to the fundamental mode 9 and their resonance frequencies are not as well predicted by the theory as in the fundamental case. It must be emphasized that the motor can operate in the neighborhood of these three resonance frequencies but the best performance of the motor is achieved around the fundamental frequency, due to the special design of the stator made for operating in this mode. These results suggest that there is a need to identify the model of the motor only around the fundamental resonance frequency.

3.3.10 The nonlinearities of the motor

The piezoelectric materials in general exhibit at least three kinds of nonlinearities which are electrical hysteresis, mechanical hysteresis and thermal hysteresis. The overall hysteresis of any piezoelectrical transducer is difficult to define and therefore impossible to model, but the admittance measurement of a piezoelectrical transducer can give an idea of how this hysteresis can result in a nonlinear admittance of the system.

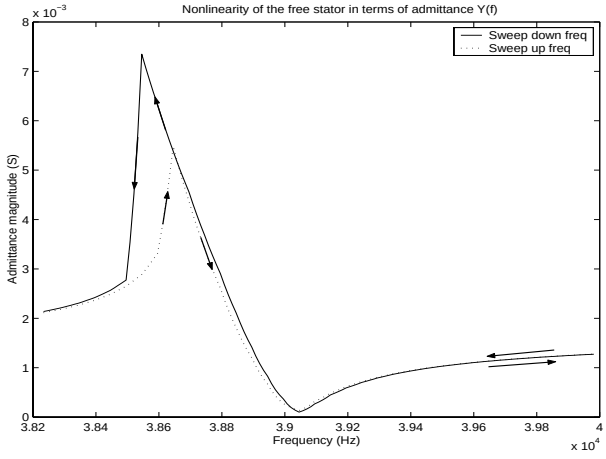

Figure 3.14: Nonlinearity of the free stator around the fundamental frequency

The results of figure 3.14 are obtained for a free stator supplied by a constant voltage $(40\ Vpp)$. Figure 3.14 shows two admittance measurements of the same stator under the same operating conditions except for the frequency span sweep condition. It can be noticed that during the sweep up and sweep down frequency mode the admittance exhibits a nonlinear (hysteresis) behavior around the resonance frequency, which suggests that care must be taken to avoid the nonlinear zone from the frequency range when frequency mode is selected for controlling the PEM.

3.3.11 The electrical admittance of the loaded motor at various amplitudes of the voltage supply

The admittance measurement of any electromechanical system is a constant voltage method, which means that the voltage must be maintained at its constant value during the whole process of admittance measurement. The foregoing results have been carried out for a free stator which showed that the stator exhibits resonance frequencies at locations predicted by the laws of physics applied to an unforced annular vibrating plate. The stator of the complete motor (mainly composed by a rotor pressed against the stator) should no longer obey the same laws with regard to resonance frequencies as the free stator unless the external axial force to the stator (i.e. normal forcing) is balanced by an internal forcing provided by the excited stator itself. The main source of generating force (strain-stress) within the stator is the applied voltage, therefore it is necessary to investigate the effect of varying voltage on the frequency response of the complete motor.

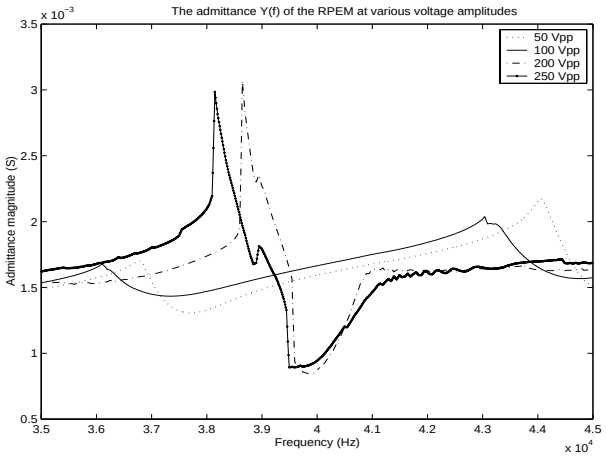

Figure 3.15: The admittance of the RPEM at various voltage amplitudes of the power supply

The results are obtained for the following nominal values of the remaining parameters

Phase shift (deg)	90^o
Normal forcing (N)	160
Load torque (Nm)	0

From figure 3.15 it can be noticed that for lower voltages the admittance exhibits resonance frequencies which are both damped in magnitude and located far beyond those of the free stator. This behavior can be explained by the imbalance existing between the applied normal forcing and the generated piezoelectric forcing. For higher voltages we can notice that the normal forcing is balanced by the piezoelectric forcing which results in a frequency response similar to that of the free stator with resonance frequencies located in the neighborhood of those predicted by the laws of physics applied to the free vibrating annular plate. From figure 3.15 it can be concluded that the effect of increasing the voltage results in a resonance frequency shift towards lower frequencies, consequently the increase in normal forcing results in a resonance frequency shift towards higher frequencies. Therefore, it is important to notice that for controlling the PEM, the voltage and the normal forcing must be maintained at their nominal values thereby avoiding this complexity. These results suggest that, for stability reasons, the model identification should be carried out from the admittance measurement of the free stator around the resonance frequency.

3.3.12 The electrical admittance of the loaded motor at various load torques

The previous results showed that the admittance of the RPEM is dependent on voltage and normal forcing, but they can be fixed at their nominal values, which eases the identification of the model and simplifies the control strategies of the motor. The load torque varies by nature, and the motor must be able to achieve the performance objectives in terms of speed and position for any load torque in the range of its capability. Therefore, the influence of the load torque on the behavior of the motor should be examined in terms of admittance

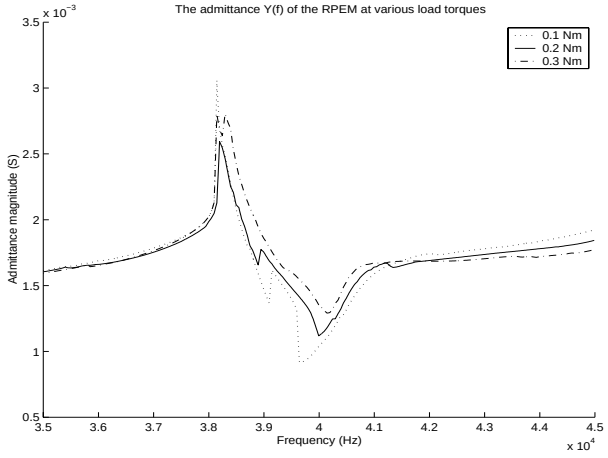

Figure 3.16: The admittance of the RPEM at various load torques

The results are obtained for the following nominal values of the remaining parameters

Phase shift (deg)	90^o
Amplitude voltage (Vrms)	100
Normal forcing (N)	160

From figure 3.16 it can clearly be seen that the effect of increasing the load torque results in the antiresonance frequency shift towards higher frequencies together with a certain damping of the admittance magnitude around this frequency. This suggests that the resonance frequency is subjected to the same law/phenomenon, which is partly hidden by the nonlinear behavior of the PEM around this frequency. It is important to notice that both the shift and the damping are roughly proportional to the torque changes. This result suggests that for control purposes the effect of the load torque can be accounted for by a tracking capability of the resonance frequency together with a correcting factor for the amplitude drop of the feedback signal.

Chapter 4

Equivalent Circuit Model

In this chapter, the background of the equivalent circuit method is first exposed, second the equivalent circuit model derivation is performed on the basis of the experimental results combined with the electrical network method, and finally the validation of the model is carried out by comparing the simulation results with the experimental results.

4.1 Background of the equivalent circuit method

Piezoelectricity is regarded by scientists as a linear interaction between electrical and mechanical systems. Therefore most of the work in this field has been carried out in order to establish linear relationships between different parameters that describe piezoelectric phenomena. The theoretical approach provides linear equations which describe the electromechanical behavior in any piezoelectric transducer by applying the basic laws of physics. The empirical approach based on the measurement of the electromechanical constants in terms of impedance or admittance and equivalent circuit information constitutes a powerful alternative to the theoretical approach for solving practical problems and thereby avoiding the complexity and the large discrepancy between linear theory and the real nonlinear physical piezoelectric transducer.

4.1.1 The ring type transducer

The electromechanical constants of any piezoelectric material are determined by the admittance measurements of a transducer with varying frequency. For practical purposes it is sufficient to observe the admittance around its fundamental resonance frequency.

The admittance Y of any piezoelectric transducer is given by the sum of the damped Y_d and the motional Y_m admittance

$$Y = Y_d + Y_m \tag{4.1}$$

Where

$$\begin{cases} Y_d = 1/R_d + j\omega C_d \\ Y_m = 1/[R + j(\omega L - 1/\omega C)]. \end{cases} \tag{4.2}$$

Figures 4.1 and 4.2 show the admittance locus and the frequency response respectively for a transducer with a high mechanical quality factor Q, (Ikeda (1996)).

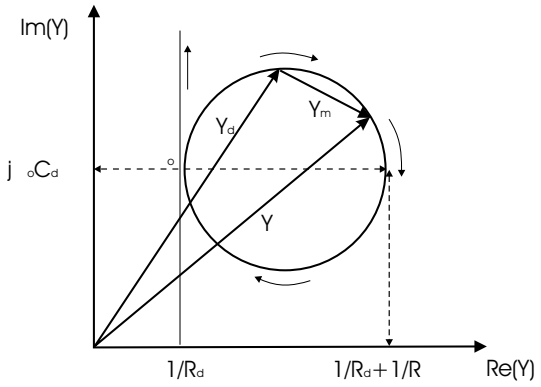

Figure 4.1: Admittance locus (Nyquist diagram) of a piezoelectric transducer

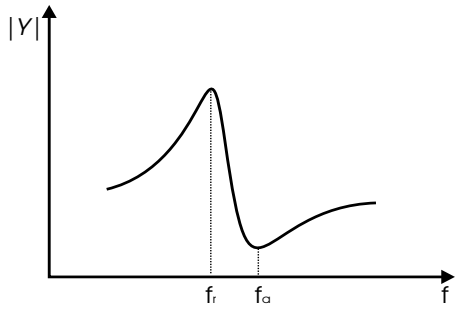

Figure 4.2: Frequency response (Bode magnitude diagram) of a piezoelectric transducer

4.1.1.1 Equivalent circuit modeling of a ring type stator

The stator of the rotary traveling wave motor is an annular plate composed of two different layers undergoing bending deformations. These two layers are the piezoceramic ring and the elastic substrate which are bonded together. To simplify the model, the curvature of the undeformed ring is disregarded and the stator is therefore regarded as a straight beam with infinite length as shown in figure 4.3

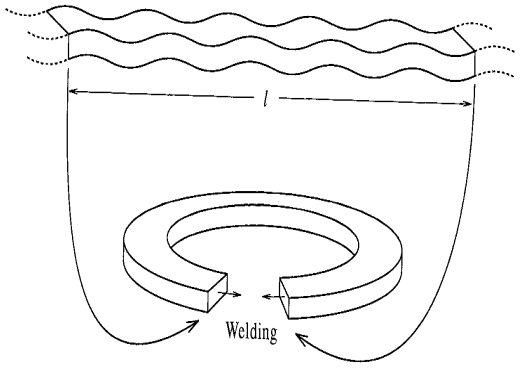

Figure 4.3: The stator of the traveling wave motor regarded as a straight beam

Mason's equivalent circuit model for a T-effect bar transducer

Consider a beam of section $\mathcal{A} = be$ and length dx, lying between x and $x+dx$, subjected to a bending deformation of a transverse type (T-effect) driven by an alternating voltage, as shown in figure 4.4

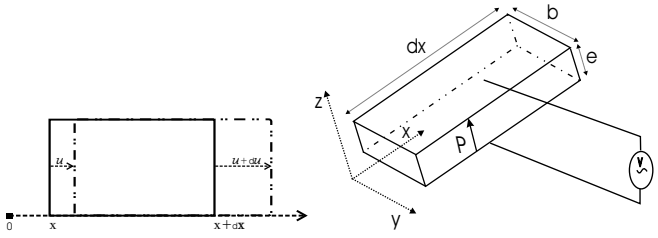

Figure 4.4: Elementary section of a piezoelectric beam subject to bending deformation of transverse type

The relevant fundamental relation is of the (T,E)-type given by

$$\begin{cases} S_1 = s_{11}^E T_1 + d_{31} E_3 \\ D_3 = d_{31} T_1 + \varepsilon_{33}^T E_3 \end{cases} \tag{4.3}$$

a rearranged relation of the (S,E)-type is used

$$\begin{cases} T_1 = \frac{1}{s_{11}^E} S_1 - \frac{d_{31}}{s_{11}^E} E_3 \\ D_3 = \frac{d_{31}}{s_{11}^E} S_1 + \varepsilon_{33}^S E_3 \end{cases} \tag{4.4}$$

The first fundamental law of dynamics applied to the forced vibrating beam reads

$$\vec{F}_{ext} = m \vec{\mathtt{a}} \tag{4.5}$$

where $\vec{F}_{ext}$ denotes the external forces acting on the body, m is the vibrating mass of the beam and finally $\vec{\mathtt{a}}$ is the acceleration of the vibrating edge, which is given by

$$\vec{\mathtt{a}} = \frac{\partial^2 \vec{u}}{\partial t^2} \tag{4.6}$$

where $\vec{u}$ is the displacement vector of the vibrating edge. By projecting this vector equation along the x direction and rearranging the terms the following is obtained

$$\frac{\partial F_{ext}}{\partial x} = \rho \mathcal{A} \frac{\partial^2 u}{\partial t^2} \tag{4.7}$$

where ρ is the mass density of the beam and $\rho \mathcal{A} dx$ is the mass of the elementary section of the piezoelectric beam subjected to the external force ∂F_{ext} given by

$$\partial F_{ext} = F_1(x + dx) - F_1(x) \tag{4.8}$$

The stress T_1 and the strain S_1 terms at the edges of the piezoceramic beam are given by

$$T_1 = \frac{F_{ext}}{\mathcal{A}} \tag{4.9}$$

$$S_1 = \frac{\partial u}{\partial x} \tag{4.10}$$

By substituting (4.9) and (4.10) in the first equation of the (S,E)-type relation (4.4) and rearranging the terms the following is obtained

$$F_{ext} = \frac{\mathcal{A}}{s_{11}^E} \frac{\partial u}{\partial x} - \frac{\mathcal{A} d_{31}}{s_{11}^E} E_3 \tag{4.11}$$

Furthermore, by substituting (4.11) in (4.7) and considering the electrical condition

$$\frac{\partial E_3}{\partial x} = 0 \tag{4.12}$$

i.e. E_3 is harmonic only in time, and thereafter rearranging the terms the following equation of motion is derived

$$\frac{\partial^2 u}{\partial x^2} = \rho s_{11}^E \frac{\partial^2 u}{\partial t^2} \tag{4.13}$$

where the phase velocity v_{ph}, the wave number k, the wave length λ and the angular frequency ω of the plane wave $u(x,t)$ in the beam propagating in x direction, solution of (4.13), are given by

$$v_{ph} = \frac{1}{\sqrt{\rho s_{11}^E}} \tag{4.14}$$

$$k = \frac{\omega}{v_{ph}} \tag{4.15}$$

$$\lambda = \frac{2\pi}{k} \tag{4.16}$$

For simplicity reasons only the non dissipative transducer case is considered (i.e. we assume that no losses take place). Thus in this ideal case, the the solution for the equation of motion (4.13) in complex notation reads

$$\underline{u}(x,t) = [\underline{p}\sin(kx) + \underline{q}\cos(kx)]e^{j\omega t} \tag{4.17}$$

where in complex notation the electric field reads $\underline{E}_3 = E_3 e^{j\omega t}$ and the coefficients $\underline{p}$ and $\underline{q}$ are given by

$$\underline{p} = [\frac{\dot{\underline{u}}\ (l,t)}{j\omega \sin(kl)} - \frac{\dot{\underline{u}}\ (0,t)}{j\omega \tan(kl)}]e^{-j\omega t} \tag{4.18}$$

$$\underline{q} = \frac{\dot{\underline{u}}\ (0,t)}{j\omega} e^{-j\omega t} \tag{4.19}$$

Furthermore, the stress $\underline{T}_1$, strain $\underline{S}_1$ and electrical field $\underline{E}_3$ for a piezoelectric beam of length l powered by a voltage $\underline{V}(t)$, see figure 4.5, are given in complex notation by

$$\underline{T}_1 = \frac{-\underline{F}_1}{\mathcal{A}} \tag{4.20}$$

$$\underline{S}_1 = \frac{\partial \underline{u}}{\partial x} \tag{4.21}$$

$$\underline{E}_3 = \frac{\underline{V}(t)}{e} \tag{4.22}$$

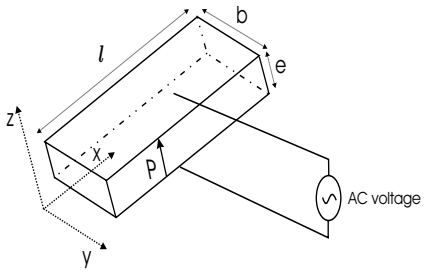

Figure 4.5: Piezoelectric straight beam of lenght l subject to bending deformation of transverse type powered by an AC voltage

By substituting (4.20), (4.21) and (4.22) in the (S,E)-type relation (4.4), the following equation

$$\underset{-}{T}_1 = \frac{1}{s_{11}^E}\underset{-}{S}_1 - \frac{d_{31}}{s_{11}^E}\underset{-}{E}_3 \tag{4.23}$$

leads, after rearranging the terms, to

$$\underset{-}{F}_1(x,t) = -\frac{k\mathcal{A}}{s_{11}^E}[\underset{-}{p}\cos kx - \underset{-}{q}\sin kx]e^{j\omega t} + \frac{d_{31}}{s_{11}^E}b\underset{-}{V}(t) \tag{4.24}$$

By using the equations (4.14) and (4.15) the following is obtained

$$\frac{k\mathcal{A}}{\omega s_{11}^E} = \rho\mathcal{A}v_{ph} \tag{4.25}$$

By substituting (4.18), (4.19) and (4.25) in the above equation (4.24), and rearranging the terms, the force produced at each point of the beam becomes

$$\underset{-}{F}_1(x,t) = \frac{\rho\mathcal{A}v_{ph}}{j}[(\sin kx + \frac{\cos kx}{\tan kl})\ \underset{-}{\dot{u}}\ (0,t) - \frac{\cos kx}{\sin kl}\ \underset{-}{\dot{u}}\ (l,t)] + \frac{d_{31}}{s_{11}^E}b\underset{-}{V}(t) \tag{4.26}$$

For each value of $x\epsilon\{0,l\}$ corresponding to the edges of the beam we get the following equations for the force produced at these edges

$$\underset{-}{F}_1(0,t) = \frac{\rho\mathcal{A}v_{ph}}{j}[\frac{1}{\tan kl}\ \underset{-}{\dot{u}}\ (0,t) - \frac{1}{\sin kl}\ \underset{-}{\dot{u}}\ (l,t)] + \frac{d_{31}}{s_{11}^E}b\underset{-}{V}(t) \tag{4.27}$$

$$\underset{-}{F}_1(l,t) = \frac{\rho\mathcal{A}v_{ph}}{j}[(\sin kl + \frac{\cos kl}{\tan kl})\ \underset{-}{\dot{u}}\ (0,t) - \frac{1}{\tan kl}\ \underset{-}{\dot{u}}\ (l,t)] + \frac{d_{31}}{s_{11}^E}b\underset{-}{V}(t) \tag{4.28}$$

where by observing that

$$\frac{\rho \mathcal{A} v_{ph}}{j}(\sin kl + \frac{\cos kl}{\tan kl}) = \frac{\rho \mathcal{A} v_{ph}}{j}\frac{1}{\sin kl} \tag{4.29}$$

$$\frac{\rho \mathcal{A} v_{ph}}{j \sin kl} + j\rho A v_{ph} \tan \frac{kl}{2} = \frac{\rho \mathcal{A} v_{ph}}{j}\frac{1}{\tan kl} \tag{4.30}$$

then (4.27) and (4.28) can be written in the following form

$$\begin{cases} \underline{F}_0(t) = (\underline{Z} + \underline{Z}_o)\underline{s}_o(t) - \underline{Z}\,\underline{s}_l(t) + \Pi \underline{V}(t) \\ \underline{F}_l(t) = \underline{Z}\,\underline{s}_o(t) - (\underline{Z} + \underline{Z}_o)\underline{s}_l(t) + \Pi \underline{V}(t) \end{cases} \tag{4.31}$$

where

$$\begin{cases} \underline{s}_o(t) = \dot{\underline{u}}(0,t) \text{ and } \underline{s}_l(t) = \dot{\underline{u}}(l,t) \\ \underline{F}_0(t) = \underline{F}_1(0,t) \text{ and } \underline{F}_l(t) = \underline{F}_1(l,t) \end{cases}$$

and where

$$\begin{cases} \underline{Z} = \frac{\rho \mathcal{A} v_{ph}}{j \sin kl} \\ \underline{Z}_o = j\rho \mathcal{A} v_{ph} \tan \frac{kl}{2} \\ \Pi = b\frac{d_{31}}{s_{11}^E} = \left[\frac{F}{V}\right]^u \end{cases} \tag{4.32}$$

$\underline{Z}$ and $\underline{Z}_o$ are elastic impedances depending only on the design and the mechanical parameters of the piezoelectric beam. Π is the electromechanical force factor of the piezoelectric beam produced under constant displacement ($u = constant$).

The electric current flowing into the piezoceramic powered by a voltage $\underline{V}(t)$ reads

$$\underline{I}(t) = \int_0^b \int_0^l j\omega \underline{D}_3 \, dxdy \tag{4.33}$$

By substituting (4.21) and (4.22) in the (S,E)-type relation (4.4), then the following equation

$$\underline{D}_3 = \frac{d_{31}}{s_{11}^E}\underline{S}_1 + \varepsilon_{33}^S \underline{E}_3 \tag{4.34}$$

writes

$$\underline{D}_3 = \frac{d_{31}}{s_{11}^E}\frac{\partial \underline{u}}{\partial x} + \varepsilon_{33}^S \frac{\underline{V}(t)}{e} \tag{4.35}$$

By inserting (4.35) in (4.33), and thereafter calculate the integral and rearrange the terms, then the following relation is obtained

$$\underline{I}(t) = \frac{d_{31}b}{s_{11}^{E}}(\underline{\dot{u}}\ (l,t) - \underline{\dot{u}}\ (0,t)) + j\omega\varepsilon_{33}^{S}\frac{bl}{e}\underline{V}(t) \tag{4.36}$$

which is further written by

$$\underline{I}(t) = -\underline{\Pi}\ \underline{s}_{o}(t) + \Pi\ \underline{s}_{l}(t) + j\omega C_d \underline{V}(t) \tag{4.37}$$

where

$$\begin{cases} C_d = \varepsilon_{33}^{S}\frac{bl}{e} \\ \varepsilon_{33}^{S} = \varepsilon_{33}^{T}(1-\mathbb{k}_{31}^{2}) \\ \mathbb{k}_{31} = \frac{d_{31}}{\sqrt{s_{11}^{E}\varepsilon_{33}^{T}}} \end{cases} \tag{4.38}$$

and where C_d is the clamped capacitance of the piezoceramic and $\mathbb{k}_{31}$ is the electromechanical coupling factor derived by using (2.15) when applied to the (T,E)-type relation (4.3).

From the above analysis and the derived equations (4.31) and (4.37) the electromechanical coupling in the piezoceramic beam is represented by the following relation

$$\begin{cases} \underline{I}(t) = -\underline{\Pi}\ \underline{s}_{o}(t) + \Pi\ \underline{s}_{l}(t) + j\omega C_d\ \underline{V}(t) \\ \underline{F}_{0}(t) = (\underline{Z} + \underline{Z}_o)\underline{s}_{o}(t) - \underline{Z}\ \underline{s}_{l}(t) + \Pi\underline{V}(t) \\ \underline{F}_{l}(t) = \underline{Z}\ \underline{s}_{o}(t) - (\underline{Z} + \underline{Z}_o)\ \underline{s}_{l}(t) + \Pi\underline{V}(t) \end{cases} \tag{4.39}$$

This system is further represented by Mason in the form of a six terminal equivalent circuit information as shown in figure 4.6.

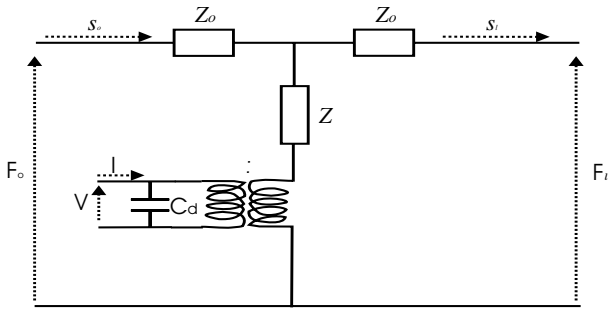

Figure 4.6: Mason's six input terminal ECM of the annular plate piezoelectric device

The ring type stator in T-effect mode

In the case of the piezoelectric ring, which constitutes the active part combined with a passive part of the stator in the ultrasonic motor USR60, the six terminal network is further reduced to a four terminal network due to the fact that the ends of the beam, shown in figure 4.3, are connected in a closed shape, thereby $\underline{F}_0(t) = \underline{F}_l(t) = \underline{F}(t)$ and the set of equation becomes

$$\begin{cases} \underline{I}(t) = -\Pi\, \underline{s}_o(t) + \Pi\, \underline{s}_l(t) + j\omega C_d\, \underline{V}(t) \\ \underline{F}(t) = (\underline{Z} + \underline{Z}_o)\, \underline{s}_o(t) - \underline{Z}\, \underline{s}_l(t) + \Pi \underline{V}(t) \\ \underline{F}(t) = \underline{Z}\, \underline{s}_o(t) - (\underline{Z} + \underline{Z}_o)\, \underline{s}_l(t) + \Pi \underline{V}(t) \end{cases} \tag{4.40}$$

which leads to

$$\underline{I} = \frac{2\Pi^2}{\underline{Z}_o + 2\underline{Z}} \left(\underline{V}(t) - \frac{\underline{F}(t)}{\Pi} \right) + j\omega C_d \underline{V}(t) \tag{4.41}$$

Furthermore, it can be assumed that the resulting force at each point of the stator is zero due to the symmetry in transverse directions of the extension and contraction phases underlying the traveling wave type design of the USR60. Consequently, The admittance $\underline{Y}$ of the stator reduces to

$$\underline{Y} = \frac{\underline{I}}{\underline{V}} = j\omega C_d + \frac{2\Pi^2}{\underline{Z}_o + 2\underline{Z}} = \underline{Y}_d + \underline{Y}_m \tag{4.42}$$

- $\underline{Y}_d$ is the blocking (damping) admittance, i.e. when no vibrations take place in the powered stator, and reads

$$\underline{Y}_d = j\omega C_d \tag{4.43}$$

- $\underline{Y}_m$ is the motional admittance representing the electromechanical behavior of the vibrating stator seen from the electrical side, and reads

$$\underline{Y}_m = \frac{2\Pi^2}{\underline{Z}_o + 2\underline{Z}} = \Pi^2 \underline{y}_m \tag{4.44}$$

  where Π is the electromechanical transformer known as the force factor, and $\underline{y}_m$ is the motional admittance representing the electromechanical behavior of the vibrating stator seen from the mechanical side.

By substituting (4.32) and (4.38) in (4.44) and rearranging the terms the motional admittance becomes

$$\begin{aligned} \underline{Y}_m &= 2j\frac{\Pi^2}{\rho\mathcal{A}v_{ph}}\tan(\frac{kl}{2}) = j\omega\varepsilon_{33}^T\mathbb{k}_{31}^2\frac{lb}{e}\frac{\tan(\frac{kl}{2})}{\frac{kl}{2}} \\ &= j\omega C_d\frac{\mathbb{k}_{31}^2}{1-\mathbb{k}_{31}^2}\frac{\tan(l_x)}{l_x} \end{aligned} \tag{4.45}$$

where

$$l_x = \frac{kl}{2} = \frac{\omega l}{2v_{ph}}$$

By varying the frequency under the constant voltage of the power supply, resonance and antiresonance behavior is obtained for different angular frequencies of the stator. This phenomenon can be mathematically accounted for by using the Mittag-Leffers's theorem to

$$\text{Expand the function } \vartheta_x = \frac{\tan(l_x)}{l_x} \text{ along its poles.}$$

Thus, if $\pm x_n$ are the poles of ϑ_x then

$$\vartheta_x = \sum_{n_{odd}}^{\infty}\frac{\mathfrak{q}_n}{1-(\frac{l_x}{x_n})^2} \tag{4.46}$$

where

$$\mathfrak{q}_n = \frac{8}{\pi^2(2m-1)^2}$$

By substituting (4.46) in (4.45) and rearranging the terms the motional admittance becomes

$$\underline{Y}_m(\omega) = \sum_{n_{odd}}^{\infty} j\omega\,\frac{\Pi^2}{(\frac{1}{C_n}-\omega^2\mathcal{L})} = \Pi^2\underline{y}_m(\omega) \tag{4.47}$$

where

$$\begin{cases} \mathcal{L} = \frac{1}{\omega_n^2 C_n} \\ C_n = \frac{\mathfrak{q}_n}{\Pi^2}\frac{\mathbb{k}_{31}^2}{1-\mathbb{k}_{31}^2}C_d \end{cases}$$

In terms of the four terminal equivalent circuit information, the electromechanical motional branch of the admittance is expressed by an infinite number of $(\mathcal{L}, C_n)$-series circuits in parallel, thus the equivalent circuit of the non-dissipative stator is shown in figure 4.7

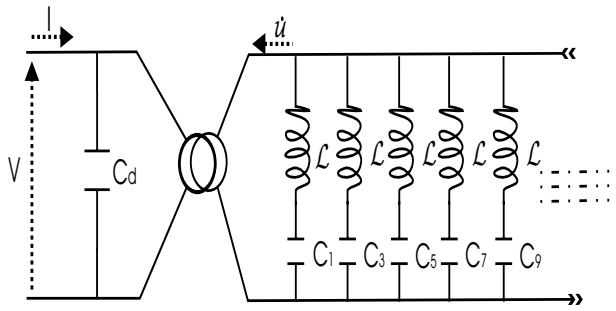

Figure 4.7: The electromechanical ECM for one phase of the ideal stator with no losses over a large span of frequencies

The electromechanical coupling factor

By solving the system of equations in the relation (4.40) for $\underline{s}_o$, $\underline{s}_l$ and $\underline{I}$ the following is obtained

$$\begin{cases} \underline{s}_o = \frac{1}{\underline{Z}_o+2\underline{Z}}\underline{F} - \frac{\Pi}{\underline{Z}_o+2\underline{Z}}\underline{V} \\ \underline{s}_l = -\frac{1}{\underline{Z}_o+2\underline{Z}}\underline{F} + \frac{\Pi}{\underline{Z}_o+2\underline{Z}}\underline{V} \\ \underline{I} = \frac{-2\Pi}{\underline{Z}_o+2\underline{Z}}\underline{F} + (\frac{2\Pi^2}{\underline{Z}_o+2\underline{Z}} + j\omega C_d)\underline{V} \end{cases} \tag{4.48}$$

By denoting the speed of vibration of the closed stator by $\underline{\dot{u}}$ such that

$$\underline{\dot{u}} = \underline{s}_o - \underline{s}_l$$

then the relation (4.48) can be rewritten in the following four terminal expression form

$$\begin{cases} \underline{\dot{u}} = \frac{2}{\underline{Z}_o+2\underline{Z}}\underline{F} - \frac{2\Pi}{\underline{Z}_o+2\underline{Z}}\underline{V} \\ \underline{I} = \frac{-2\Pi}{\underline{Z}_o+2\underline{Z}}\underline{F} + (\frac{2\Pi^2}{\underline{Z}_o+2\underline{Z}} + j\omega C_d)\underline{V} \end{cases} \tag{4.49}$$

By using the definition of the electromechanical coupling factor defined in section 2.2.4 and observing that (4.49) has the following four terminal expression form

$$\begin{cases} \dot{u} = \varrho_{11}F + \varrho_{12}V \\ I = \varrho_{12}F + \varrho_{22}V \end{cases} \tag{4.50}$$

where

$$\varrho_{11} = \frac{2}{\underline{Z}_o + 2\underline{Z}} \tag{4.51}$$

$$\varrho_{12} = -\frac{2\Pi}{\underline{Z}_o + 2\underline{Z}} \tag{4.52}$$

$$\varrho_{22} = \frac{2\Pi^2}{\underline{Z}_o + 2\underline{Z}} + j\omega C_d \tag{4.53}$$

Then the electromechanical coupling factor is given by

$$\Bbbk^2 = \lim_{\omega \longrightarrow 0} \frac{\varrho_{12}^2}{\varrho_{11}\varrho_{22}} \tag{4.54}$$

By substituting (4.51), (4.52) and (4.53) in (4.54) and rearranging the terms then the coupling factor reads

$$\Bbbk^2 = \lim_{\omega \longrightarrow 0} \frac{\frac{2\Pi^2}{\underline{Z}_o + 2\underline{Z}}}{\frac{2\Pi^2}{\underline{Z}_o + 2\underline{Z}} + j\omega C_d} = \lim_{\omega \longrightarrow 0} \frac{\underline{Y}_m}{\underline{Y}_d + \underline{Y}_m} \tag{4.55}$$

By considering only the vibrating mode of rank n and substituting (4.43) and (4.44) in (4.55) then the effective coupling factor of this mode is

$$\Bbbk_{31}^2 = \lim_{\omega \longrightarrow 0} \frac{\Pi^2 C_n}{C_d + \Pi^2 C_n - \pounds C_d C_n \omega^2} = \frac{\Pi^2 C_n}{C_d + \Pi^2 C_n} \tag{4.56}$$

The overall intrinsic coupling factor of the piezomaterials $\Bbbk_{31_{int}}$ for all transverse modes of vibration is further given by

$$\Bbbk_{31_{int}}^2 = \frac{\Pi^2 C_{eq}}{C_d + \Pi^2 C_{eq}} \tag{4.57}$$

where

$$\begin{cases} \sum\limits_n \mathfrak{q}_n = 1 \\ C_{eq} = \sum\limits_n C_n \end{cases}$$

are used.

4.1.2 The free stator around the fundamental resonance

In practice only the fundamental frequency is of interest, and therefore it is only necessary to identify the admittance around this frequency and represent the motional admittance with one $(\pounds, C_1)$-series tank. When no load is considered the output terminal of the motional admittance is a short circuit as shown in figure 4.8

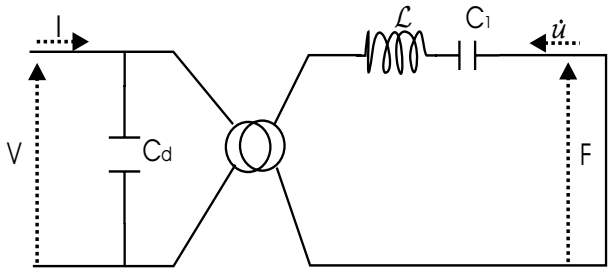

Figure 4.8: The electromechanical ECM for one phase of the ideal stator with no losses around the fundamental resonance frequency

In order to take into account the dissipative sources in the real stator, it is necessary to integrate the losses of energy within the system in terms of equivalent circuit information both at the input terminal and the output terminal.This is done by adding a resistance R_d, representing the dielectrical losses, in parallel with the blocking capacitance and another resistance R_1, representing the electromechanical (conversion) losses, in series with the motional $(\pounds, C_1)$-series tank. To represent further disturbances and influences such as temperature, friction and eventual load, a box referred to by $LOAD$ is added in series with the $(R_{1,}\pounds, C_1)$-series tank of the dissipative motional admittance as shown in figure 4.9

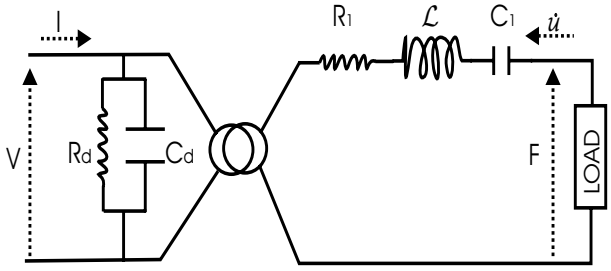

Figure 4.9: The electromechanical ECM for one phase of the real stator integrating the losses around the fundamental resonance frequency

The electromechanical transformer, which serves no useful function in the two terminal equivalent circuit, is normally eliminated by transforming the mechanical elements $\pounds$ and C_1 across the electrical side. Consequently, the electromechanical elements seen as their electrical equivalents become

$$\boxed{R = \frac{R_1}{\Pi^2}\ ,\ L = \frac{\pounds}{\Pi^2}\ ,\ C = \Pi^2 C_1} \tag{4.58}$$

and the electrical equivalent circuit model is shown in figure 4.10

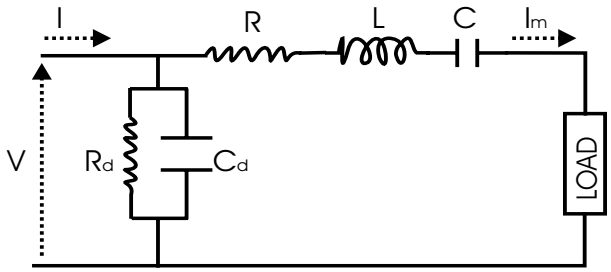

Figure 4.10: The ECM for one phase of the real stator integrating the losses, around the fundamental resonance frequency, and where the mechanical parameters are seen as their electrical equivalents

In general there is a one to one correlation between the mechanical and electrical parameters of the equivalent circuit information used for the analysis of any piezoelectric transducer. Therefore, the use of the electrical equivalent of the mechanical parameters is preferred when the electrical network method is to be used for extracting the parameters of the circuit. Consequently, the analysis of the behavior of any transducer in various working conditions can be carried out by using only the electrical elements, and reference to their mechanical equivalent is made when this is necessary. The correlation between electrical and mechanical parameters for any piezoelectric transducer is shown in the following table

Electrical	Unit	Mechanical	Units
Current I	A	Velocity $\dot{u}$	$m.s^{-1}$
Charge q	C	Displacement u	m
Resistance R	Ω	Damping D	$N.s.m^{-1}$
Inductance L	H	Mass M	kg
Capacitance C	F	Elasticity K	$N.m^{-1}$
Force factor Π	$C.m^{-1}$	Force factor Π	$N.V^{-1}$

Table 4.1: Correlation between the electrical and the mechanical parameters

4.1.2.1 Identification of the parameters in the equivalent circuit model

The unloaded stator is accurately represented near its fundamental resonance by the two terminal equivalent circuit model, where the electrical and the electromechanical parameters are represented by their electrical equivalents. The identification of the parameters is carried out by using the electrical network method to extract the parameters from the admittance locus (Nyquist diagram) of any electromechanical system.

- The global admittance Y of the system is the sum of the damping admittance Y_d and the motional admittance Y_m

$$Y = Y_d + Y_m$$

  where in terms of the equivalent circuit parameters

  – The damping admittance Y_d reads

$$Y_d = \frac{1}{R_d} + jw_oC_d$$

  – The motional admittance Y_m reads

$$Y_m = \frac{R}{R^2 + (L\omega - \frac{1}{C\omega})^2} + j\frac{(\frac{1}{C\omega} - L\omega)}{R^2 + (L\omega - \frac{1}{C\omega})^2}$$

  – The global admittance Y reads

$$Y = \frac{1}{R_d} + \frac{R}{R^2 + (L\omega - \frac{1}{C\omega})^2} + j(w_oC_d + \frac{(\frac{1}{C\omega} - L\omega)}{R^2 + (L\omega - \frac{1}{C\omega})^2})$$

The following figure 4.11 represents the locus of the admittance in Nyquist plane where the curve describes a vertical line with increasing frequency, except in the region around the mechanical resonance and antiresonance where it describes a motional admittance circle. The maximum and the minimum of the motional admittance occur at the mechanical resonance (series) f_s and antiresonance (parallel) f_p respectively. The resonance and the antiresonance of the whole system are given byf_r and f_a respectively whereas the maximum and the minimum of the total admittance are given by the pair f_h and f_l respectively. The admittance is capacitive over the whole range of frequencies except for the narrow interval of frequencies lying between f_r and f_a where the admittance is inductive. The three pairs of characteristic frequencies (f_r,f_a), (f_s,f_p) and (f_h,f_l) are therefore the frequencies of principal interest in the process of identification of the parameters of all two terminal equivalent circuit applications.

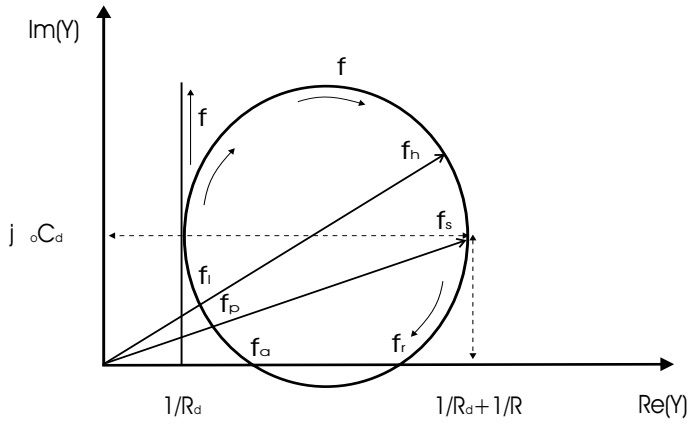

Figure 4.11: Nyquist diagram of the electromechanical transducer around its fundamental resonance and antiresonance frequencies

The electrical network method also uses the information provided by the frequency response as a Bode magnitude diagram where the three pairs of characteristic frequencies are identified in the neighborhood of the resonance and antiresonance sharpness of the diagram as shown in figure 4.12

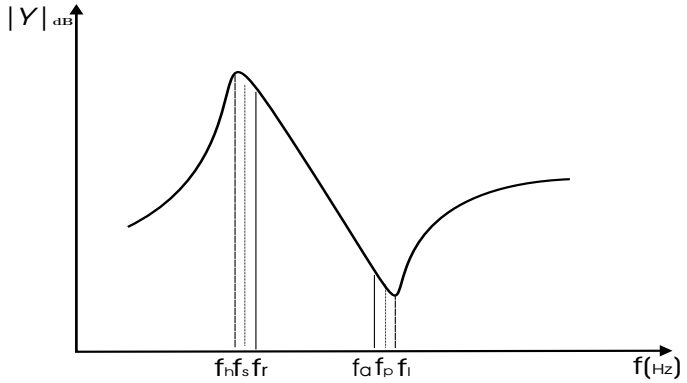

Figure 4.12: Bode magnitude diagram of the electromechanical transducer around its fundamental resonance and antiresonance frequencies

For convenience, definitions of characteristic parameters obtained from the admittance diagram are listed in table 4.2

f_s	motional (series) resonance frequency	$f_s = \frac{1}{2\pi\sqrt{LC}}$
f_p	parallel resonance frequency	$f_p = \frac{\sqrt{(1+\frac{C_d}{C})}}{2\pi\sqrt{LC}}$
f_r	resonance frequency	$Re(Y) = 0$
f_a	antiresonance frequency	$Re(Y) = 0$
f_h	frequency at maximum admittance	
f_l	frequency at minimum admittance	
Q	mechanical quality factor	$Q = 2\pi f_s \frac{L}{R}$
$\frac{C_d}{C}$	capacitance ratio	$\frac{C_d}{C} = \frac{f_s^2}{f_p^2 - f_s^2}$

Table 4.2: The characteristic parameters of the electrical network method

The characteristic frequencies which are commonly used in the evaluation of the equivalent circuit parameters are f_s and f_p. It must be emphasized that in the lossless case the three pairs of frequencies coincide ($f_s = f_h = f_r$ and $f_p = f_l = f_a$) and these occur at the minimum and the maximum of the impedance respectively, and when the losses are small then the pair (f_h, f_l) can be used instead of the pair (f_s, f_p), and when the quality factor is sufficiently high $(Q > 100)$ then the pair (f_s, f_p) is obtained from the average of the two other pairs

$$(f_s, f_p) = \frac{(f_h, f_l) + (f_r, f_a)}{2} \tag{4.59}$$

The quality factor Q is determined from either the Nyquist diagram or the Bode diagram. In the Bode case, the sharpness of the admittance around the resonance frequency as shown in figure 4.13 is used to determine Q from the pass band at $-3dB$ of the frequency response

$$Q = \frac{f_s}{\Delta f}_{-3dB} \tag{4.60}$$

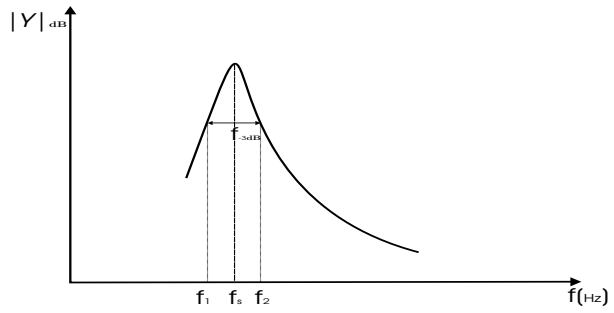

Figure 4.13: Bode magnitude diagram of the electromechanical transducer around its fundamental resonance frequency

From the Nyquist diagram the quality factor is

$$Q = 2\pi f_s \frac{L}{R} = \frac{1}{2\pi f_s RC} = \frac{1}{R}\sqrt{\frac{L}{C}} \tag{4.61}$$

Finally, the following set of equations gives the evaluation formula for each parameter in the two terminal equivalent circuit information (Nogarede and Piecourt (1994))

$$\begin{cases} f_s = \frac{f_h + f_r}{2} \\ f_p = \frac{f_l + f_a}{2} \\ R_d = \frac{1}{Re(Y(f))} \text{ for } f \ll f_s \\ C_d = \frac{Im(Y(f_s))}{2\pi f_s} \\ R = \frac{1}{Re(Y(f_s)) - \frac{1}{R_0}} \\ L = \frac{1}{4\pi^2 C_d (f_p^2 - f_s^2)} \\ C = C_d \frac{f_p^2 - f_s^2}{f_s^2} \\ Q = 2\pi f_s \frac{L}{R} > 100 \text{ for verification} \end{cases} \tag{4.62}$$

4.1.3 The complete motor around the fundamental resonance

The ultrasonic motor considered in this work is a two phase motor type USR60. The design and the shape of the stator of the USR60 give rise to a traveling wave resulting from the superposition of two standing waves provided by each excited phase of the motor. The analysis in terms of equivalent circuit information leads to two four terminal equivalent circuits to represent the complete motor (i.e. one circuit per excited phase).

The equivalent circuit that represents the complete motor is shown in figure 4.14 where the load box represents all the phenomena that intervene beyond the stator at the interface contact between the stator and the rotor.

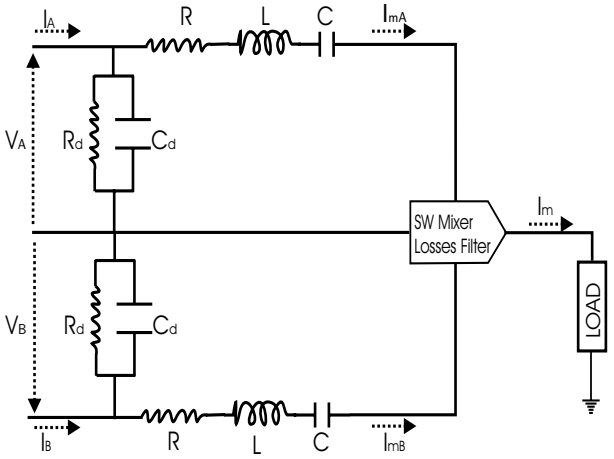

Figure 4.14: The ECM of the two phase complete RPEM

However, due to the symmetrical nature of the stator of the USR60 only one four terminal equivalent circuit is necessary in order to represent the electromechanical behavior of the stator. Consequently, the final equivalent circuit model of the complete motor can be reduced to a mono-phase four terminal circuit, which provides the prediction of the performance characteristics of the motor operating under various working conditions.

Figure 4.15 shows the mono-phase equivalent circuit model of the complete motor

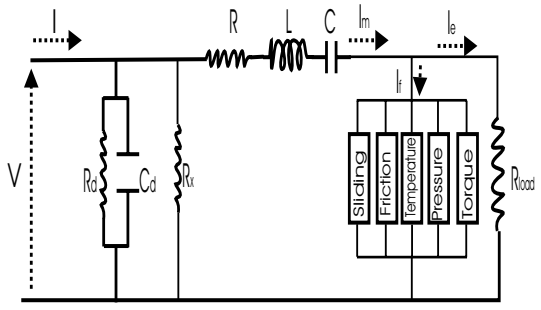

Figure 4.15: The ECM of the complete RPEM

4.1.4 Speed and feedback signal relationship for the motor

The feedback electrode of the motor, which is a neutral part of length ($\lambda/4$), is subjected to bending deformations created by the traveling wave. According to the piezoelectric direct effect the total current $\underline{I}_x$ flowing out of this electrode is related to the tangential vibration velocity $\underline{\vartheta}$ of the particles of the stator in complex notation by a force factor

$$\underline{I}_x = \eta_x \, \underline{\vartheta} \tag{4.63}$$

It must be emphasized that the feedback electrode is a neutral part and therefore behaves like a blocking capacitance C_x. The developed voltage V_x within this electrode is related to the current I_x flowing out of it by

$$\underline{V}_x = \frac{\underline{I}_x}{j\omega C_x} \tag{4.64}$$

The maximum of the tangential velocity ϑ of the particles of the stator, located at the middle radius R_o of the annular plate, is related to the ideal rotary speed Ω_{id} of the motor, when no sliding is assumed, by

$$\vartheta = R_o \Omega_{id} \tag{4.65}$$

By substituting (4.65) in (4.63), and thereafter (4.63) in (4.64) and rearranging the terms

$$V_x = \frac{\eta_x R_o}{\omega C_x} \Omega_{id} \tag{4.66}$$

where η_x is the direct modal force factor, it can be concluded from the equation (4.66) that the feedback voltage is proportional to the ideal rotary speed of the motor at any fixed frequency. Furthermore, the maximum tangential velocity of the particles of the stator, see section 4.2.1.2, is given by

$$\vartheta = \frac{kh}{R_o} R_r A \omega = R_o \Omega_{id} \tag{4.67}$$

where R_r is the modal shape constant in radial direction, A and ω are the amplitude and angular frequency of the traveling wave, respectively. Finally, by substituting (4.67) in (4.66) then the following is obtained

$$V_x = \frac{\eta_x k h R_r}{R_o C_x} A \tag{4.68}$$

where it can be noticed that there is a proportionality between the amplitude of the traveling wave and the amplitude of the feedback voltage. This result suggests that the feedback voltage is a valuable parameter for predicting and controlling the motor.

4.2 Equivalent circuit model derivation

The equivalent circuit modeling of the traveling wave motor USR60 is done stepwise by first considering the free stator then the unloaded motor and finally the loaded motor.

4.2.1 The free stator

The identification of the parameters of the equivalent circuit model is carried out by applying the electrical network method as stated in the previous section 4.1.2.1. The stator of the USR60 is a two phase symmetrical system with each phase providing a standing wave. Due to the special design of the stator these standing waves are combined and create a traveling wave within the body of the stator. The admittance of each phase of the stator was measured in the same conditions and their compared results are plotted in figure 4.16

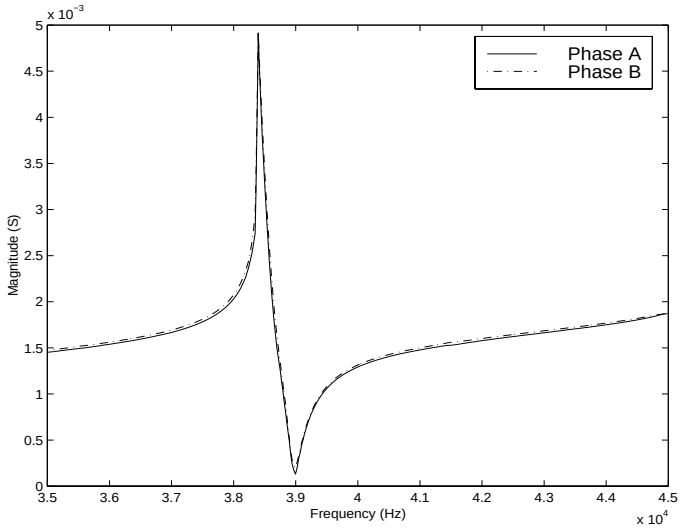

Figure 4.16: Comparison between the admittance of phase A and the admittance of phase B of the stator around the fundamental resonance frequency

From figure 4.16 it can be noticed that the two phases exhibit almost the same admittance, consequently the stator can be assumed to be perfectly symmetrical and therefore only one phase needs to be identified. The two terminal equivalent circuit representation of one phase of the free stator, where the electromechanical parameters are seen as their electrical equivalents, is shown in figure 4.17.

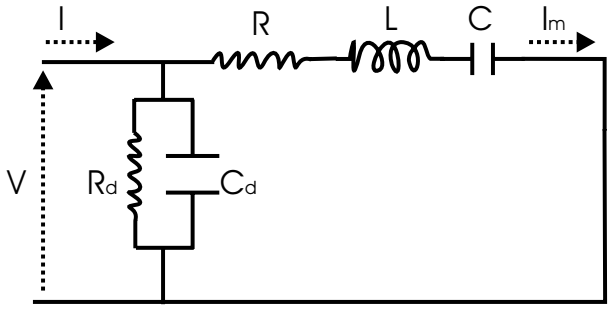

Figure 4.17: The electrical equivalent circuit model of one phase of the free stator

The admittance of the free stator is provided for one phase around the fundamental frequency, and the results are plotted in figure 4.18 in the form of Bode and Nyquist diagrams.

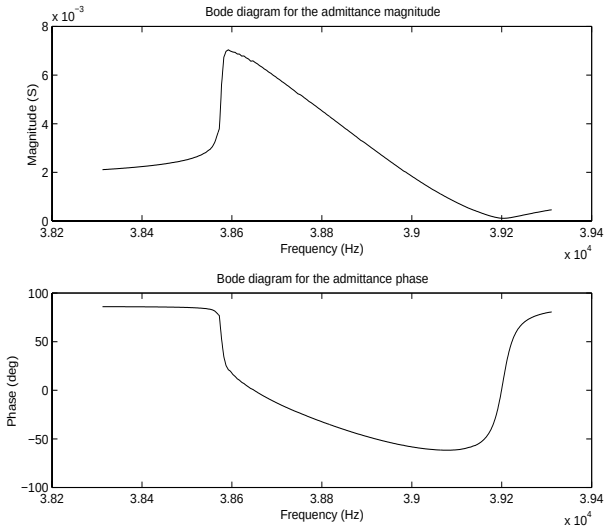

Figure 4.18: Bode magnitude and phase diagram of the electrical admittance of the stator around the fundamental resonance frequency

From the Bode diagram it can easily be seen that the admittance exhibits resonance and antiresonance behavior in the explored range of frequencies. The extraction of the parameters is therefore possible by using the Nyquist diagram in figure 4.19 according to the previously stated method in section 4.1.2.1.

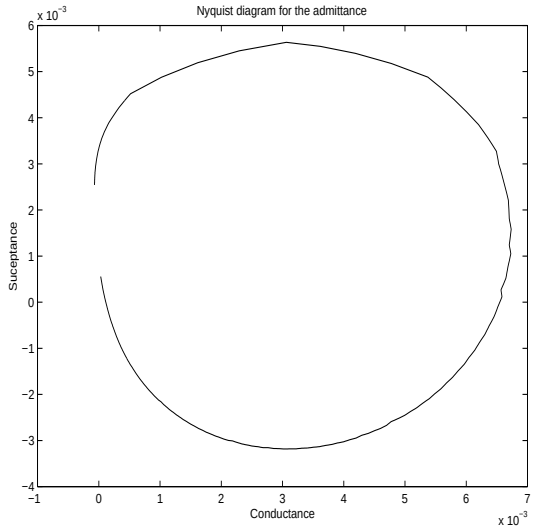

Figure 4.19: Nyquist diagram of the electrical admittance of the stator around the fundamental resonance frequency

The exploitation of the Nyquist diagram leads to the following values

f_s =	$3.862\,10^4$	R =	149.75
f_p =	$3.920\,10^4$	L =	0.102
R_d =	$3.12\,10^4$	C =	$1.66\,10^{-10}$
C_d =	$5.4\,10^{-9}$	Q =	166

Table 4.3: The identified parameters of the electrical admittance

The quality factor Q which is over 100 in this case enhances the validity of the approximation made to derive the parameters of the network.

The stator is by nature an electromechanical system with an electrical input terminal and a mechanical output terminal. The admittance of the stator derived in the above gave the mechanical parameters of the network in terms of their electrical equivalents, but it is possible and also more convenient to derive these mechanical parameters directly by measuring the ElectroMechanical (EM) admittance of the vibrating gain of the stator. The EM admittance is the ratio between the speed of vibration at the surface of the stator and the input voltage. It must be emphasised that the speed of vibration can be measured only in normal direction.

4.2.1.1 Normal and tangential force factors

Due to the elliptical motion of the particles at the surface of the stator it will be shown that the speed of vibration in tangential direction can be obtained as a function of the speed of vibration in normal direction. Hence, by assuming that the traveling wave at the surface of the stator is given by (4.69), see sections 4.2.1.2 and 5.2.1

$$w(r,\theta,t) = R_r A \cos(\omega t - k\theta) \tag{4.69}$$

and by applying Kirchhoff's law, the displacement u_P of a point P, in the (θ, z)-plane, at the surface of the stator, located at distance h from the centerline is given by

$$\begin{aligned} u_P &= u_z\ \vec{e}_z + u_\theta\ \vec{e}_\theta \\ &= w(r,\theta,t)\ \vec{e}_z - \frac{h}{r}\frac{\partial w}{\partial \theta}(r,\theta,t)\ \vec{e}_\theta \\ &= R_r A \cos(\omega t - k\theta)\ \vec{e}_z + \frac{kh}{r} R_r A \sin(\omega t - k\theta)\ \vec{e}_\theta \end{aligned} \tag{4.70}$$

where $\vec{e}_z$ and $\vec{e}_\theta$ are unit vectors in vertical and circumferential direction respectively. Consequently, the elliptical motion of the point P in the (θ, z)-plane is given by

$$(\frac{u_z}{R_r A})^2 + (\frac{u_\theta}{\frac{kh}{r} R_r A})^2 = 1 \tag{4.71}$$

By taking the derivative of equation (4.71) with respect to time the following is obtained

$$(\frac{kh}{r})^2 u_z \dot{u}_z + u_\theta \dot{u}_\theta = 0 \tag{4.72}$$

which leads to

$$\dot{u}_z = -(\frac{r}{kh})^2 \frac{u_\theta}{u_z} \dot{u}_\theta = -\frac{r}{kh} \tan(\omega t - k\theta) \dot{u}_\theta \tag{4.73}$$

This relation (4.73) shows that, for any point at the surface of the stator, the speed of vibration in normal direction can be obtained from the speed of vibration in tangential direction. Consequently, this result suggests that the equivalent circuit representation presented in section 4.1.2 can be used for predicting the speed of vibration in normal direction. Hence, by using (4.70) the speed of vibration in normal direction $\dot{u}_z$ and the speed of vibration in tangential direction $\dot{u}_\theta$ read

$$\dot{u}_z = -R_r A \omega \sin(\omega t - k\theta) = -\hat{\dot{u}}_z \sin(\omega t - k\theta) \tag{4.74}$$

$$\dot{u}_\theta = \frac{kh}{r} R_r A \omega \cos(\omega t - k\theta) = \hat{\dot{u}}_\theta \cos(\omega t - k\theta) \tag{4.75}$$

where

$$\hat{\dot{u}}_z = R_r A \omega \tag{4.76}$$

$$\hat{\dot{u}}_\theta = \frac{kh}{r} R_r A \omega \tag{4.77}$$

Furthermore, the maximum I_m of the motional sinusoidal current, flowing into the motional branch of the equivalent circuit, is related to the maximum of the vibration velocity in normal direction $\hat{\dot{u}}_z$ and the maximum of the vibration velocity in tangential direction $\hat{\dot{u}}_\theta$ by respectively a normal force factor Π_n and a tangential force factor Π_t such that

$$I_m = \Pi_n \hat{\dot{u}}_z = \Pi_t \hat{\dot{u}}_\theta \tag{4.78}$$

where by using (4.76) and (4.77) leads to the following relationship between the normal force factor Π_n and the tangential force factor Π_t such that

$$\Pi_n = \frac{kh}{r}\Pi_t \tag{4.79}$$

For convenience, as only the speed of vibration in normal direction can be measured, in the remaining developments the normal force factor will be denoted by Π and will be referred to by the force factor and the speed of vibration in normal direction will be denoted by $\dot{u}$ and will be referred to by the speed of vibration. Furthermore, the maximum of the speed of vibration in normal direction will be denoted ϑ and reads

$$\vartheta = \frac{I_m}{\Pi} \tag{4.80}$$

Consequently, the two terminal equivalent circuit representation of one phase of the free stator, to be identified, is shown in figure 4.20

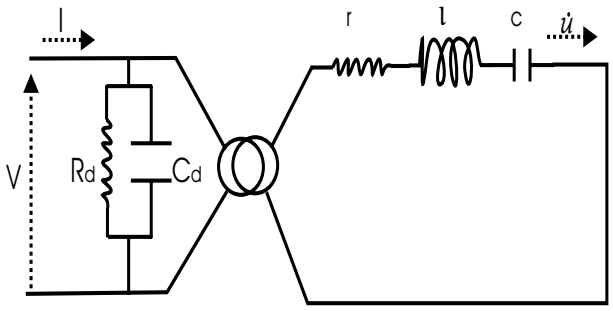

Figure 4.20: The electromechanical equivalent circuit model of the free stator

where the blocking admittance Y_d, the motional admittance y_m and the total admittance Y are respectively given by

$$Y_d = 1/R_d + j\omega C_d \tag{4.81}$$

$$y_m = 1/[r + j(\omega l - 1/\omega c)] \tag{4.82}$$

$$Y = Y_d + \Pi^2 y_m \tag{4.83}$$

and where the relationship between the electromechanical elements and their electrical equivalents is given by

$$R = \frac{r}{\Pi^2} \qquad L = \frac{l}{\Pi^2} \qquad C = \Pi^2 c \tag{4.84}$$

The identification of the parameters is carried out by using the electrical network method, see section 4.1.2.1. Figure 4.21 presents the Bode magnitude and the Nyquist diagrams of the EM admittance.

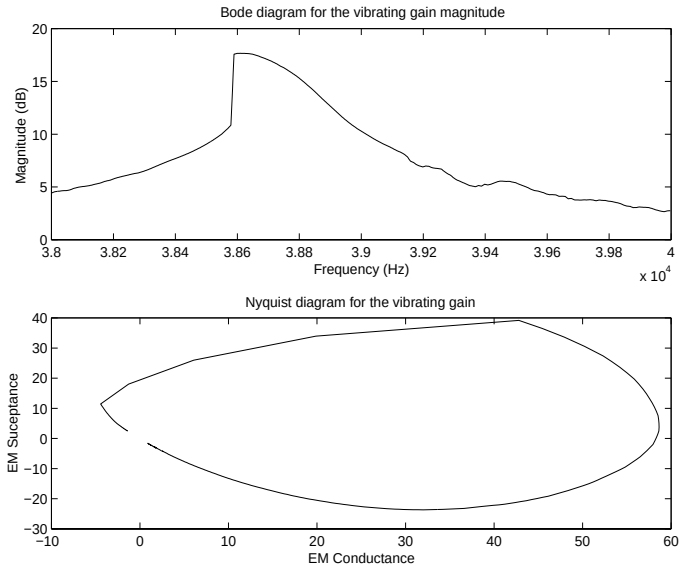

Figure 4.21: Bode and Nyquist diagrams of the EM vibrating gain admittance of the stator around the fundamental resonance frequency

The exploitation of the diagrams reported in figure 4.21 according to the sharpness of the EM admittance around the resonance frequency and the derivation of the quality factor from the pass band at -3dB of the frequency response together with the radius of the Nyquist diagram lead to the following values

f_r =	$3.8644\ 10^4$	r =	15.4
Δf_{-3dB} =	242.19	l =	0.0101
Q =	159.55	c =	$1.68\ 10^{-9}$

Table 4.4: The identified parameters of the electromechanical motional admittance

The quality factor which is slightly different from the previous case enhances both the validity of the approximation and the compatibility of these two methods. The above mechanical (r,l,c) values can be seen as their electrical equivalents and thereby, by using (4.84), deduce the force factor

$$\Pi = 0.32$$

The identified values are thereafter used in a simulated equivalent circuit model environment, and for each case an admittance is provided over a certain range of frequencies around the fundamental resonance and the results are then compared to the experimental data.

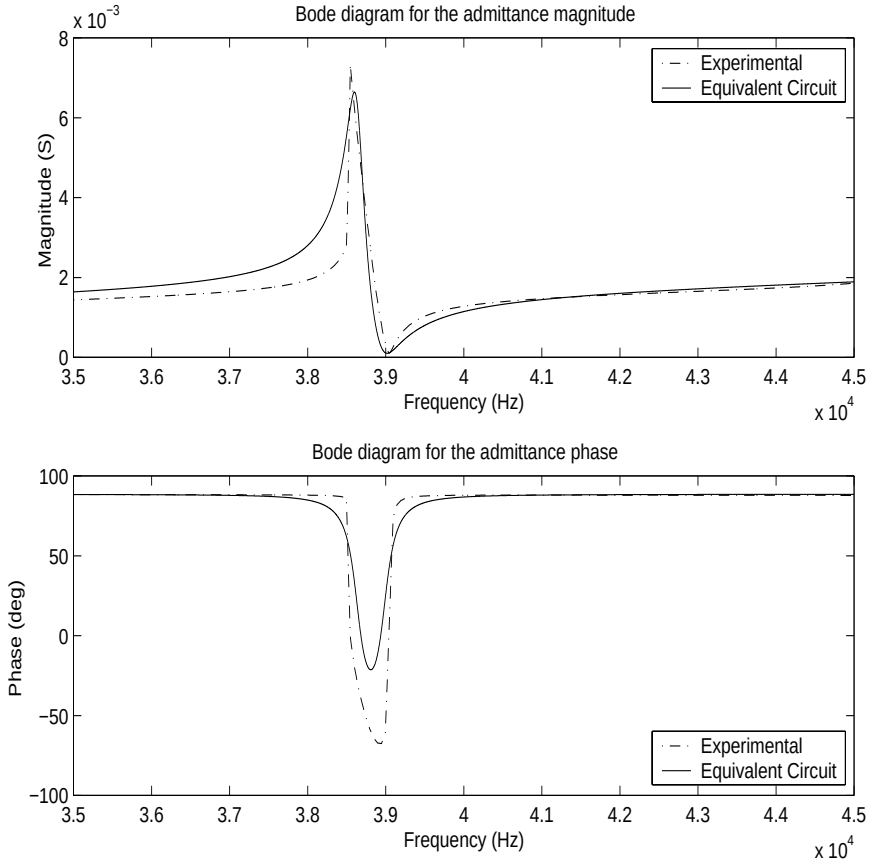

Figure 4.22: Prediction of the electrical admittance of the stator around the fundamental resonance frequency

From figure 4.22 it can be noticed that the simulated model predicts most of the electrical admittance characteristic especially in the range of frequencies located above the fundamental resonance, however a small and harmless discrepancy can be observed for the phase prediction which is caused by the nonlinear behavior of the stator between its resonance and antiresonance behavior.

For control purposes the most important part of the equivalent circuit model is the mechanical output terminal, therefore it is important to compare the EM admittance prediction to the experimental data.

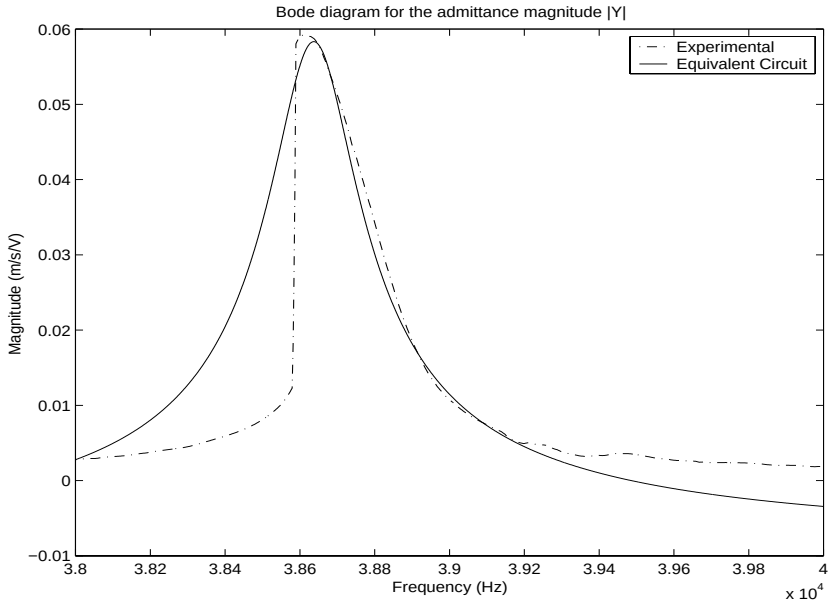

Figure 4.23: Prediction of the EM vibrating gain admittance of the stator around the fundamental resonance frequency

From figure 4.23 it can be noticed that most of the performance of the stator in terms of the EM admittance gain can be predicted fairly well in a simulated environment. However, this is valid only in the range of frequencies lying above the fundamental frequency.

The behavior of the stator over a large span of frequencies can also be predicted by a simulated equivalent circuit model provided that each excited mode in this range is identified and an electrical branch is allocated for it in the model. Figure 4.24 shows the comparison between experimental data and model prediction over the span of frequencies $[20\ kHz, 60\ kHz]$.

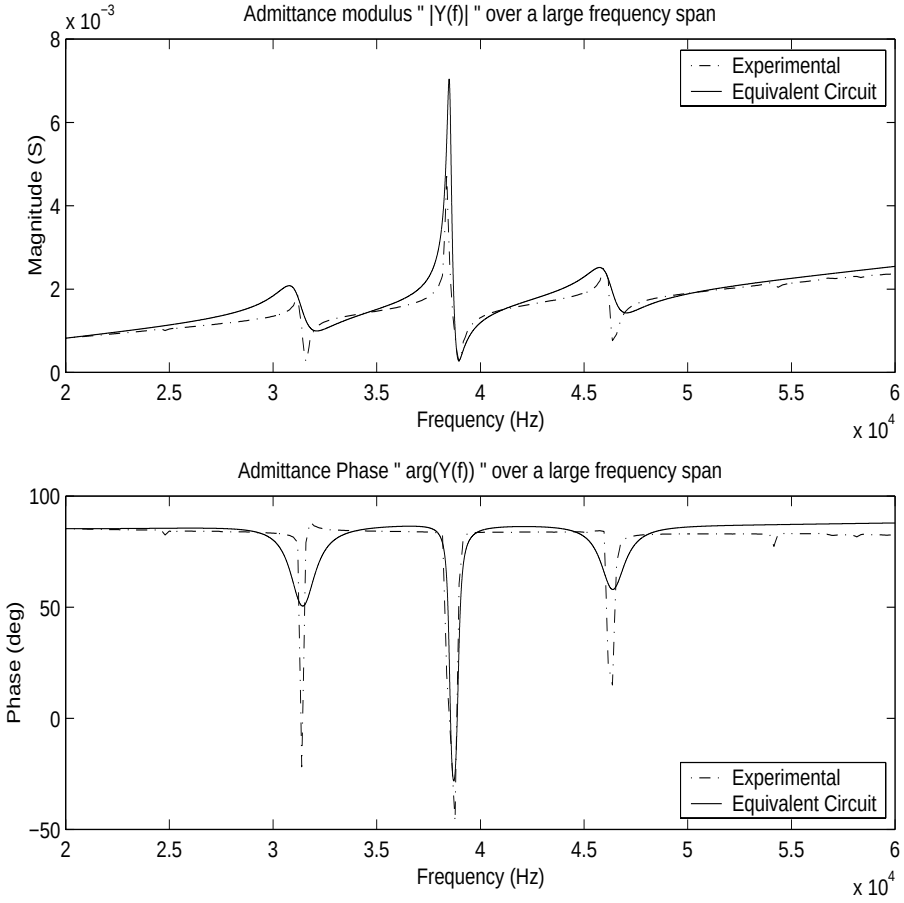

Figure 4.24: Prediction of the admittance of the stator over a large span of frequencies

From figure 4.24 it can be noticed that a good prediction is achieved in the neighborhood of the fundamental frequency whereas the quality of prediction deteriorates for the other modes. The large discrepancies observed in the neighborhood of other resonance frequencies than the fundamental resonance can be explained by the fact that the stator is especially designed to operate in its fundamental resonance mode and even if the remaining modes can be excited they are maintained at a cost of a different stress-strain relationship affecting the dielectric and electromechanical behavior of the whole structure, which results mainly in drastic changes of the blocking admittance. Therefore, a better prediction for these modes requires the reidentification of the blocking admittance for each mode.

4.2.1.2 The modal force factor

The stator of USR60 is a two phase system in which a traveling wave is generated by the superposition of two standing waves provided by two excited mechanical orthogonal modes $\cos k\theta$ and $\sin k\theta$. The traveling wave can be mathematically expressed in terms of a summation over the excited mechanical modes weighted by their respective modal amplitudes ξ_1 and ξ_2 such that

$$w(r,\theta,t) = R_r(\xi_1 \cos k\theta + \xi_2 \sin k\theta\ ) = R_r A \cos(\omega t - k\theta) \tag{4.85}$$

where A is the maximum amplitude of the temporal modes and R_r is the shape of the traveling wave in radial direction. The speed of the traveling wave in normal direction (i.e. the rate of vibration) can be expressed by

$$\frac{dw}{dt} = -\vartheta \sin(\omega t - k\theta) = R_r(\dot{\xi}_1 \cos k\theta + \dot{\xi}_2 \sin k\theta\ ) \tag{4.86}$$

where

$$\begin{cases} \xi_1 = A\cos\omega t \\ \xi_2 = A\sin\omega t \\ \vartheta = R_r A\omega \end{cases} \tag{4.87}$$

According to the piezoelectric direct effect the electrical charge that flows in each electrode powering the electromechanical system is related to the generated displacement by a force factor. Consequently, the modal amplitude of each excited mechanical mode is related by a modal force factor to the charge flowing into the motional part of the corresponding phase in the following way

$$\begin{cases} q_{Am} = \eta\ \xi_1 \\ q_{Bm} = \eta\ \xi_2 \end{cases} \tag{4.88}$$

which leads to the useful relation for the current and the modal amplitude velocity

$$\begin{cases} I_{Am} = \eta\ \dot{\xi}_1 \\ I_{Bm} = \eta\ \dot{\xi}_2 \end{cases} \tag{4.89}$$

Under the assumption that the two phases are symmetrical and powered by a common voltage the currents flowing in the motional part of the electromechanical system exhibit the same amplitude and therefore the following notation for the motional charge and current can be used

$$\begin{cases} q_{Am} = q_m \cos\omega t \\ q_{Bm} = q_m \sin\omega t \\ I_{Am} = -I_m \sin\omega t \\ I_{Bm} = I_m \cos\omega t \end{cases} \tag{4.90}$$

by rewriting the foregoing equation in terms of modal force factor and motional current the following is obtained

$$\begin{cases} w(r,\theta,t) = R_r(\frac{q_m}{\eta}\cos\omega t\cos k\theta + \frac{q_m}{\eta}\sin\omega t\sin k\theta\ ) \\ \frac{dw}{dt} = \frac{R_r}{\eta}(-I_m\sin\omega t\cos k\theta + I_m\cos\omega t\sin k\theta\ ) = -R_r\frac{I_m}{\eta}\sin(\omega t - k\theta) \end{cases} \tag{4.91}$$

which leads to the following relation between the maximum of the vibration velocity and the maximum of the motional current flowing into each phase of the stator

$$\vartheta = R_r\frac{I_m}{\eta} \tag{4.92}$$

According to the force factor derived from the electromechanical parameters of the motional part seen as their electrical equivalents in the foregoing analysis, see section 4.2.1.1, the same relation is given by

$$\vartheta = \frac{I_m}{\Pi} \tag{4.93}$$

which leads to the following relation between the modal force factor and the force factor of the USR60

$$\eta = R_r\,\Pi \tag{4.94}$$

where R_r is a radial function depending on the design of the stator and the modal shape of the traveling wave in the radial direction. In general this function is given by the following relation

$$R_r = (\frac{r-a}{b-a})^\gamma \tag{4.95}$$

where a and b are the inner and outer radius of the stator annular plate respectively and γ is a constant depending on the modal shape of the deformation of the stator in the radial direction. By assuming that the contact interface between the stator and the rotor is mainly concentrated around the middle radius of the annular plate i.e. $R_o = \frac{b-a}{2}$ then R_r becomes a constant depending only on the amplitude of the radial mode at the point of contact. The choice of γ is, however, difficult but possible to derive from the motional part seen as its electrical equivalent powered by only one source of power leading to the same amplitude of vibration at the surface of the stator.

The total power $\mathcal{P}$ needed to supply the two symmetrical phase USR60 is given by

$$\mathcal{P} = V_A I_A + V_B I_B = 2VI \tag{4.96}$$

which can be written as

$$\mathcal{P} = (\sqrt{2}V)(\sqrt{2}I) = V_c\ I_c \tag{4.97}$$

This suggests that if only one power source (i.e. one phase) is used to supply the stator of USR60 to obtain the same condition of vibration then the current that will flow in the motional part of the electromechanical system is given by

$$I_{cm} = \sqrt{2}\, I_m \tag{4.98}$$

The relation between the motional current and the vibration velocity is then given by

$$\vartheta = \frac{I_{cm}}{\Pi} = \frac{\sqrt{2}\, I_m}{\Pi} \tag{4.99}$$

The same amplitude of the vibration velocity could be achieved by the motional current I_m flowing through one phase of the stator by using the modal force factor η necessary to create a standing wave within the stator such that

$$\vartheta = \frac{I_m}{\eta} \tag{4.100}$$

which leads to

$$\Pi = \sqrt{2}\eta \tag{4.101}$$

and consequently

$$\begin{cases} \gamma = \frac{1}{2} \\ R_r = \frac{1}{\sqrt{2}} \end{cases} \tag{4.102}$$

4.2.2 The unloaded motor

The case of the unloaded motor with a rotor pressed against the stator with a normal forcing $F = 160\ N$ is the next step of the modeling process. Under the forcing process the piezoelectric converse effect tends to balance the external forcing when sufficient voltage is applied to the piezoceramic, and thereby achieves the same resonance behavior within the stator around the fundamental resonance frequency. By assuming that the blocking admittance (R_d, C_d) characterizing the dielectric behavior of the stator remains constant under pressure and that the modal vibrating mass l of the stator body is a mechanical constant, then the only parameters subject to changes and therefore needing adjustments are (r, c) parameters of the mechanical output terminal. Some extra resistance needs to be added in parallel with the blocking admittance at the input terminal in order to take into account the extra losses of power, which are needed to overcome the external pressure and thereby meet the resonance of the stator.

4.2.2.1 Modeling the applied pressure and the losses

The extra losses due to pressure conditions can be integrated in the ECM as a power source $\mathcal{P}_x$ represented by a resistance R_x. For the USR60 these quantities can be approximately defined by the following relation (Nogarede and Piecourt (1994))

$$\begin{cases} \mathcal{P}_x = \frac{F}{80} \\ R_x = \frac{V^2}{\mathcal{P}_x} \end{cases} \tag{4.103}$$

Under the nominal conditions of operation $F = 160\ N$ and $V = 100\ Vrms$, the loss of power is $\mathcal{P}_x = 2\ W$ per phase which leads to a resistance $R_x = 5\ k\Omega$ to be integrated in parallel with the blocking admittance at the input terminal.

Besides the losses of power the frictional phenomenon at the stator and rotor contact points is responsible for more losses and also for performance deterioration in terms of speed drop. The losses due to friction can be integrated in the model by readjusting the value of r at the mechanical output terminal and readjusting the output speed of the model by subtracting from the motional current at the output terminal an amount image of the speed drop seen as its electrical equivalent.

The readjustment of the mechanical resistance is done by simulation and by comparison to the experimental data gathered in terms of admittance of the unloaded motor operating under nominal conditions.

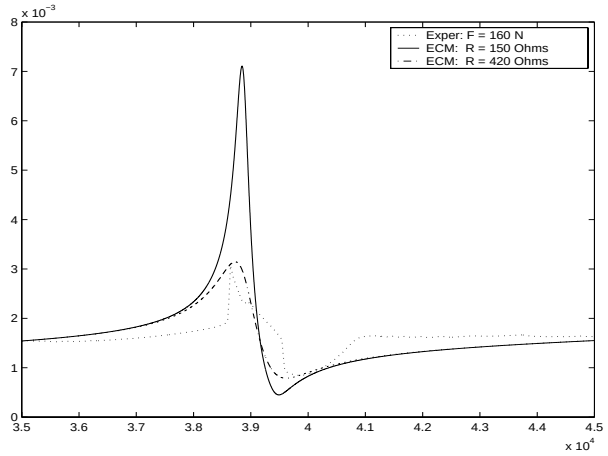

Figure 4.25: Readjustment of the mechanical damping by simulation in terms of the admittance prediction of the RPEM

Figure 4.25 shows that the mechanical resistance seen as an electrical equivalent should be readjusted to $R = 420\ Ohms$ when the motor is operating under its nominal values $(100\ Vrms, 160\ N)$ in unloaded condition.

The speed drop can be provided by sensing the amplitude of the feedback voltage at different normal forcings under constant excitation frequency, which is maintained at its nominal value of $40\ kHz$. It is assumed that in the ideal case the contact between the stator and the rotor is of a non sliding type. Consequently, the velocity of the rotor is opposite and equal to the maximum of the tangential velocity of the particles at the surface of the stator, see sections 4.2.1.2 and 4.2.1.1, and thereby the maximum of the speed of vibration ϑ in normal direction reads

$$\vartheta = R_r A\omega = \frac{R_o}{kh} R_o \Omega_{id} \tag{4.104}$$

where A and ω are the amplitude and the angular frequency of the traveling wave at the surface of the stator, R_r is a mechanical constant depending only on the geometry of the stator, R_o is the middle radius of the driving contact and finally Ω_{id} is the rotary ideal speed of the shaft of the motor.

From figure 3.10, which shows the speed-feedback characteristics, it is clear that the speed of the unloaded motor depends on the normal forcing which is responsible for the sliding and the stick-slip behavior at the contact surface of the driving mechanism (friction). The measured speed Ω_o can be related to the ideal speed Ω_{id} by

$$\Omega_o = \Omega_{id} - \Delta\Omega_f \tag{4.105}$$

where $\Delta\Omega_f$ is the speed drop due to the normal forcing. Figure 3.10 suggests that the speed drop is almost proportional to the normal forcing, at any amplitude of the feedback signal, and their relationship is given by

$$\Delta\Omega_f \cong \alpha\ F \tag{4.106}$$

where for the USR60 the slope is $\alpha = 2\ 10^{-2}\ rad.s^{-1}.N^{-1}$.

The measured speed, drop speed and ideal speed can all be seen as their electrical equivalents and therefore integrated in the equivalent circuit model of the unloaded motor. The speed relation leads to its current image relation for the current flowing into the motional impedance of the motor (Nogarede and Piecourt (1994))

$$\begin{cases} I_{m_o} = I_{id} - I_f \\ Arg(I_{m_o}) = Arg(I_{id}) = Arg(I_f) \end{cases} \tag{4.107}$$

Furthermore the speed current relationship obeys the following relation

$$\frac{\Omega_o}{I_{m_o}} = \frac{\Omega_{id}}{I_{id}} = \frac{\Delta\Omega_f}{I_f} = \aleph \tag{4.108}$$

The proportionality factor is easily derived from the ideal situation where by using (4.99) and (4.104) the motional current is related to the tangential vibrating speed and the rotary speed by

$$I_{id}\sqrt{2} = \Pi\vartheta = \Pi\frac{R_o}{kh} R_o \Omega_{id} \tag{4.109}$$

which leads to

$$\aleph = \frac{kh\sqrt{2}}{\Pi R_o^2} \tag{4.110}$$

For the USR60 $R_o = 26.75$ mm, $\Pi = 0.32$, $k = 9$, $h = 1.5$ mm, the proportionality factor $\aleph = 83\ rad.s^{-1}.A^{-1}$ and $I_f = 9.7\,mA$.

Finally the rotary speed of the unloaded motor can be directly deduced from the motional current I_{m_o} by

$$\boxed{\begin{cases} \Omega_o = \aleph\, I_{m_o} & \text{for} \quad I_f \leqslant I_{m_o} \\ \Omega_o = 0 & \text{for} \quad I_f > I_{m_o} \end{cases}} \tag{4.111}$$

The equivalent circuit model of the unloaded motor can finally be represented by only a two terminal electrical network as shown in figure 4.26 where all mechanical parameters are seen as their electrical equivalent.

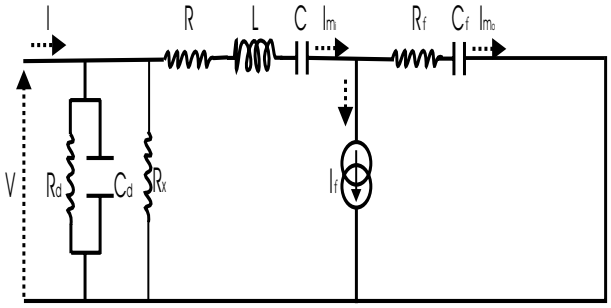

Figure 4.26: The ECM of the unloaded RPEM

It must be emphasized that the capacitance C_f in the two terminal equivalent circuit should be adjusted in order to match the mechanical resonance frequency of the unloaded motor under operation. The information on the mechanical resonance frequency is obtained by sensing the feedback signal, see section 3.3.5. Figure 3.9 suggests that the mechanical resonance frequency of the feedback signal is $f_r \approx 39.8kHz$. Thereby, the value of C_f is updated in the following way

$$C_f = \frac{C}{LC(2\pi f_r)^2 - 1} \tag{4.112}$$

For the USR60: $fr = 39.8\ kHz$, $L = 102\ mH$, $C = .166\ nF$ and $C_f = 2.5866\ nF$

4.2.3 The loaded motor

The speed of the loaded motor depends on the amount of the load torque at the output shaft of the motor. The variational nature of the torque gives rise to nonlinear dynamical changes affecting the sliding and stick-slip behavior at the contact surface of the driving mechanism (friction). The measured speed Ω can be related to the ideal speed Ω_{id} by

$$\Omega = \Omega_{id} - \Delta\Omega_f - \Delta\Omega_\tau \tag{4.113}$$

where $\Delta\Omega_\tau$ is the speed drop due to the load torque. Figures 3.11 and 3.8, which show the speed-feedback characteristics at various load torques and the speed-torque characteristics at various excitation frequencies respectively, suggest that the speed drop is almost proportional to the load torque in the range of frequencies that are of interest i.e. $[40kHz, 41.5kHz]$. Consequently, the relationship between the speed drop and the load torque can be represented by the following linear equation where the coefficient β is the average slope of the speed-torque characteristics

$$\Delta\Omega_\tau \cong \beta\,\mathcal{T} \tag{4.114}$$

where for the USR60 the slope is $\beta = 6.7\ rad.s^{-1}.N^{-1}.m^{-1}$.

The measured, drop and ideal speed can all be seen as their electrical equivalents and therefore integrated in the equivalent circuit model of the unloaded motor. The speed relation leads to its current image relation for the current flowing into the motional impedance of the motor (Nogarede and Piecourt (1994))

$$\begin{cases} I_m = I_{id} - I_f - I_\tau \\ Arg(I_m) = Arg(I_{id}) = Arg(I_f) = Arg(I_\tau) \end{cases} \tag{4.115}$$

Furthermore the speed current relationship obeys the following relation

$$\frac{\Omega}{I_m} = \frac{\Omega_{id}}{I_{id}} = \frac{\Delta\Omega_f}{I_f} = \frac{\Delta\Omega_\tau}{I_\tau} = \aleph \tag{4.116}$$

Finally the rotary speed of the loaded motor can be directly deduced from the motional current I_m by

$$\boxed{\begin{cases} \Omega = \aleph\, I_m & \text{for} \quad I_f + I_\tau \leqslant I_m \\ \Omega = 0 & \text{for} \quad I_f + I_\tau > I_m \end{cases}} \tag{4.117}$$

The proportionality factor $\aleph$ is easily derived from the ideal situation as shown in (4.110). The equivalent circuit model of the loaded motor can finally be represented by a two terminal electrical network where all the mechanical parameters are seen as their electrical equivalents as shown in figure 4.27

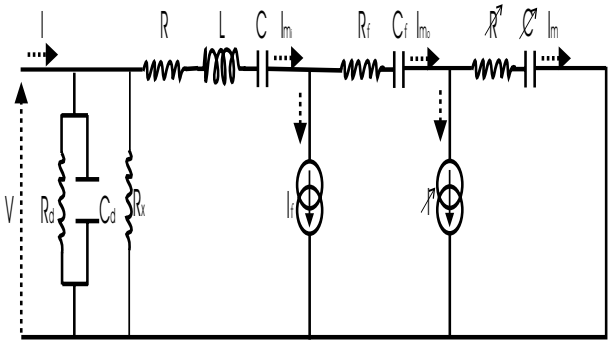

Figure 4.27: The ECM of the loaded RPEM

where the current I_τ image of the speed drop is torque dependent and given by

$$I_\tau = \frac{\beta}{\aleph}\mathcal{T} \tag{4.118}$$

It must be emphasized that the (R_τ, C_τ) branch can be neglected in the simulation process.

4.2.4 Temperature integration in the final equivalent circuit model

The resonance and antiresonance frequencies changes with the temperature which in terms of equivalent circuit modeling can be represented by the same model as before but with varying parameters as shown in figure 4.28

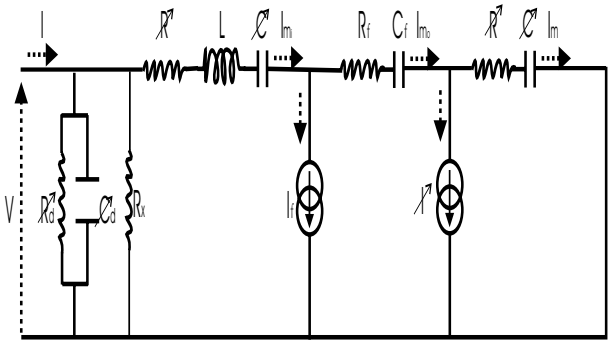

Figure 4.28: The complete ECM of the RPEM integrating the effect of temperature changes

The effect of the heating process that takes place within the body of the stator on the performance of the PEM can be monitored by the feedback signal. By sensing this signal as a function of the temperature of the PEM, see section 3.3.8, the characteristic shown in figure 3.12 is obtained when operating under nominal conditions. It is clear from figure 3.12 that the resonance frequency of the feedback signal shifts towards lower frequencies as the temperature of the PEM increases during the operation process.

It must be emphasized that it is difficult to monitor the effect of temperature on the antiresonance frequency, but fortunately, only the mechanical resonance frequency is of crucial importance when the main target is the output performance in terms of speed and position. Therefore it is only necessary to integrate a tracking capability of the mechanical resonance frequency in the model in order to maintain the output performance of the motor despite the temperature changes. Given the fact that the modal mass is a mechanical constant then the only parameters subject to variation under temperature changes are the damping and the stiffness/elasticity of the motional part whereas the changes of the blocking admittance exist but are overlooked in the modeling process. The following relation represents the resonance behavior of the motional impedance as a function of temperature

$$\begin{cases} C_T = \frac{C\ C_f}{C+C_f} \\ LC_T(2\pi f_r)^2 = 1 \\ LC_{T_o}(2\pi f_{r_o})^2 = 1 \\ f_r = f_{r_o} - \ell\ \Delta\Theta \end{cases} \tag{4.119}$$

where f_{r_o} and f_r are resonance frequencies at the ambient and working temperature respectively, $\Delta\Theta$ is the temperature gradient during operation and ℓ is the slope of the resonance-temperature characteristic. In terms of equivalent circuit information the total capacitance C_T should be updated during the temperature changes in the following way

$$\begin{aligned} C_T &= \frac{1}{L(2\pi f_r)^2} = \frac{1}{L[2\pi(f_{r_o} - \ell\ \Delta\Theta)]^2} \\ &= \frac{1}{L(2\pi f_{r_o})^2(1 - \frac{\ell}{f_{r_o}}\ \Delta\Theta)^2} \approx C_{T_o}(1 + 2\frac{\ell}{f_{r_o}}\ \Delta\Theta) \end{aligned}$$

where

$$\begin{cases} C_{T_o} = \frac{1}{L(2\pi f_{r_o})^2} \\ C_T = C_{T_o}(1 + 2\frac{\ell}{f_{r_o}}\ \Delta\Theta) \end{cases} \tag{4.120}$$

For the USR60: $\ell = 5\ Hz.\deg^{-1}$ and $2\frac{\ell}{f_{r_o}} \approx 2.5\ 10^{-4}$.

4.2.5 Simulation of the effect of varying temperature

The mechanical resonance frequency of the motor shifts towards lower frequencies during the operation of the motor due to the temperature increase within the body of the stator. In order to overcome this problem in a simulated environment and therefore predict the performance characteristics of the motor despite the changes in its temperature, a tracking facility which updates the temperature sensitive parameters is introduced in the equivalent circuit model. Figure 4.29 shows the prediction results achieved for the speed of the motor subject to temperature variation.

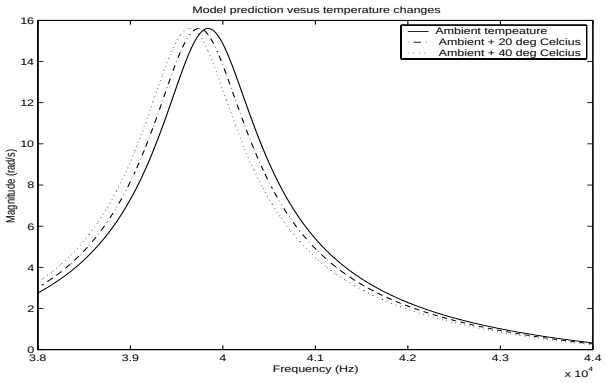

Figure 4.29: Speed prediction under varying temperature of the RPEM

From figure 4.29 it can be noticed that the resonance frequency is a decreasing function of temperature and consequently for a fixed frequency above the resonance frequency the performance of the motor in terms of speed deteriorates. The main conclusion to be drawn is that for speed control purposes the influence of temperature changes must be integrated in model prediction for long term operations.

4.3 Simulation and model validation

The derived equivalent circuit model of the RPEM is implemented in Matlab-Simulink environment using the power-system toolbox. The results achieved by the simulated model are then compared to the measured characteristics in order to enhance the validity of the model.

4.3.1 The effect of the driving frequency on the motor

The performance of the simulated model is given in terms of the output speed performance under varying frequency. The range of frequencies between 38 kHz and 44 kHz is explored and the achieved results are given in figure 4.30

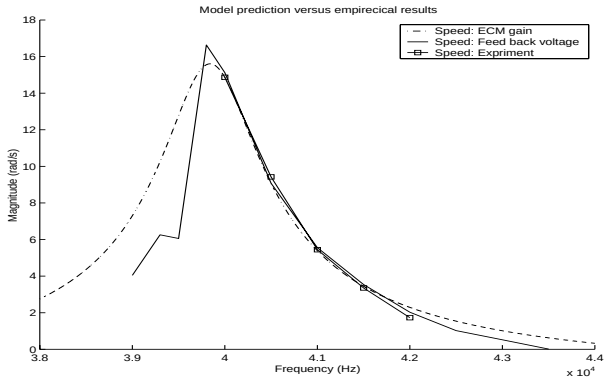

Figure 4.30: Comparison of speed-frequency characteristics for the unloaded RPEM: simulation, feedback prediction and measurement

It must be emphasized that the results reported in this figure are obtained for the free motor (i.e. no load) operating under its nominal conditions. In the same figure 4.30 are reported the results achieved by feedback prediction based on the proportionality between the feedback voltage amplitude and the output speed of the motor together with the real speed measured directly on the motor. It can be noticed that there is agreement between the simulated model, feedback prediction and the measured data, which validates both the equivalent circuit modeling of the free motor and the proportionality relationship between the amplitude of the feedback voltage and the rotary speed of the motor.

4.3.2 The effect of the varying torque on the loaded motor

The speed-torque relationship is the most important characteristic of any electromechanical motor and therefore model validation should respect this criterion. Figure 4.31 represents speed-frequency characteristics under different load torques obtained from direct measurement and feedback prediction when working under nominal conditions.

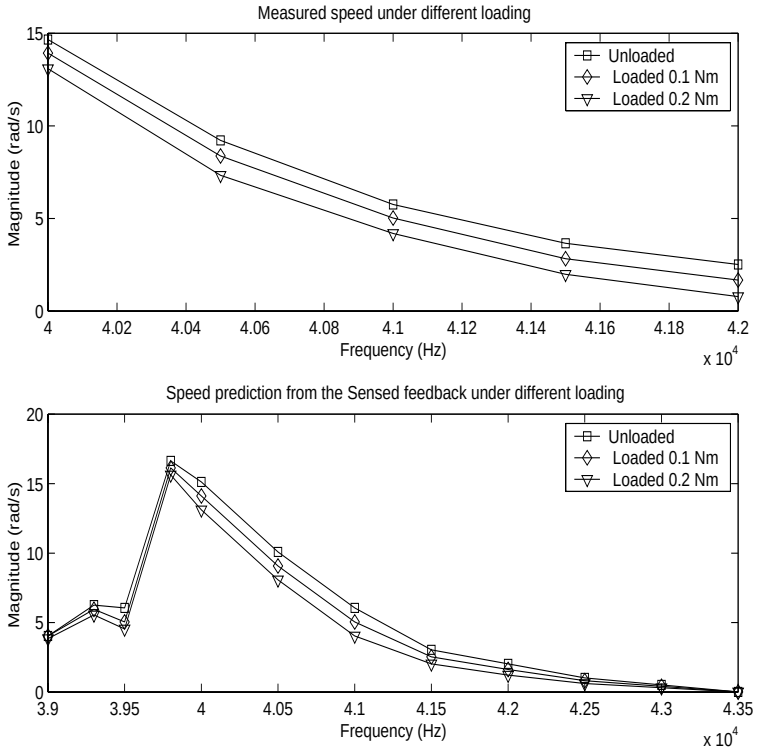

Figure 4.31: Speed-frequency characteristics of the RPEM under different load torques: measurement and feedback prediction

The range of torques between 0 Nm and 0.32 Nm is explored and the results achieved by the simulated model are given in figure 4.32 for the load torques 0.1 Nm and 0.2 Nm respectively.

It can be noticed from the compared results that there is agreement between the simulated results, feedback prediction results and the measured results, which validates the model in the range of torques $[0\ Nm, 0.32\ Nm]$ and frequencies of interest i.e. in the neighborhood above the fundamental resonance frequency.

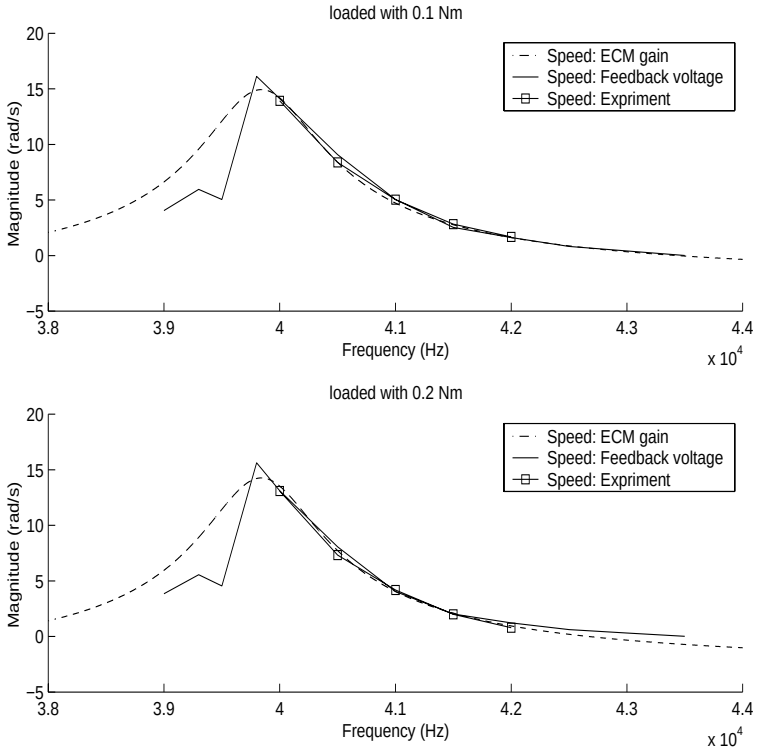

Figure 4.32: Comparison of speed-frequency characteristics for the RPEM subject to different load torques: simulation, feedback prediction and measurement

4.4 Conclusion and perspectives

In this chapter the modeling of the traveling wave motor USR60 has been addressed on the basis of the experimental investigation of the behavior of the motor in various working conditions and by observing the electromechanical admittance of the motor around its fundamental frequency. The equivalent circuit model has been derived by using the electrical network method together with various performance characteristics of the motor gathered from the experimental setup. This has made it possible to identify the electromechanical parameters of the motor. Thereafter, the derived model has been simulated in a Matlab-Simulink environment by using the power-system toolbox and the results achieved have been compared to the real performance of the motor and thereby the validity of the model has been established.

4.4.1 Advantages and performances

The main advantage of the ECM method is its simplicity compared to the highly demanding theoretical background necessary for understanding and modeling the piezoelectric transducers due to the extremely high nonlinearities of these devices. Consequently, by observing the admittance of any piezoelectric transducer in a narrow range of frequencies around its fundamental resonance frequency makes it possible to capture most of its features. This is necessary in order to predict the performance characteristics of the transducer by a simulated ECM model. Moreover, the computational burden of the ECM method is extremely low compared to other modeling methods such as FEM (Finite Element Method) usually used for modeling and analyzing these kinds of devices.

4.4.2 Drawbacks and limitations

There are many drawbacks of using the ECM method for modeling the RPEM, these are mainly related to its inability to accurately model the mechanical contact between the stator and the rotor and also the effect of temperature variation during long term operation on the performance of the motor. The stick-slip behavior at the contact surface of the driving mechanism has been simplified in the ECM model which hides some of the nonlinear behaviors of the real RPEM especially in the loaded case.

4.4.3 The alternatives

The results achieved by the ECM method can be used with benefit for modeling the stator part of the RPEM, whereas for modeling the contact mechanism other more suitable methods are necessary in order to take into account the nonlinearities of the real RPEM. The stick-slip behavior of the contact surface should be modeled by using the fundamental laws of dynamics and the theory of analytical contact mechanics. The objective is then to combine the strength of the ECM method with the fundamental laws of physics in order to overcome this highly demanding problem. The most appropriate method to be compared and then combined with the ECM modeling seems to be the analytical method which uses the energy method based on the variational work by applying Hamilton's principle.

Chapter 5

Analytical Model

In this chapter the necessary theoretical background of the electromechanical behavior in the rotary piezoelectric motor is first given, next, the state space model of the complete Rotary Piezo-Electrical Motor (RPEM) is derived by applying the basic laws of variational work and elasticity theory (Hamilton's principle). Thereafter, a reduced state space model is derived on the basis of the special design of the motor of interest (i.e. two phase symmetrical system). Finally, a further simplified model of the motor is given within the framework of various assumptions on the behavior of the stator. This makes it possible to predict the performance of the stator by a single second order system. Consequently, the complexity of the model is reduced.

5.1 The general framework model of the traveling wave piezoelectric motor

In this section the general framework mathematical model of the rotary piezoelectric motor will be introduced. The formulation of the problem is based on the energy method which uses Hamilton's principle.

5.1.1 The background of the general framework model derivation

The derivation begins by applying Hamilton's principle modified for general electromechanical systems (Hagood and Andrew (1995))

$$\delta \int_{t_1}^{t_2} L \, dt + \int_{t_1}^{t_2} \delta W \, dt = 0 \tag{5.1}$$

where L is the Lagrangian of the system and δW is the variational work done by the external forces. The Lagrangian is given by

$$L = E_k - E_p + E_e \tag{5.2}$$

where E_k is the kinetic energy, E_p is the potential energy and E_e is the electrical energy of the piezoelectric transducer. For the ring type piezoelectric stator shown in figure 5.1

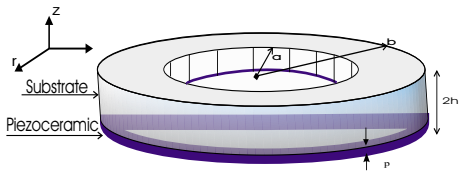

Figure 5.1: The ring type stator

These quantities are given by

$$E_k = \frac{1}{2}\int_{V_s} \rho_s \, \dot{\mathbf{u}}_o^t \dot{\mathbf{u}}_o \, dV + \frac{1}{2}\int_{V_p} \rho_p \, \dot{\mathbf{u}}_o^t \dot{\mathbf{u}}_o \, dV \tag{5.3}$$

$$E_p = \frac{1}{2}\int_{V_s} \mathbf{S}^t \mathbf{T} dV + \frac{1}{2}\int_{V_p} \mathbf{S}^t \mathbf{T} dV \tag{5.4}$$

$$E_e = \frac{1}{2}\int_{V_p} \mathbf{E}^t \mathbf{D} dV \tag{5.5}$$

where the superscript "t" denotes the mathematical transpose.

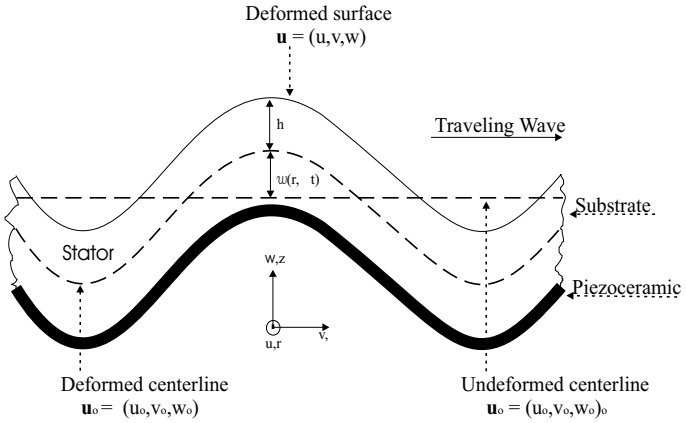

Figure 5.2: Section of the ring type stator undergoing bending deformations

where $\dot{\mathbf{u}}_o$ represents the three dimensional centerline velocity, which is the time derivative of the centerline displacement $\mathbf{u}_o$, in the r, θ and z directions, see figure 5.2, such that

$$\dot{\mathbf{u}}_o\ (r,\theta,z,t) = \frac{d}{dt}\begin{pmatrix} u_o(r,\theta,z,t) \\ v_o(r,\theta,z,t) \\ w_o(r,\theta,z,t) \end{pmatrix} \tag{5.6}$$

and where ρ_s and V_s are the mass density and the volume of the substrate respectively, ρ_p and V_p are the mass density and the volume of the piezo plate respectively, $\mathbf{S}$ represents the strain vector, $\mathbf{T}$ the stress vector, $\mathbf{D}$ is the electrical displacement vector and finally $\mathbf{E}$ is the electrical field vector.

Within the substrate, the strain-stress normal constitutive relation holds true

$$\mathbf{T} = \mathbf{c}_s \mathbf{S} \tag{5.7}$$

where $\mathbf{c}_s$ denotes the plane stress stiffness matrix within the substrate.

- **Hooke's law**: According to the generalized Hooke's law applied to an isotropic elastic thin layer the strain-stress relationship is given by the following stiffness matrix

$$\mathbf{c} = \begin{pmatrix} c_{11} & c_{12} & 0 \\ c_{21} & c_{22} & 0 \\ 0 & 0 & c_{66} \end{pmatrix} \tag{5.8}$$

  where

$$\begin{aligned} c_{11} &= c_{22} = \frac{J}{1-\nu^2} \\ c_{12} &= c_{21} = \frac{\nu J}{1-\nu^2} \\ c_{66} &= \mathtt{G} \end{aligned}$$

  and where J is Young's modulus, ν is the Poisson ratio and finally $\mathtt{G}$ is the shear modulus.

Within the piezoelectric material, the relevant fundamental constitutive relation is of the (S,E)-type given by

$$\begin{cases} \mathbf{D} = \varepsilon^S\ \mathbf{E} + \mathbf{e}\ \mathbf{S} \\ \mathbf{T} = -\mathbf{e}^t\ \mathbf{E} + \mathbf{c}^E\ \mathbf{S} \end{cases} \tag{5.9}$$

where the superscripts "S" and "E" refer to values taken at constant strain and constant electric field respectively and the superscript "t" denotes the mathematical transpose.

After the assumption that the depolarizing field is oriented parallel to axis 3 and also that the electrical field is applied parallel to the same axis 3, see section 2.2.2, both the electrical field and the electrical displacement vectors are reduced to one element

$$\begin{cases} \mathbf{D} = D_3 \\ \mathbf{E} = E_3 \end{cases}$$

i.e.

$$D_1 = D_2 = 0 \quad \text{and} \quad E_1 = E_2 = 0$$

Upon making the plane stress assumptions, the stress and the strain vectors are reduced to three elements in cylindrical coordinates

$$\begin{cases} \mathbf{S} = [S_1\ S_2\ S_6]^t \\ \mathbf{T} = [T_1\ T_2\ T_6]^t \end{cases}$$

i.e.

$$S_3 = S_4 = S_5 = 0 \quad \text{and} \quad T_3 = T_4 = T_5 = 0$$

This leads to the following reduced constitutive relations given by

$$\begin{pmatrix} D_3 \\ T_1 \\ T_2 \\ T_6 \end{pmatrix} = \begin{pmatrix} \varepsilon_{33}^S & e_{31} & e_{31} & 0 \\ -e_{31} & c_{11}^E & c_{12}^E & 0 \\ -e_{31} & c_{12}^E & c_{11}^E & 0 \\ 0 & 0 & 0 & c_{66}^E \end{pmatrix} \begin{pmatrix} E_3 \\ S_1 \\ S_2 \\ S_6 \end{pmatrix} \tag{5.10}$$

The strain-displacement relationship

The strain-displacement relations must be developed in cylindrical coordinates. According to Kirchoff's plate theory, which is valid only for thin plates

- **Kirchoff's statement**: The displacement of any point in the plate is a function of the plate's
  - Centerline displacements
    $$(u_o, v_o, w_o)$$
  - Centerline slope
    $$(\frac{\partial w_o}{\partial r}, \frac{1}{r}\frac{\partial w_o}{\partial \theta})$$
  - and the offset of that point from the centerline (z).

The displacement vector can then be written in cylindrical coordinates as

$$\begin{aligned}\mathbf{u}(r,\theta,z,t) &= \begin{pmatrix} u(r,\theta,z,t) \\ v(r,\theta,z,t) \\ w(r,\theta,z,t) \end{pmatrix} \\ &= \begin{pmatrix} u_o(r,\theta,z,t) - z\frac{\partial w_o(r,\theta,z,t)}{\partial r} \\ v_o(r,\theta,z,t) - z\frac{1}{r}\frac{\partial w_o(r,\theta,z,t)}{\partial \theta} \\ w_o(r,\theta,z,t) \end{pmatrix} \end{aligned} \tag{5.11}$$

Proceeding to the strain-displacement relationship in cylindrical coordinates, the strain vector is defined by

$$\begin{aligned}\mathbf{S}(r,\theta,z,t) &= \begin{pmatrix} S_1(r,\theta,z,t) \\ S_2(r,\theta,z,t) \\ S_6(r,\theta,z,t) \end{pmatrix} \\ &= \begin{pmatrix} \frac{\partial u(r,\theta,z,t)}{\partial r} \\ \frac{u(r,\theta,z,t)}{r} + \frac{1}{r}\frac{\partial v(r,\theta,z,t)}{\partial \theta} \\ \frac{1}{r}\frac{\partial u(r,\theta,z,t)}{\partial \theta} + \frac{\partial v(r,\theta,z,t)}{\partial r} - \frac{v(r,\theta,z,t)}{r} \end{pmatrix} \end{aligned} \tag{5.12}$$

The mid-plane deflections $\mathbf{u}_o(r,\theta,t)$ can be defined in several assumed modes, and are generally approximated via shape functions, (Hagood and Andrew (1995))

$$\mathbf{u}_o(r,\theta,t) = \Phi_m(r,\theta)\xi(t) \tag{5.13}$$

where ξ is the mechanical modal amplitude vector dependent only on time and Φ_m is the assumed mechanical mode matrix (called deflection matrix) dependent only on r and θ. It must be emphasized that the solution remains general for n assumed modes.

$$\mathbf{u}_o(r,\theta,z,t) = \begin{pmatrix} u_o(r,\theta,z,t) \\ v_o(r,\theta,z,t) \\ w_o(r,\theta,z,t) \end{pmatrix} = \begin{pmatrix} \phi_{u_1}(r,\theta) & .... & \phi_{u_n}(r,\theta) \\ \phi_{v_1}(r,\theta) & .... & \phi_{v_n}(r,\theta) \\ \phi_{w_1}(r,\theta) & .... & \phi_{w_n}(r,\theta) \end{pmatrix} \begin{pmatrix} \xi_1(t) \\ : \\ \xi_n(t) \end{pmatrix}$$

The relationship between the strain $\mathbf{S}$ and the centerline displacement is obtained by substituting (5.11) in (5.12) and rearranging the terms as follows

$$\begin{aligned} S_1 &= \frac{\partial}{\partial r}(u_o - z\frac{\partial w_o}{\partial r}) \\ &= \begin{pmatrix} \frac{\partial}{\partial r} & 0 & -z\frac{\partial^2}{\partial r^2} \end{pmatrix} \mathbf{u}_o \end{aligned} \tag{5.14}$$

$$\begin{aligned} S_2 &= \frac{1}{r}(u_o - z\frac{\partial w_o}{\partial r}) + \frac{1}{r}\frac{\partial}{\partial \theta}(v_o - z\frac{1}{r}\frac{\partial w_o}{\partial \theta}) \\ &= \begin{pmatrix} \frac{1}{r} & \frac{\partial}{r\partial \theta} & -\frac{z\partial}{r\partial r} - \frac{z\partial^2}{r^2\partial \theta^2} \end{pmatrix} \mathbf{u}_o \end{aligned} \tag{5.15}$$

$$\begin{aligned} S_6 &= \frac{1}{r}\frac{\partial}{\partial\theta}(u_o - z\frac{\partial w_o}{\partial r}) + \frac{\partial}{\partial r}(v_o - z\frac{1}{r}\frac{\partial w_o}{\partial\theta}) - \frac{1}{r}(v_o - z\frac{1}{r}\frac{\partial w_o}{\partial\theta}) \\ &= \begin{pmatrix} \frac{\partial}{r\partial\theta} & \frac{\partial}{\partial r} - \frac{1}{r} & -\frac{2z\partial^2}{r\partial r\partial\theta} + \frac{2z\partial}{r^2\partial\theta} \end{pmatrix} \mathbf{u}_o \end{aligned} \tag{5.16}$$

By gathering (5.14), (5.15) and (5.16) into a single matrix equation the strain shape vector $\mathbf{S}$ is then derived from the mid-plane deflections $\mathbf{u}_o$ as follows

$$\mathbf{S} = \mathbf{L}_m \mathbf{u}_o \tag{5.17}$$

where the (3x3)-matrix differential mapping operator $\mathbf{L}_m$, which is known as the Lazarus mapping operator, reads

$$\mathbf{L}_m = \begin{pmatrix} \frac{\partial}{\partial r} & 0 & -\frac{z\partial^2}{\partial r^2} \\ \frac{1}{r} & \frac{\partial}{r\partial\theta} & -\frac{z\partial}{r\partial r} - \frac{z\partial^2}{r^2\partial\theta^2} \\ \frac{\partial}{r\partial\theta} & \frac{\partial}{\partial r} - \frac{1}{r} & -\frac{2z\partial^2}{r\partial r\partial\theta} + \frac{2z\partial}{r^2\partial\theta} \end{pmatrix} \tag{5.18}$$

furthermore by inserting (5.13) in (5.17) the following relationship between the strain vector $\mathbf{S}$ and the modal amplitude vector $\xi(t)$ is obtained

$$\mathbf{S} = \mathbf{N}_m \xi(t) \tag{5.19}$$

where $\mathbf{N}_m$ is the strain matrix function of the coordinates (r, θ, z) and given by

$$\mathbf{N}_m = \mathbf{L}_m \Phi_m \tag{5.20}$$

The deflection matrix can be written

$$\Phi_m = \begin{pmatrix} \Phi_u \\ \Phi_v \\ \Phi_w \end{pmatrix} \tag{5.21}$$

where Φ_u, Φ_v and Φ_w are n-dimensional row vector shape functions. In the remaining developments, it is assumed that the mid-plane symmetric nature of the piezoceramics implies that no extension will be present within the stator i.e.

$$\begin{cases} u_o = 0 & v_o = 0 \\ \Phi_u = \mathbf{0} & \Phi_v = \mathbf{0} \end{cases} \tag{5.22}$$

Thereby the deflection matrix reduces to

$$\Phi_m = \begin{pmatrix} \mathbf{0} \\ \mathbf{0} \\ \Phi_w \end{pmatrix} = \Phi_w \tag{5.23}$$

The electrical field-voltage relationship

The assumed shapes on the electric potential φ within the stator is defined by

$$\varphi = \Phi_e \mathbf{v} \tag{5.24}$$

where Φ_e is the electrical shape matrix and $\mathbf{v}$ the voltage vector at the electrodes of the stator. Thereby the electrical field is given by

$$\mathbf{E} = -grad\ \varphi = \mathbf{L}_e \varphi \tag{5.25}$$

where the operator matrix $\mathbf{L}_e$ converts the assumed shapes on the potential at the electrodes φ to an electric field within the piezoelectric materials. The electric field is assumed to be constant and present only through the thickness of the piezoceramics. Consequently $\mathbf{L}_e$ is defined as a fraction

$$\mathbf{L}_e = \frac{1}{\iota_p} \tag{5.26}$$

where ι_p is the thickness of the piezoceramics. Furthermore, by substituting (5.24) in (5.25), the electrical field and the applied voltage relationship reads

$$\mathbf{E} = \mathbf{N}_e \mathbf{v} \tag{5.27}$$

where $\mathbf{N}_e$ is the electrical mapping operator given by

$$\mathbf{N}_e = \mathbf{L}_e \Phi_e \tag{5.28}$$

The work of external forces

The variational work due to the external forces on a piezoelectric body that has a volume V bounded by a surface $\mathcal{S}$ is given by

$$\delta W = \delta W_n + \delta W_t - \delta W_e \tag{5.29}$$

where δW_n is the variational normal work, δW_t is the variational tangential work, δW_e is the variational electrical work energy. A sketch of a loaded section of the naked complete motor is shown in figure 5.3.

- The variational electrical work energy due to the external charges reads

  $$\delta W_e = \mathbf{q}^t \delta \mathbf{v} \tag{5.30}$$

  where $\mathbf{q}$ is the electrical charge vector on the electrodes of the stator which reads

  $$\mathbf{q} = \iint_{\mathcal{S}} \sigma\ dS \tag{5.31}$$

  and where σ is the electrical charge density vector on the surface $\mathcal{S}$ that bounds the volume of the piezoelectric body.

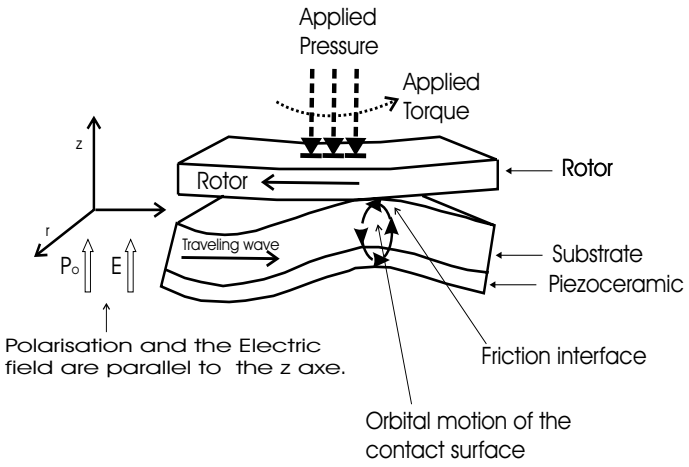

Figure 5.3: Section of the loaded ring-type piezoelectric motor where the forced stator is undergoing bending deformations

- The variational normal work reads

$$\delta W_n = \delta \xi^t \mathbf{F}_n^* \tag{5.32}$$

where $\mathbf{F_n^*}$ is the resulting normal modal forcing vector at the contact surface between the stator and the rotor. This force is expressed, see (Hagood and Andrew (1995)), by

$$\mathbf{F}_n^* = -\iint \Phi_w^t P(r,\theta,t) r dr d\theta \tag{5.33}$$

where $P(r,\theta,t)$ is the pressure distribution at the interface contact between the stator and the rotor.

- The variational tangential work reads

$$\delta W_t = \delta \xi^t \mathbf{F}_t^* \tag{5.34}$$

where $\mathbf{F_t^*}$ is the resulting tangential modal forcing vector at the contact surface between the stator and the rotor. This force vector is expressed, see (Hagood and Andrew (1995)), by

$$\begin{aligned} \mathbf{F}_t^* &= -\mu \iint (r\Phi_v^t + h\frac{\partial \Phi_w^t}{\partial \theta}) P(r,\theta,t)\ sign(v_s, v_\theta) dr d\theta \\ &= -\mu h \iint \frac{\partial \Phi_w^t}{\partial \theta} P(r,\theta,t)\ sign(v_s, v_\theta) dr d\theta \end{aligned} \tag{5.35}$$

where h is half of the height of the stator, μ is the Coulomb's friction coefficient, $\Phi_v^t = \mathbf{0}$ is assumed, see (5.22), and finally $sign(v_s, v_\theta)$ is the sign function depending on the relative velocity between the rotor and the surface of the stator. The sign function is given by

$$sign(v_s, v_\theta) = \begin{cases} +1 \text{ if } |v_s| > |v_\theta| \\ -1 \text{ if } |v_s| < |v_\theta| \end{cases} \tag{5.36}$$

where v_s is the velocity of the particles of the stator, which is a function of radius, offset distance from the centerline h and the modal amplitude time derivative and reads

$$v_s = \frac{-h}{r} \frac{\partial \Phi_w}{\partial \theta} \frac{d\xi}{dt} \tag{5.37}$$

and v_θ is the rotor velocity in circumferential direction, which is a function of the radius and angular velocity $\dot{\theta}$ and reads

$$v_\theta = r\dot{\theta} \tag{5.38}$$

The dynamic of the rotor

The dynamic of the rotor is considered by deriving its equations of motion in vertical and in spinning directions.

- The equation of the vertical motion reads

$$M_r \ddot{z} + \mathcal{D}_z \dot{z} = F_{int} - F_{app} \tag{5.39}$$

where z is the displacement in the vertical direction, M_r is the mass of the rotor, $\mathcal{D}_z$ is the damping in the vertical direction, F_{app} is the applied axial load and finally F_{int} is the force at the interface contact given by

$$F_{int} = \iint P(r, \theta, t)\, r dr d\theta \tag{5.40}$$

- The equation of the spinning motion reads

$$J_r \ddot{\theta} + \mathcal{D}_r \dot{\theta} = \mathcal{T}_{int} - \mathcal{T}_{app} \tag{5.41}$$

where θ is the angular position of the rotor, J_r is the rotor inertia, $\mathcal{D}_r$ the damping in the spinning direction, $\mathcal{T}_{app}$ is the applied torque and finally $\mathcal{T}_{int}$ is the torque at the interface contact given by

$$\mathcal{T}_{int} = \mu \iint sign(v_s, v_\theta) P(r, \theta, t) r^2 dr d\theta \tag{5.42}$$

Derivation of the equation of motion of the stator

It must be emphasized that E_k, E_p and E_e are linear elements, whereas δW_n , δW_t and δW_e are nonlinear and motion dependent. The equations of motion can be derived by making the appropriate substitutions for $E_k, E_p, E_e, \delta W_n$, δW_t and δW_e in (5.1) as shown in the following development

- **The kinetic energy**: By substituting (5.13) in (5.3) and rearranging the terms
  - The kinetic energy within the substrate reads

$$\frac{1}{2}\int_{V_s} \rho_s \ \dot{\mathbf{u}}_o^t \dot{\mathbf{u}}_o \ dV = \frac{1}{2}\int_{V_s} \dot{\xi}^t \ \Phi_m^t \rho_s \Phi_m \ \dot{\xi} \ dV = \frac{1}{2} \ \dot{\xi}^t \ \mathbf{M}_s \ \dot{\xi} \tag{5.43}$$

    where $\mathbf{M}_s$ is the modal mass matrix of the substrate

$$\mathbf{M}_s = \int_{V_s} \Phi_m^t \rho_s \Phi_m dV \tag{5.44}$$

  - The kinetic energy within the piezoelectric plate reads

$$\frac{1}{2}\int_{V_p} \rho_p \ \dot{\mathbf{u}}_o^t \dot{\mathbf{u}}_o \ dV = \frac{1}{2}\int_{V_p} \dot{\xi}^t \ \Phi_m^t \rho_p \Phi_m \ \dot{\xi} \ dV = \frac{1}{2} \ \dot{\xi}^t \ \mathbf{M}_p \ \dot{\xi} \tag{5.45}$$

    where $\mathbf{M}_p$ is the modal mass matrix of the piezoelectric plate

$$\mathbf{M}_p = \int_{V_p} \Phi_m^t \rho_p \Phi_m dV \tag{5.46}$$

  - The total modal mass matrix of the stator

$$\mathbf{M} = \mathbf{M}_s + \mathbf{M}_p \tag{5.47}$$

  Finally, by substituting (5.43), (5.45) and (5.47) in (5.3) the total kinetic energy becomes

$$E_k = \frac{1}{2} \ \dot{\xi}^t \ \mathbf{M}_s \ \dot{\xi} + \frac{1}{2} \ \dot{\xi}^t \ \mathbf{M}_p \ \dot{\xi} = \frac{1}{2} \ \dot{\xi}^t \ \mathbf{M} \ \dot{\xi} \tag{5.48}$$

- **The potential energy**: By substituting (5.7) and (5.9) in (5.4) the total potential energy reads

$$E_p = \frac{1}{2}\int_{V_s} \mathbf{S}^t \mathbf{c}_s \mathbf{S} dV + \frac{1}{2}\int_{V_p} \mathbf{S}^t (-\mathbf{e}^t \mathbf{E} + \mathbf{c}^E \mathbf{S}) dV \tag{5.49}$$

  and by substituting (5.19) and (5.27) in (5.49) and rearranging the terms

– The potential energy within the substrate reads

$$\frac{1}{2}\int_{V_s}\mathbf{S}^t\mathbf{c}_s\mathbf{S}dV = \frac{1}{2}\int_{V_s}\xi^t\mathbf{N}_m^t\mathbf{c}_s\mathbf{N}_m\xi dV = \frac{1}{2}\xi^t\mathbf{K}_s\xi \tag{5.50}$$

where $\mathbf{K}_s$ is the modal stiffness matrix of the substrate

$$\mathbf{K}_s = \int_{V_s}\mathbf{N}_m^t\mathbf{c}_s\mathbf{N}_m dV \tag{5.51}$$

– The potential energy due to the electromechanical coupling within the piezoelectric plate reads

$$\frac{1}{2}\int_{V_p}\mathbf{S}^t\mathbf{e}^t\mathbf{E}dV = \frac{1}{2}\int_{V_p}\xi^t\mathbf{N}_m^t\mathbf{e}^t\mathbf{N}_e\mathbf{v}dV = \frac{1}{2}\xi^t\mathrm{II}\mathbf{v} + \frac{1}{2}\mathbf{q}^t\mathbf{v} \tag{5.52}$$

where II is the modal electromechanical coupling matrix

$$\mathrm{II} = \int_{V_p}\mathbf{N}_m^t\mathbf{e}^t\mathbf{N}_e dV \tag{5.53}$$

– The pure mechanical potential energy within the piezoelectric plate reads

$$\frac{1}{2}\int_{V_p}\mathbf{S}^t\mathbf{c}^E\mathbf{S}dV = \frac{1}{2}\int_{V_p}\xi^t\mathbf{N}_m^t\mathbf{c}^E\mathbf{N}_m\xi dV = \frac{1}{2}\xi^t\mathbf{K}_p\xi \tag{5.54}$$

where $\mathbf{K}_p$ is the modal stiffness matrix of the piezoelectric plate

$$\mathbf{K}_p = \int_{V_p}\mathbf{N}_m^t\mathbf{c}^E\mathbf{N}_m dV \tag{5.55}$$

– The total modal stiffness matrix of the stator

$$\mathbf{K} = \mathbf{K}_s + \mathbf{K}_p \tag{5.56}$$

Finally, by substituting (5.50), (5.52), (5.54) and (5.56) in (5.49) the total potential energy becomes

$$E_p = \frac{1}{2}\xi^t\mathbf{K}_s\xi - \frac{1}{2}\xi^t\mathrm{II}\mathbf{v} + \frac{1}{2}\xi^t\mathbf{K}_p\xi = \frac{1}{2}\xi^t\mathbf{K}\xi - \frac{1}{2}\xi^t\mathrm{II}\mathbf{v} \tag{5.57}$$

- **The electrical energy**: By substituting (5.9) in (5.5) the total electrical energy reads

$$E_e = \frac{1}{2}\int_{V_p}\mathbf{E}^t(\varepsilon^S\mathbf{E} + \mathbf{e}\mathbf{S})dV \tag{5.58}$$

and by substituting (5.19) and (5.27) in (5.58) and rearranging the terms

– The electrical energy due to the electromechanical coupling within the piezoelectric plate reads

$$\frac{1}{2}\int_{V_p}\mathbf{E}^t\mathbf{e}\mathbf{S}dV = \frac{1}{2}\int_{V_p}\mathbf{v}^t\mathbf{N}_e^t\mathbf{e}\mathbf{N}_m\xi dV = \frac{1}{2}\mathbf{v}^t\mathrm{II}^t\xi \tag{5.59}$$

– The pure electrical energy within the piezoelectric plate reads

$$\frac{1}{2}\int_{V_p}\mathbf{E}^t\varepsilon^S\mathbf{E}dV = \frac{1}{2}\int_{V_p}\mathbf{v}^t\mathbf{N}_e^t\varepsilon^S\mathbf{N}_e\mathbf{v}dV = \frac{1}{2}\mathbf{v}^t\mathbf{C}_p\mathbf{v} \tag{5.60}$$

where $\mathbf{C}_p$ is the modal piezoelectric capacitance matrix

$$\mathbf{C}_p = \int_{V_p}\mathbf{N}_e^t\varepsilon^S\mathbf{N}_e dV \tag{5.61}$$

Finally, by substituting (5.59), (5.60) in (5.58) the total electrical energy becomes

$$E_e = \frac{1}{2}\mathbf{v}^t\mathbf{C}_p\mathbf{v}+\frac{1}{2}\mathbf{v}^t\mathrm{II}^t\xi \tag{5.62}$$

- **The Lagrangian**: By substituting (5.48), (5.57) and (5.62) in (5.2) the Lagrangian becomes

$$L = \frac{1}{2}\dot{\xi}^t\mathbf{M}\dot{\xi} - \frac{1}{2}\xi^t\mathbf{K}\xi+\frac{1}{2}\xi^t\mathrm{II}\mathbf{v}+\frac{1}{2}\mathbf{v}^t\mathbf{C}_p\mathbf{v}+\frac{1}{2}\mathbf{v}^t\mathrm{II}^t\xi \tag{5.63}$$

By further observing that the following propriety holds true, due to the fact that the transpose of a scalar is itself.

$$\xi^t\mathrm{II}\mathbf{v} = \mathbf{v}^t\mathrm{II}^t\xi \tag{5.64}$$

Then the Lagrangian reduces to

$$L = \frac{1}{2}\dot{\xi}^t\mathbf{M}\dot{\xi} - \frac{1}{2}\xi^t\mathbf{K}\xi + \xi^t\mathrm{II}\mathbf{v}+\frac{1}{2}\mathbf{v}^t\mathbf{C}_p\mathbf{v} \tag{5.65}$$

- **The variation of the Lagrangian**: A small variation of (5.65) is given by

$$\delta L = \delta(\frac{1}{2}\dot{\xi}^t\mathbf{M}\dot{\xi}) - \delta(\frac{1}{2}\xi^t\mathbf{K}\xi) + \delta(\xi^t\mathrm{II}\mathbf{v}) + \delta(\frac{1}{2}\mathbf{v}^t\mathbf{C}_p\mathbf{v}) \tag{5.66}$$

Furthermore, the following derivation properties will be used

$$\delta(\frac{1}{2}\dot{\xi}^t\mathbf{M}\dot{\xi}) = \delta\dot{\xi}^t\mathbf{M}\dot{\xi}=\dot{\xi}^t\mathbf{M}\delta\dot{\xi} \tag{5.67}$$

$$\delta(\frac{1}{2}\xi^t \mathbf{K}\xi) = \delta\xi^t\ \mathbf{K}\ \xi = \xi^t\ \mathbf{K}\ \delta\xi \tag{5.68}$$

$$\delta(\xi^t \amalg \mathbf{v}) = \delta\xi^t\ \amalg\mathbf{v} + \xi^t \amalg\ \delta\mathbf{v} \tag{5.69}$$

$$\delta(\frac{1}{2}\mathbf{v}^t \mathbf{C}_p \mathbf{v}) = \delta\mathbf{v}^t\ \mathbf{C}_p\mathbf{v} = \mathbf{v}^t\mathbf{C}_p\ \delta\mathbf{v} \tag{5.70}$$

By substituting (5.67), (5.68), (5.69) and (5.70) in (5.66) and rearranging the terms the variation of the Lagrangian becomes

$$\delta L = \dot{\xi}^t\ \mathbf{M}\ \delta\ \dot{\xi} - \delta\xi^t\ \mathbf{K}\ \xi + \delta\xi^t\ \amalg\mathbf{v} + \xi^t \amalg\ \delta\mathbf{v} + \mathbf{v}^t\mathbf{C}_p\ \delta\mathbf{v} \tag{5.71}$$

The kinetic energy term will be integrated by part. Thus the following derivation property will be used

$$\dot{\xi}^t\ \mathbf{M}\ \delta\ \dot{\xi} = \delta\ \dot{\xi}^t\ \mathbf{M}\ \dot{\xi} = \frac{d}{dt}(\delta\xi^t\ \mathbf{M}\ \dot{\xi}) - \delta\xi^t\ \mathbf{M}\ \ddot{\xi} \tag{5.72}$$

By substituting (5.72) in (5.71) the variation of the Lagrangian reads

$$\delta L = \frac{d}{dt}(\delta\xi^t\ \mathbf{M}\ \dot{\xi}) - \delta\xi^t\ \mathbf{M}\ \ddot{\xi} - \delta\xi^t\ \mathbf{K}\ \xi + \delta\xi^t\ \amalg\mathbf{v} + \xi^t \amalg\ \delta\mathbf{v} + \mathbf{v}^t\mathbf{C}_p\ \delta\mathbf{v}$$

After rearranging the terms the variation of the Lagrangian becomes

$$\delta L = \frac{d}{dt}(\delta\xi^t\ \mathbf{M}\ \dot{\xi}) - \delta\xi^t\ (\mathbf{M}\ \ddot{\xi} + \mathbf{K}\ \xi - \amalg\mathbf{v}\ ) + (\xi^t\ \amalg + \mathbf{v}^t\ \mathbf{C}_p)\delta\mathbf{v} \tag{5.73}$$

- **The variational work**: By substituting (5.30), (5.32) and (5.34) in (5.29) the variational work of the external forces becomes

$$\delta W = \delta\xi^t\ \mathbf{F}_n^* + \delta\xi^t\ \mathbf{F}_t^* - \mathbf{q}^t\ \delta\mathbf{v} \tag{5.74}$$

- **Model derivation**: The equation of motion will be derived by substitution of (5.73) and (5.74) in (5.1), which after rearranging the terms reads

$$\int_{t_1}^{t_2} [\frac{d}{dt}(\delta\xi^t\ \mathbf{M}\ \dot{\xi}) - \delta\xi^t\ (\mathbf{M}\ \ddot{\xi} + \mathbf{K}\ \xi - \amalg\mathbf{v}\ - \mathbf{F}_n^* - \mathbf{F}_t^*) + (\xi^t\ \amalg + \mathbf{v}^t\ \mathbf{C}_p - \mathbf{q}^t)\ \delta\mathbf{v}]\ dt = 0 \tag{5.75}$$

where the derivations $\delta\xi$ and $\delta\mathbf{v}$ are independent of each other and arbitrary quantities. By allowing arbitrary variation for ξ and $\mathbf{v}$, two matrix equations of motion, known as actuator equation and sensor equation respectively, are obtained

  - **The actuator equation**

$$\mathbf{M}\ \ddot{\xi} + \mathbf{K}\ \xi - \amalg\mathbf{v} - \mathbf{F}_n^* - \mathbf{F}_t^* = \mathbf{0} \tag{5.76}$$

  - **The sensor equation**

$$\amalg^t\ \xi + \mathbf{C}_p\mathbf{v} = \mathbf{q} \tag{5.77}$$

5.1.2 The general compact model representation

It must be noticed that in the non ideal case a damping matrix $\mathcal{D}$ must be added in the actuator equation (5.76) such that

$$\mathbf{M}\,\ddot{\xi} + \mathcal{D}\,\dot{\xi} + \mathbf{K}\,\xi - \mathrm{II}\mathbf{v} - \mathbf{F}_n^* - \mathbf{F}_t^* = \mathbf{0} \tag{5.78}$$

The actuator equation of motion of the stator (5.78) together with the rotor model in vertical (5.39) and spinning (5.41) directions constitute the following general model of the complete motor

$$\begin{cases} \mathbf{M}\,\ddot{\xi} + \mathcal{D}\,\dot{\xi} + \mathbf{K}\xi = \mathrm{II}\mathbf{v} + \mathbf{F}_\mathbf{n}^* + \mathbf{F}_\mathbf{t}^* \\ J_r\,\ddot{\theta} + D_r\,\dot{\theta} = \mathcal{T}_{int} - \mathcal{T}_{app} \\ M_r\,\ddot{z} + D_z\,\dot{z} = F_{int} - F_{app} \end{cases} \tag{5.79}$$

where $\mathbf{v}$ is the applied voltage through electrodes, $\mathbf{M}$ is the total mass matrix, $\mathcal{D}$ is the structural damping matrix assumed to be diagonal, $\mathbf{K}$ is the total stiffness matrix, II is the electromechanical coupling matrix. The parameters of the general model of the stator are recalled for convenience and reads

$$\mathbf{M} = \int_{V_s} \Phi_m^t \rho_s \Phi_m dV + \int_{V_p} \Phi_m^t \rho_p \Phi_m dV \tag{5.80}$$

$$\mathbf{K} = \int_{V_s} \mathbf{N}_m^t \mathbf{c}_s \mathbf{N}_m dV + \int_{V_p} \mathbf{N}_m^t \mathbf{c}_p \mathbf{N}_m dV \tag{5.81}$$

$$\mathrm{II} = \int_{V_p} \mathbf{N}_m^t \mathbf{e}^t \mathbf{N}_e dV \tag{5.82}$$

where $\mathbf{c}_p = \mathbf{c}^E$ denotes the plane stress stiffness matrix within the piezo plate, $\mathbf{N}_m$ is the strain shape matrix derived from the deflection shape matrix Φ_m by using Lazarus mapping operator matrix $\mathbf{L}_m$, $\mathbf{N}_e$ is the electrical field shape matrix derived from the electrical potential shape matrix Φ_e by using the electrical mapping operator matrix $\mathbf{L}_e$, $\mathbf{e}$ is the dielectric constant matrix, ε^S is the clamped dielectric constant matrix. The matrices $\mathbf{c}^E$, $\mathbf{e}$ and ε^S are respectively expressed in terms of the more commonly available compliance matrix $\mathbf{s}^E$, dielectric constant matrix $\mathbf{d}$ and free dielectric constant matrix ε^T as

$$\begin{cases} \mathbf{c}^E = (\mathbf{s}^E)^{-1} \\ \mathbf{e} = \mathbf{d}\mathbf{c}^E \\ \varepsilon^S = \varepsilon^T - \mathbf{d}\mathbf{c}^E\mathbf{d}^t \end{cases} \tag{5.83}$$

Within the framework of the previously made assumptions, see section 2.2.2, the different elements in (5.83) reduce to

$$\begin{aligned}
\mathbf{d} &= [d_{31}\ d_{31}\ 0] \\
\mathbf{c}^E &= \begin{pmatrix} s_{11}^E & s_{12}^E & 0 \\ s_{12}^E & s_{11}^E & 0 \\ 0 & 0 & s_{66}^E \end{pmatrix}^{-1} \\
&= \begin{pmatrix} c_{11}^E & c_{12}^E & 0 \\ c_{12}^E & c_{11}^E & 0 \\ 0 & 0 & c_{66}^E \end{pmatrix} \\
\mathbf{e} &= [e_{31}\ e_{31}\ 0] \\
\varepsilon^S &= \varepsilon_{33}^S \text{ and } \varepsilon^T = \varepsilon_{33}^T
\end{aligned}$$

where

$$c_{11}^E = \frac{s_{11}^E}{(s_{11}^E)^2 - (s_{12}^E)^2} \tag{5.84}$$

$$c_{12}^E = \frac{-s_{12}^E}{(s_{11}^E)^2 - (s_{12}^E)^2} \tag{5.85}$$

$$c_{66}^E = \frac{1}{s_{66}^E} \tag{5.86}$$

$$e_{31} = d_{31}(c_{11}^E + c_{12}^E) \tag{5.87}$$

$$\varepsilon_{33}^S = \varepsilon_{33}^T - 2d_{31}^2(c_{11}^E + c_{12}^E) \tag{5.88}$$

5.2 The state space model

Some necessary assumptions on the behavior of the stator will be stated in section 5.2.1. Then the applied voltage and the electric shape functions for the nine wave piezoelectric motor will be explicitly defined. Thereafter, in the framework of the made assumptions it will be shown that the parameters $\mathbf{M}$, $\mathbf{K}$ and Π reduce to diagonal matrices. Finally, a state space representation for the complete model of the motor will be given.

5.2.1 Assumptions

It is assumed that only two orthogonal mechanical modes ϕ_{w_1} and ϕ_{w_2} can be excited within the piezoceramic plate. These modes reads

$$\phi_{w_1} = R_r \cos k\theta \tag{5.89}$$

$$\phi_{w_2} = R_r \sin k\theta \tag{5.90}$$

Their temporal modal amplitudes, which are also orthogonal, are denoted by ξ_1 and ξ_2 respectively and reads

$$\xi_1(t) = A\cos\omega t \tag{5.91}$$

$$\xi_2(t) = A\sin\omega t \tag{5.92}$$

The superposition of their corresponding standing waves results in a traveling wave at the surface of the stator expressed by

$$\begin{aligned} w(r,\theta,t) &= \phi_{w_1}\xi_1(t) + \phi_{w_2}\xi_2(t) \\ &= R_r A\cos(\omega t - k\theta) \end{aligned} \tag{5.93}$$

where

$$A = \sqrt{\xi_1^2 + \xi_2^2} \tag{5.94}$$

$$R_r = (\frac{r-a}{b-a})^{\gamma} \tag{5.95}$$

$$k = \frac{2\pi R_o}{\lambda} \tag{5.96}$$

$$R_o = \frac{b-a}{2} \tag{5.97}$$

where A is the maximum temporal amplitude of the traveling wave, ω is the angular frequency, R_r is the shape of the traveling wave in radial direction, a and b are the inner and outer radius of the annular plate of the stator respectively and γ is a constant depending on the modal shape of the deformation of the stator in the radial direction, k is the wave number which is also the number of nodal diameters, λ is the wave length, R_o is the middle radius of the annular plate where the contact interface between the stator and the rotor is mainly concentrated. The geometrical parameters of the stator are shown in figure 5.4

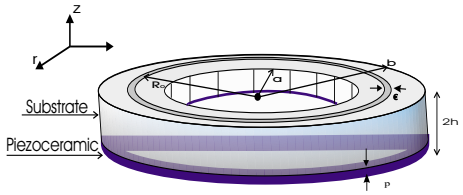

Figure 5.4: The geometry of the stator

Under these assumptions the mechanical mode matrix reduces to

$$\Phi_m = \begin{pmatrix} 0 & 0 \\ 0 & 0 \\ \phi_{w_1} & \phi_{w_2} \end{pmatrix} = \Phi_w \tag{5.98}$$

5.2.2 The applied voltage

The rotary PEM which is considered in this thesis is a nine wave two phase motor, where the annular plate of the stator is divided into three sections see figure 5.5. One section is the phase *A* supplied by voltage V_A, the second is phase *B* supplied by voltage V_B and the third is phase *C* connected to the ground. It must be emphasized that section *C* is made of two separated parts, a small part of length $(\lambda/4)$ used as a feedback electrode and a large part of length $(3\lambda/4)$ directly connected to the ground. The electrical potential φ at the free surface of the nine wave piezoceramic ring is the product of the electrical shape functions and the applied voltage, which can be written in vector notation as follows

$$\varphi = \Phi_e \mathbf{v} = \left(\phi_A(\theta)\ \phi_B(\theta) \right) \begin{pmatrix} V_A(t) \\ V_B(t) \end{pmatrix} \tag{5.99}$$

where the components of the applied voltage **v** are explicitly given by

$$\begin{cases} V_A(t) = \hat{V} \cos \omega t \\ V_B(t) = \hat{V} \sin \omega t \end{cases} \tag{5.100}$$

and the electrical shape functions for the nine wave motor are explicitly defined by

$$\begin{aligned} \phi_A(\theta) &= \begin{cases} 1 \text{ if } \frac{\pi}{18} + k\lambda < \theta < \frac{3\pi}{18} + k\lambda \\ -1 \text{ if } \frac{3\pi}{18} + k\lambda < \theta < \frac{5\pi}{18} + k\lambda \end{cases} \\ \phi_B(\theta) &= \begin{cases} 1 \text{ if } \pi + k\lambda < \theta < \frac{10\pi}{9} + k\lambda \\ -1 \text{ if } \frac{10\pi}{9} + k\lambda < \theta < \frac{11\pi}{9} + k\lambda \end{cases} \\ & for\ k = 0, .., 4. \end{aligned} \tag{5.101}$$

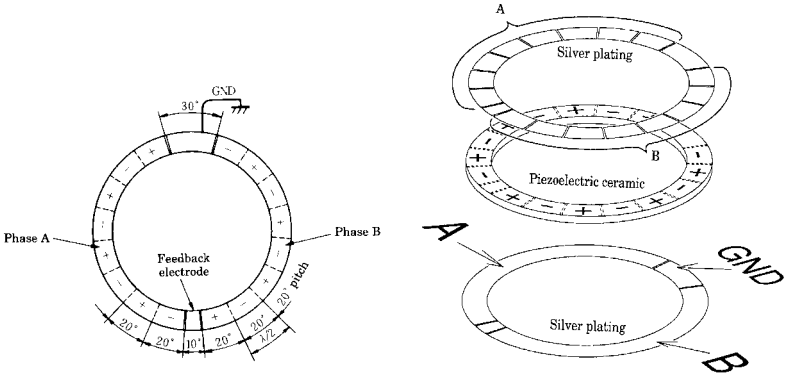

Figure 5.5: The nine wave piezoceramic ring

5.2.3 Calculation and diagonalization of the modal mass matrix

The modal mass matrix $\mathbf{M}$ of any vibrating plate of volume mass density ρ and total volume V_t is a function of the mechanical deflection matrix Φ_m and reads

$$\mathbf{M} = \int_{V_t} \Phi_m^t \rho \Phi_m dV \tag{5.102}$$

Consequently, the total modal mass matrix $\mathbf{M}$ of the piezoelectric stator is constituted by the modal mass matrix $\mathbf{M}_s$ of the substrate and the modal mass matrix $\mathbf{M}_p$ of the piezoelectric plate, such that

$$\begin{aligned} \mathbf{M} &= \mathbf{M}_s + \mathbf{M}_p \\ &= \rho_s \int_{V_s} \Phi_m^t \Phi_m dV + \rho_p \int_{V_p} \Phi_m^t \Phi_m dV \end{aligned}$$

where ρ_s and V_s are the mass density and the volume of the substrate respectively, ρ_p and V_p are the mass density and the volume of the piezo plate respectively, and where by using (5.98), (5.89) and (5.90) the following reads

$$\begin{aligned} \Phi_m^t \Phi_m &= \begin{pmatrix} \phi_{w_1}^2 & \phi_{w_1}\phi_{w_2} \\ \phi_{w_1}\phi_{w_2} & \phi_{w_2}^2 \end{pmatrix} \\ &= \begin{pmatrix} R_r^2 \cos^2 k\theta & R_r^2 \cos k\theta \sin k\theta \\ R_r^2 \cos k\theta \sin k\theta & R_r^2 \sin^2 k\theta \end{pmatrix} \end{aligned}$$

and finally the total modal mass matrix is given by

$$\mathbf{M} = \rho_s \int_{\iota_p}^{2h} \begin{pmatrix} m_{11} & m_{12} \\ m_{21} & m_{22} \end{pmatrix} dz + \rho_p \int_0^{\iota_p} \begin{pmatrix} m_{11} & m_{12} \\ m_{21} & m_{22} \end{pmatrix} dz \tag{5.103}$$

where ι_p is the thickness of the piezoelectric plate and $2h - \iota_p$ is the thickness of the substrate and where the m_{ij} components are given by

$$\begin{cases} m_{11} = \iint R_r^2 \cos^2 k\theta \; r dr d\theta \\ m_{12} = \iint R_r^2 \cos k\theta \sin k\theta \; r dr d\theta \\ m_{21} = \iint R_r^2 \cos k\theta \sin k\theta \; r dr d\theta \\ m_{22} = \iint R_r^2 \sin^2 k\theta \; r dr d\theta \end{cases} \tag{5.104}$$

By further calculating the integrals in (5.104) , over the surface of contact between the stator and the rotor, the following is obtained

$$\begin{cases} m_{11} = m_{22} = m_z \\ m_{12} = m_{21} = 0 \end{cases}$$

Finally, the modal mass matrix is diagonalized and reads

$$\mathbf{M} = \begin{pmatrix} M & 0 \\ 0 & M \end{pmatrix} \tag{5.105}$$

where M is the modal mass of the stator.

$$M = \rho_s \int_{\iota_p}^{2h} m_z dz + \rho_p \int_0^{\iota_p} m_z dz \tag{5.106}$$

5.2.4 Calculation and diagonalization of the modal stiffness matrix

The modal stiffness matrix $\mathbf{K}$ of any vibrating plate of volume stiffness matrix $\mathbf{c}$ and total volume V_t is a function of the strain shape matrix $\mathbf{N}_m$ and reads

$$\mathbf{K} = \int_{V_t} \mathbf{N}_m^t \mathbf{c} \mathbf{N}_m dV \tag{5.107}$$

where the volume stiffness matrix $\mathbf{c}$ of the elastic plate is given in (5.8). The strain shape matrix $\mathbf{N}_m$ is derived from the deflection shape matrix $\mathbf{\Phi}_m$ by using Lazarus mapping operator matrix $\mathbf{L}_m$ given in (5.18) such that

$$\begin{aligned}
\mathbf{N}_m &= \mathbf{L}_m \mathbf{\Phi}_m = \begin{pmatrix} \frac{\partial}{\partial r} & 0 & -\frac{z\partial^2}{\partial r^2} \\ \frac{1}{r} & \frac{\partial}{r\partial\theta} & -\frac{z\partial}{r\partial r} - \frac{z\partial^2}{r^2\partial\theta^2} \\ \frac{\partial}{r\partial\theta} & \frac{\partial}{\partial r} - \frac{1}{r} & -\frac{2z\partial^2}{r\partial r\partial\theta} + \frac{2z\partial}{r^2\partial\theta} \end{pmatrix} \begin{pmatrix} 0 & 0 \\ 0 & 0 \\ \phi_{w_1} & \phi_{w_2} \end{pmatrix} \\
&= \begin{pmatrix} -\frac{z\partial^2(R_r\cos k\theta)}{\partial r^2} & -\frac{z\partial^2(R_r\sin k\theta)}{\partial r^2} \\ -\frac{z\partial(R_r\cos k\theta)}{r\partial r} - \frac{z\partial^2(R_r\cos k\theta)}{r^2\partial\theta^2} & -\frac{z\partial(R_r\sin k\theta)}{r\partial r} - \frac{z\partial^2(R_r\sin k\theta)}{r^2\partial\theta^2} \\ -\frac{2z\partial^2(R_r\cos k\theta)}{r\partial r\partial\theta} + \frac{2z\partial(R_r\cos k\theta)}{r^2\partial\theta} & -\frac{2z\partial^2(R_r\sin k\theta)}{r\partial r\partial\theta} + \frac{2z\partial(R_r\sin k\theta)}{r^2\partial\theta} \end{pmatrix}
\end{aligned}$$

where it is assumed in section 5.2.1 that $R_r = \left(\frac{r-a}{b-a}\right)^\gamma$ is the shape of the traveling wave in radial direction, with γ a rational number. The first and the second derivative of R_r are given below

$$\begin{cases} \frac{\partial R_r}{\partial r} = \frac{\gamma}{r-a} R_r \\ \frac{\partial^2 R_r}{\partial r^2} = \frac{\gamma(\gamma-1)}{(r-a)^2} R_r \end{cases} \tag{5.108}$$

which leads to the following assumed strain shape matrix

$$\mathbf{N}_m = \begin{pmatrix} -\frac{z\gamma(\gamma-1)}{(r-a)^2} R_r \cos k\theta & -\frac{z\gamma(\gamma-1)}{(r-a)^2} R_r \sin k\theta \\ -\frac{z}{r}[\frac{\gamma}{r-a} - \frac{k^2}{r}] R_r \cos k\theta & -\frac{z}{r}[\frac{\gamma}{r-a} - \frac{k^2}{r}] R_r \sin k\theta \\ \frac{2zk}{r}[\frac{\gamma}{r-a} - \frac{1}{r}] R_r \sin k\theta & -\frac{2zk}{r}[\frac{\gamma}{r-a} - \frac{1}{r}] R_r \cos k\theta \end{pmatrix} = \begin{pmatrix} \mathbf{I} & \mathbf{J} \end{pmatrix} \tag{5.109}$$

where **I** and **J** are vectors given by

$$\mathbf{I} = \begin{pmatrix} i_1 \\ i_2 \\ i_3 \end{pmatrix} = \begin{pmatrix} -\frac{z\gamma(\gamma-1)}{(r-a)^2} R_r \cos k\theta \\ -\frac{z}{r}[\frac{\gamma}{r-a} - \frac{k^2}{r}] R_r \cos k\theta \\ \frac{2zk}{r}[\frac{\gamma}{r-a} - \frac{1}{r}] R_r \sin k\theta \end{pmatrix} \tag{5.110}$$

$$\mathbf{J} = \begin{pmatrix} j_1 \\ j_2 \\ j_3 \end{pmatrix} = \begin{pmatrix} -\frac{z\gamma(\gamma-1)}{(r-a)^2} R_r \sin k\theta \\ -\frac{z}{r}[\frac{\gamma}{r-a} - \frac{k^2}{r}] R_r \sin k\theta \\ -\frac{2zk}{r}[\frac{\gamma}{r-a} - \frac{1}{r}] R_r \cos k\theta \end{pmatrix} \tag{5.111}$$

The stiffness matrix of a thin layer of the annular plate will be derived as follow

$$\begin{aligned} \mathbf{N}_m^t \mathbf{c} \mathbf{N}_m &= \begin{pmatrix} i_1 & i_2 & i_3 \\ j_1 & j_2 & j_3 \end{pmatrix} \begin{pmatrix} c_{11} & c_{12} & 0 \\ c_{12} & c_{11} & 0 \\ 0 & 0 & c_{66} \end{pmatrix} \begin{pmatrix} i_1 & j_1 \\ i_2 & j_2 \\ i_3 & j_3 \end{pmatrix} \\ &= \begin{pmatrix} n_{11} & n_{12} \\ n_{21} & n_{22} \end{pmatrix} \end{aligned} \tag{5.112}$$

where

$$\begin{cases} n_{11} = (i_1^2 + i_2^2)c_{11} + 2i_1 i_2 c_{12} + i_3^2 c_{66} \\ n_{22} = (j_1^2 + j_2^2)c_{11} + 2j_1 j_2 c_{12} + j_3^2 c_{66} \\ n_{12} = (i_1 j_1 + i_2 j_2)c_{11} + (i_1 j_2 + i_2 j_1)c_{12} + i_3 j_3 c_{66} \\ n_{12} = n_{21} \end{cases} \tag{5.113}$$

and where by using the following functions

$$\begin{cases} \Upsilon_1(r,z) = [\frac{z^2\gamma^2(\gamma-1)^2}{(r-a)^4} + \frac{z^2}{r^2}(\frac{\gamma}{r-a} - \frac{k^2}{r})^2] R_r^2 \\ \Upsilon_2(r,z) = 2\frac{z^2\gamma(\gamma-1)}{r(r-a)^2}[\frac{\gamma}{r-a} - \frac{k^2}{r}] R_r^2 \\ \Upsilon_3(r,z) = \frac{4z^2k^2}{r^2}[\frac{\gamma}{r-a} - \frac{1}{r}]^2 R_r^2 \end{cases}$$

hence, the coefficients in relation (5.113) are given by

$$\begin{cases} i_1^2 + i_2^2 = \Upsilon_1(r,z)\cos^2 k\theta \\ 2i_1 i_2 = \Upsilon_2(r,z)\cos^2 k\theta \\ i_3^2 = \Upsilon_3(r,z)\sin^2 k\theta \\ j_1^2 + j_2^2 = \Upsilon_1(r,z)\sin^2 k\theta \\ 2j_1 j_2 = \Upsilon_2(r,z)\sin^2 k\theta \\ j_3^2 = \Upsilon_3(r,z)\cos^2 k\theta \\ i_1 j_1 + i_2 j_2 = \Upsilon_1(r,z)\sin k\theta \cos k\theta \\ i_1 j_2 + i_2 j_1 = \Upsilon_2(r,z)\sin k\theta \cos k\theta \\ i_3 j_3 = \Upsilon_3(r,z)\sin k\theta \cos k\theta \end{cases}$$

which leads to

$$\begin{cases} n_{11} = [\Upsilon_1(r,z)c_{11} + \Upsilon_2(r,z)c_{12}]\cos^2 k\theta + \Upsilon_3(r,z)c_{66}\sin^2 k\theta \\ n_{22} = [\Upsilon_1(r,z)c_{11} + \Upsilon_2(r,z)c_{12}]\sin^2 k\theta + \Upsilon_3(r,z)c_{66}\cos^2 k\theta \\ n_{12} = [\Upsilon_1(r,z)c_{11} + \Upsilon_2(r,z)c_{12} + \Upsilon_3(r,z)c_{66}]\sin k\theta\cos k\theta \\ n_{12} = n_{21} \end{cases}$$

By using the following periodic properties of the cosine basis in calculating (5.107) and (5.112)

$$\begin{cases} \int_0^{2\pi} cos^2 k\theta d\theta = \int_0^{2\pi} sin^2 k\theta d\theta \\ \int_0^{2\pi} \sin k\theta\cos k\theta d\theta = 0 \end{cases}$$

the following stiffness matrix is derived

$$\mathbf{K} = \int_{V_t} \begin{pmatrix} n_{11} & n_{12} \\ n_{21} & n_{22} \end{pmatrix} dV = \begin{pmatrix} K_i & 0 \\ 0 & K_i \end{pmatrix} \tag{5.114}$$

where

$$\begin{cases} \int_{V_t} n_{11} dV = \int_{V_t} n_{22} dV = K_i \\ \int_{V_t} n_{12} dV = \int_{V_t} n_{21} dV = 0 \end{cases}$$

Thereby, the diagonalization of the stiffness matrix of an elastic plate is achieved. Consequently, the total stiffness matrix of the stator which is the summation of the stiffness matrix of the piezoelectric plate and the stiffness matrix of the substrate such that

$$\begin{aligned} \mathbf{K} &= \mathbf{K}_p + \mathbf{K}_s \\ &= \int_{V_p} \mathbf{N}_m^t \mathbf{c}_p \mathbf{N}_m dV + \int_{V_s} \mathbf{N}_m^t \mathbf{c}_s \mathbf{N}_m dV \end{aligned} \tag{5.115}$$

leads to the following diagonal form

$$\mathbf{K} = \begin{pmatrix} K_o & 0 \\ 0 & K_o \end{pmatrix} \tag{5.116}$$

where

$$K_o = K_p + K_s$$

is the total modal stiffness of the stator, which is the summation of the modal stiffness of the piezo plate and the modal stiffness of the substrate.

5.2.5 Calculation and diagonalization of the electromechanical coupling matrix

The electromechanical coupling matrix II of any vibrating piezoelectric plate of dielectric constant matrix $\mathbf{e}$ and volume V_p is a function of the electrical field shape matrix $\mathbf{N}_e$ and of the strain shape matrix $\mathbf{N}_m$ and reads

$$\mathrm{II} = \int_{V_p} \mathbf{N}_m^t \mathbf{e}^t \mathbf{N}_e dV \tag{5.117}$$

Within the framework of the assumptions made in section 2.2.2 the dielectric constant matrix $\mathbf{e}$ reduces to the following vector

$$\mathbf{e}^t = \left[\begin{array}{ccc} e_{31} & e_{31} & 0 \end{array} \right]^t \tag{5.118}$$

where e_{31} is the dielectric constant defined in (5.87). The electrical field shape matrix is given in (5.28) and reads

$$\mathbf{N}_e = \mathbf{L}_e \mathbf{\Phi}_e = \frac{1}{\iota_p} \left(\begin{array}{cc} \phi_A & \phi_B \end{array} \right) \tag{5.119}$$

where $\mathbf{L}_e = \frac{1}{\iota_p}$ is the electrical mapping operator, ι_p is the thickness of the piezo plate and finally ϕ_A and ϕ_B are the assumed shapes of the electric potential within the stator defined in (5.101).

Moreover by using (5.119), (5.118) and (5.109) the following matrix equation

$$\mathbf{N}_m^t \mathbf{e}^t \mathbf{N}_e = \frac{e_{31}}{\iota_p} \left(\begin{array}{cc} (i_1 + i_2)\,\phi_A & (i_1 + i_2)\,\phi_B \\ (j_1 + j_2)\,\phi_A & (j_1 + j_2)\,\phi_B \end{array} \right)$$

leads to the following matrix integral equation

$$\begin{aligned} \mathrm{II} &= \frac{e_{31}}{\iota_p} \int_{V_p} \left(\begin{array}{cc} (i_1 + i_2)\,\phi_A & (i_1 + i_2)\,\phi_B \\ (j_1 + j_2)\,\phi_A & (j_1 + j_2)\,\phi_B \end{array} \right) dV \\ &= \left(\begin{array}{cc} \eta_{11} & \eta_{12} \\ \eta_{21} & \eta_{22} \end{array} \right) \end{aligned} \tag{5.120}$$

By using the following function in (5.120)

$$\chi(r,z) = -[\frac{z\gamma(\gamma-1)}{(r-a)^2} + \frac{z}{r}(\frac{\gamma}{r-a} - \frac{k^2}{r})]R_r$$

then, the following writes

$$\left\{ \begin{array}{l} i_1 + i_2 = \chi(r,z)\cos k\theta \\ j_1 + j_2 = \chi(r,z)\sin k\theta \end{array} \right. \tag{5.121}$$

which leads to the following components of the electromechanical coupling matrix

$$\begin{cases} \eta_{11} = \frac{e_{31}}{\iota_p} \int_{V_p} \chi(r,z) \cos k\theta \; \phi_A dV \\ \eta_{12} = \frac{e_{31}}{\iota_p} \int_{V_p} \chi(r,z) \cos k\theta \; \phi_B dV \\ \eta_{21} = \frac{e_{31}}{\iota_p} \int_{V_p} \chi(r,z) \sin k\theta \; \phi_A dV \\ \eta_{22} = \frac{e_{31}}{\iota_p} \int_{V_p} \chi(r,z) \sin k\theta \; \phi_B dV \end{cases} \tag{5.122}$$

Furthermore, by using the potential functions defined in (5.101) and by proceeding to further calculations of the integrals in (5.122), over the total volume of the piezoelectric plate, the following is obtained

$$\begin{cases} \eta_{11} = \eta_{22} = \eta \\ \eta_{12} = \eta_{21} = 0 \end{cases}$$

Finally, the electromechanical coupling matrix is diagonalized and reads

$$\text{II} = \begin{pmatrix} \eta & 0 \\ 0 & \eta \end{pmatrix} \tag{5.123}$$

where η is the modal electromechanical force factor.

5.2.6 The state space representation

After substituting (5.105), (5.116) and (5.123) in (5.79) and rearranging the terms, the following general model of the complete motor is obtained

$$\begin{cases} M \; \ddot{\xi}_1 + \mathcal{D}_o \; \dot{\xi}_1 + K_o \xi_1 = \eta V_A + F_{n1} + F_{t1} \\ M \; \ddot{\xi}_2 + \mathcal{D}_o \; \dot{\xi}_2 + K_o \xi_2 = \eta V_B + F_{n2} + F_{t2} \\ J_r \; \ddot{\theta} + \mathcal{D}_r \; \dot{\theta} = \mathcal{T}_{int} - \mathcal{T}_{app} \\ M_r \; \ddot{z} + \mathcal{D}_z \; \dot{z} = F_{int} - F_{app} \end{cases} \tag{5.124}$$

where the assumed diagonal form of the damping matrix $\mathcal{D}$, the components of the normal force vector $\mathbf{F}_n^*$ and the components of the tangential force vector $\mathbf{F}_t^*$, which are respectively given by

$$\mathcal{D} = \begin{pmatrix} \mathcal{D}_o & 0 \\ 0 & \mathcal{D}_o \end{pmatrix} \tag{5.125}$$

$$\mathbf{F}_n^* = \begin{pmatrix} F_{n1} \\ F_{n2} \end{pmatrix} \tag{5.126}$$

$$\mathbf{F}_t^* = \begin{pmatrix} F_{t1} \\ F_{t2} \end{pmatrix} \tag{5.127}$$

are used.

This analytical model is the state space description of the equation of motion of the motor given by

$$\dot{\mathbf{x}} = A_* \mathbf{x} + B_* \mathbf{u} \tag{5.128}$$

where the total state vector is composed by the state components of the stator and the rotor respectively and is given by

$$\mathbf{x} = \begin{bmatrix} \xi_1 & \xi_2 & \dot{\xi}_1 & \dot{\xi}_2 & \theta & \dot{\theta} & z & \dot{z} \end{bmatrix}^t \tag{5.129}$$

and where the input components are

$$\mathbf{u} = \begin{pmatrix} \eta V_A + F_{n1} + F_{t1} \\ \eta V_B + F_{n2} + F_{t2} \\ \mathcal{T}_{int} - \mathcal{T}_{app} \\ F_{int} - F_{app} \end{pmatrix} \tag{5.130}$$

and finally the transfer matrices

$$A_* = \begin{pmatrix} 0 & 0 & 1 & 0 & 0 & 0 & 0 & 0 \\ 0 & 0 & 0 & 1 & 0 & 0 & 0 & 0 \\ \frac{-K_o}{M} & 0 & \frac{-\mathcal{D}_o}{M} & 0 & 0 & 0 & 0 & 0 \\ 0 & \frac{-K_o}{M} & 0 & \frac{-\mathcal{D}_o}{M} & 0 & 0 & 0 & 0 \\ 0 & 0 & 0 & 0 & 0 & 1 & 0 & 0 \\ 0 & 0 & 0 & 0 & 0 & -\frac{\mathcal{D}_r}{J_r} & 0 & 0 \\ 0 & 0 & 0 & 0 & 0 & 0 & 0 & 1 \\ 0 & 0 & 0 & 0 & 0 & 0 & 0 & \frac{-\mathcal{D}_z}{M_r} \end{pmatrix}$$

$$B_* = \begin{pmatrix} 0 & 0 & 0 & 0 \\ 0 & 0 & 0 & 0 \\ \frac{\eta}{M} & 0 & 0 & 0 \\ 0 & \frac{\eta}{M} & 0 & 0 \\ 0 & 0 & 0 & 0 \\ 0 & 0 & \frac{1}{J_r} & 0 \\ 0 & 0 & 0 & 0 \\ 0 & 0 & 0 & \frac{1}{M_r} \end{pmatrix}$$

5.3 The explicit state space model

In this section the pressure distribution at the stator-rotor interface contact will first be defined. Thereafter, the nonlinear elements in the state space model will be derived explicitly as a function of the excited modes and load characteristics. Finally, an explicit state space representation of the complete motor will be given.

5.3.1 The pressure distribution at the stator-rotor interface contact

It is assumed that the stator is a rigid body along the contact interface, whereas the rotor can be modeled as a linear spring (Hagood and Andrew (1995)). The overlap between the stator and the rotor defines the compression of the spring, thereby the pressure distribution that acts on the stator at the interface contact with the rotor is given by

$$P(r,\theta,t) = \begin{cases} \varkappa_r g(r,\theta,z,t) & \text{if} \quad g(r,\theta,z,t) > 0 \\ 0 & \text{if} \quad g(r,\theta,z,t) < 0 \end{cases} \tag{5.131}$$

where

$$\begin{aligned} g(r,\theta,z,t) &= w(r,\theta,t) + h - z(t) \\ &= R_r A \cos(\omega t - k\theta) + h - z(t) \end{aligned} \tag{5.132}$$

and where $\varkappa_r$ is the rotor stiffness, which is essentially a stiffness per unit area of contact. A sketch of the contact mechanism is shown in figure 5.6 where $w(r,\theta,t)$, h and $z(t)$ can be noticed.

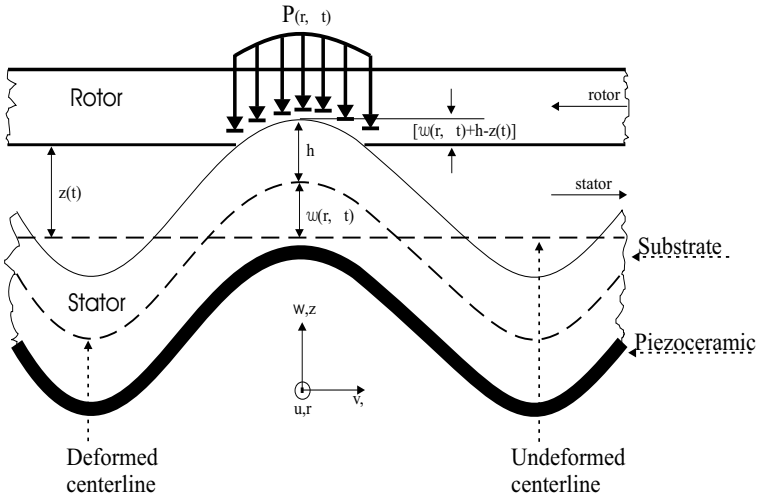

Figure 5.6: Section of the loaded stator undergoing bending deformations

The pressure distribution is a function of time because it travels along with the wave crests at the speed of the traveling wave, therefore it is more appropriate to introduce a wave oriented coordinate system rotating with the traveling wave in which to write the equations describing the mutual interaction between the stator and the rotor at the interface contact, see figure 5.7 where x is used instead of θ.

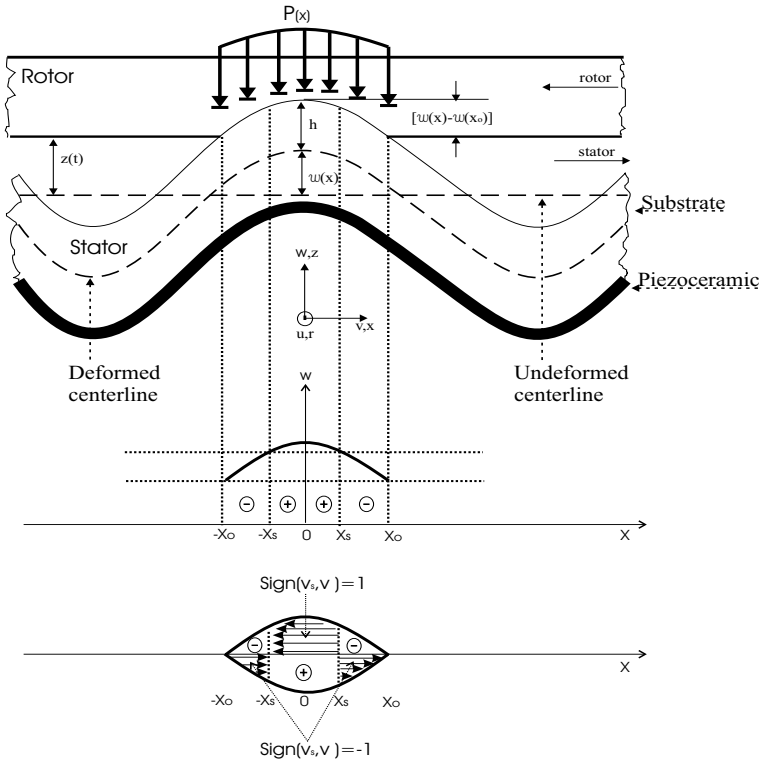

Figure 5.7: Section of the loaded stator undergoing bending deformations in the moving coordinate system

The pressure in this coordinate system along the contact region $-x_0 \leqslant x \leqslant x_0$ over one wave length becomes

$$\begin{aligned} P(x) &= \varkappa_r[w(x) - w(x_o)] \\ &= \varkappa_r R_r A(\cos kx - \cos kx_0) \end{aligned} \tag{5.133}$$

where

$$\begin{cases} w(x) = w(r,\theta,t) = R_r A \cos kx \\ w(x_o) = h - z(t) = R_r A \cos kx_0 \\ kx = \omega t - k\theta \end{cases}$$

which leads to the following slip point expression of the half width of the contact zone

$$x_0 = \frac{1}{k} \arccos(\frac{h - z(t)}{R_r A}) \tag{5.134}$$

5.3.2 The explicit normal modal forcing vector

The normal modal forcing vector $\mathbf{F}_n^*$ is the frictional pressure $P(r,\theta,t)$ at the interface contact weighted by the vertical deflection vector Φ_w and integrated over the whole area of contact, see (5.33), and reads

$$\begin{aligned}\mathbf{F}_n^* &= -\iint \Phi_w^t P(r,\theta,t) r dr d\theta \\ &= \begin{pmatrix} -\iint R_r \cos k\theta \; P(r,\theta,t) r dr d\theta \\ -\iint R_r \sin k\theta \; P(r,\theta,t) \; r dr d\theta \end{pmatrix} \\ &= \begin{pmatrix} F_{n1} \\ F_{n2} \end{pmatrix} \end{aligned} \tag{5.135}$$

where (5.98),(5.89) and (5.90) are used. By inserting (5.132) in (5.135) and using the following variable changes

$$kx = \omega t - k\theta \tag{5.136}$$

and thereafter, by using (5.91), (5.92), (5.94), (5.133) and the following approximating formula

$$\Lambda = \int_{R_0-\frac{\epsilon}{2}}^{R_0+\frac{\epsilon}{2}} R_r^2 A r dr \approx R_r^2 A R_0 \epsilon \tag{5.137}$$

lead to

$$\begin{cases} F_{n1} = -\varkappa_r \Lambda k \int_{-x_0}^{x_0} cosk\theta (coskx - coskx_0) dx \\ F_{n2} = -\varkappa_r \Lambda k \int_{-x_0}^{x_0} sink\theta (coskx - coskx_0) dx \end{cases} \tag{5.138}$$

For the sake of easing the remaining developments, the following notations will be used

$$\begin{aligned} l_1(x) &= \sin k\theta \; (\cos kx - \cos kx_0) \\ &= \gamma_1(x) \sin \omega t - \gamma_2(x) \cos \omega t \end{aligned} \tag{5.139}$$

$$\begin{aligned} l_2(x) &= \cos k\theta \; (\cos kx - \cos kx_0) \\ &= \gamma_1(x) \cos \omega t + \gamma_2(x) \sin \omega t \end{aligned} \tag{5.140}$$

where (5.136) and the following trigonometric relation is used

$$\begin{cases} sink\theta = \cos kx \; sin\omega t - \; sinkx \; cos\omega t \\ cosk\theta = \cos kx \; cos\omega t + \; sinkx \; sin\omega t \end{cases} \tag{5.141}$$

and where the functions $\gamma_1(x)$ and $\gamma_2(x)$ are given by

$$\begin{cases} \gamma_1(x) = \cos^2 kx - \cos kx_0 \cos kx \\ \gamma_2(x) = \cos kx \sin kx - \cos kx_0 \sin kx \end{cases} \tag{5.142}$$

This leads to rewrite (5.138) as follows

$$\begin{cases} F_{n1} = -\varkappa_r \Lambda k \int_{-x_0}^{x_0} l_2(x)dx \\ F_{n2} = -\varkappa_r \Lambda k \int_{-x_0}^{x_0} l_1(x)dx \end{cases} \tag{5.143}$$

and by substituting (5.139) and (5.140) in (5.143) the following is obtained

$$\begin{cases} F_{n1} = -\varkappa_r \Lambda k [\cos\omega t \int_{-x_0}^{x_0} \gamma_1(x)dx + \sin\omega t \int_{-x_0}^{x_0} \gamma_2(x)dx] \\ F_{n2} = -\varkappa_r \Lambda k [\sin\omega t \int_{-x_0}^{x_0} \gamma_1(x)dx - \cos\omega t \int_{-x_0}^{x_0} \gamma_2(x)dx] \end{cases} \tag{5.144}$$

By observing that

$$\int_{-x_0}^{x_0} \gamma_2(x)dx = 0$$

because the integrated function is odd over a symmetrical interval. This leads to rewrite (5.144) as follows

$$\begin{cases} F_{n1} = -\varkappa_r \Lambda k \ \cos\omega t \int_{-x_0}^{x_0} \gamma_1(x)dx \\ F_{n2} = -\varkappa_r \Lambda k \ \sin\omega t \int_{-x_0}^{x_0} \gamma_1(x)dx \end{cases} \tag{5.145}$$

Thereby, after calculating and rearranging the terms the following is obtained

$$\begin{cases} F_{n1} = -f_n \psi(x_o)\xi_1(t) \\ F_{n2} = -f_n \psi(x_o)\xi_2(t) \end{cases} \tag{5.146}$$

where

$$f_n = R_r^2 R_0 \varepsilon \varkappa_r \tag{5.147}$$

and

$$\begin{aligned} \psi(x_o) &= k \int_{-x_0}^{x_0} \gamma_1(x)dx \\ &= kx_0 - \frac{\sin 2kx_0}{2} \end{aligned} \tag{5.148}$$

5.3.3 The explicit tangential modal forcing vector

The tangential modal forcing vector $\mathbf{F}_t^*$ is the frictional pressure $P(r,\theta,t)$ at the interface contact weighted by respectively the tangent to the vertical deflection vector Φ_w in circumferential direction, the sign of the relative velocity ζ_v between the particles of the

stator and the rotor and the Coulomb's friction coefficient μ and finally integrated over the whole area of contact, see (5.35). This forcing vector reads

$$\begin{aligned}\mathbf{F}_t^* &= -\mu \iint h \frac{\partial \Phi_w^t}{\partial \theta} P(r,\theta,t)\, \zeta_v dr d\theta \\ &= \begin{pmatrix} \mu hk \iint R_r \sin k\theta\, P(r,\theta,t)\, \zeta_v dr d\theta \\ -\mu hk \iint R_r \cos k\theta\, P(r,\theta,t)\, \zeta_v dr d\theta \end{pmatrix} \\ &= \begin{pmatrix} F_{t1} \\ F_{t2} \end{pmatrix} \end{aligned} \tag{5.149}$$

where (5.98),(5.89) and (5.90) are used. The coefficient μ is assumed to model only the slip effects of Coulomb's friction law and ζ_v is the sign function given by

$$\zeta_v = sign(v_s, v_\theta) = \begin{cases} +1 \text{ if } |v_s| > |v_\theta| \\ -1 \text{ if } |v_s| < |v_\theta| \end{cases} \tag{5.150}$$

where v_s is the velocity of the particles of the stator and v_θ is the rotor velocity in circumferential direction. By using (5.91), (5.92), (5.94), (5.89), (5.90), (5.133), (5.136) and the following approximating formula

$$\Lambda^* = \int_{R_0 - \frac{\epsilon}{2}}^{R_0 + \frac{\epsilon}{2}} R_r^2 A dr \approx R_r^2 A \epsilon \tag{5.151}$$

lead to the following tangential forcing vector given by

$$\begin{pmatrix} F_{t1} \\ F_{t2} \end{pmatrix} = f_t^* \begin{pmatrix} \Gamma_1 \\ -\Gamma_2 \end{pmatrix} \tag{5.152}$$

where f_t^* is given by

$$f_t^* = \mu hk \Lambda^* \varkappa_r \tag{5.153}$$

and where Γ_1 and Γ_2 are given by

$$\begin{cases} \Gamma_1 = k \int_{-x_0}^{x_0} \zeta_v sink\theta\, (\cos kx - \cos kx_0)\, dx \\ \Gamma_2 = k \int_{-x_0}^{x_0} \zeta_v \cos k\theta\, (\cos kx - \cos kx_0)\, dx \end{cases}$$

In the new coordinate systems the state where

$$|v_s| = |v_\theta| \tag{5.154}$$

is defined by the stick point x_s which leads to the following

$$\Gamma_1 = 2k \left(\int_0^{x_s} l_1(x) dx - \int_{xs}^{x_0} l_1(x) dx \right) \tag{5.155}$$

$$\Gamma_2 = 2k \left(\int_0^{x_s} l_2(x) dx - \int_{xs}^{x_0} l_2(x) dx \right) \tag{5.156}$$

where (5.139) and (5.140) are used. By using (5.38) and (5.37) the relation in (5.154) becomes $R_o\dot{\theta} = khR_rR_o^{-1}A\omega\cos kx$, thereby, the stick point is derived and reads

$$x_s = \frac{1}{k}\arccos(\frac{R_o^2\,\dot{\theta}}{khR_rA\omega}) \tag{5.157}$$

The equations (5.155) and (5.156) are further written as

$$\Gamma_1 = 2k\left[L_1(x)\sin\omega t - L_2(x)\cos\omega t\right] \tag{5.158}$$

$$\Gamma_2 = 2k\left[L_1(x)\sin\omega t + L_2(x)\cos\omega t\right] \tag{5.159}$$

where

$$\begin{cases} L_1(x) = \int_0^{x_s}\gamma_1(x)dx - \int_{x_s}^{x_0}\gamma_1(x)dx \\ L_2(x) = \int_0^{x_s}\gamma_2(x)dx - \int_{x_s}^{x_0}\gamma_2(x)dx \end{cases} \tag{5.160}$$

Furthermore, by using (5.142) the following indefinite integrals

$$\Delta_1(x) = k\int\gamma_1(x)\,dx \tag{5.161}$$

$$= \frac{kx}{2} + \frac{\sin 2kx}{4} - \cos kx_0\sin kx$$

$$\Delta_2(x) = k\int\gamma_2(x)\,dx \tag{5.162}$$

$$= \frac{\sin^2 kx}{2} + \cos kx_0\cos kx$$

will be used in order to ease the writing of the remaining expressions and thus

$$\Gamma_1 = [\zeta_v\Delta_1(x)]_{-x_0}^{x_0}\sin\omega t - [\zeta_v\Delta_2(x)]_{-x_0}^{x_0}\cos\omega t$$

$$= G_1(x_0,x_s)\sin\omega t - G_2(x_0,x_s)\cos\omega t \tag{5.163}$$

$$\Gamma_2 = [\zeta_v\Delta_1(x)]_{-x_0}^{x_0}\cos\omega t + [\zeta_v\Delta_2(x)]_{-x_0}^{x_0}\sin\omega t$$

$$= G_1(x_0,x_s)\cos\omega t + G_2(x_0,x_s)\sin\omega t \tag{5.164}$$

where

$$\left\| \begin{array}{c} \Delta_1(0) = 0 \text{ and } \Delta_2(0) = 1 \\ G_1(x_0,x_s) = 2\left(2\Delta_1(x_s) - \Delta_1(x_0)\right) \\ G_2(x_0,x_s) = 2\left(2\Delta_2(x_s) - \Delta_2(x_0) - 1\right) \end{array} \right.$$

which finally, by substituting (5.163) and (5.164) in (5.152), leads to

$$\begin{cases} F_{t_1} = f_t\left[G_1(x_0,x_s)\xi_2(t) - G_2(x_0,x_s)\xi_1(t)\right] \\ F_{t_2} = -f_t\left[G_1(x_0,x_s)\xi_1(t) + G_2(x_0,x_s)\xi_2(t)\right] \end{cases} \tag{5.165}$$

where

$$f_t = \mu hk R_r^2\epsilon\varkappa_r \tag{5.166}$$

5.3.4 The explicit interface force

The force at the interface contact F_{int} is the frictional pressure $P(r,\theta,t)$ at the interface integrated over the whole area of contact and reads

$$\begin{aligned} F_{int} &= \iint P(r,\theta,t)\, r dr d\theta \\ &= \Lambda_0 \varkappa_r\, k \int_{-x_0}^{x_0} (\cos kx - \cos kx_0)\, dx \end{aligned} \tag{5.167}$$

where (5.133) , (5.136) and the following approximation formulae

$$\Lambda_0 = \int_{R_0-\frac{\epsilon}{2}}^{R_0+\frac{\epsilon}{2}} R_r A r dr \approx R_r A R_0 \epsilon \tag{5.168}$$

are used. By further using

$$\begin{aligned} \Phi(x) &= k \int (\cos kx - \cos kx_0) dx \\ &= \sin kx - kx \cos kx_0 \end{aligned} \tag{5.169}$$

this leads to

$$F_{int} = f_i \Phi(x_0) \tag{5.170}$$

where

$$f_i = 2\Lambda_0 \varkappa_r = 2 R_r A R_0 \epsilon \varkappa_r \tag{5.171}$$

5.3.5 The explicit interface torque

The torque $\mathcal{T}_{int}$ at the interface contact is the frictional pressure $P(r,\theta,t)$ at the interface weighted by the radius r and integrated over the whole area of contact and reads

$$\begin{aligned} \mathcal{T}_{int} &= \mu \iint \zeta_v P(r,\theta,t) r^2 dr d\theta \\ &= \mu \Lambda_0^* \varkappa_r\, k \int_{-x_0}^{x_0} \zeta_v (\cos kx - \cos kx_0)\, dx \\ &= 2\mu \Lambda_0^* \varkappa_r \left([\Phi(x)]_0^{x_s} + [-\Phi(x)]_{x_s}^{x_0} \right) \\ &= 2\mu \Lambda_0^* \varkappa_r \left(2\Phi(x_s) - \Phi(x_0) \right) \end{aligned} \tag{5.172}$$

where (5.133) , (5.136), (5.150), (5.169) and the following cappproximation formulae

$$\Lambda_0^* = \int_{R_0-\frac{\epsilon}{2}}^{R_0+\frac{\epsilon}{2}} R_r A r^2 dr \approx R_r A R_0^2 \epsilon \tag{5.173}$$

are used. For clarity reasons this is further written

$$\mathcal{T}_{int} = \tau_i \Phi(x_0, x_s) \tag{5.174}$$

where

$$\begin{cases} \tau_i = 2\mu\Lambda_0^* \varkappa_r = 2\mu R_r A R_0^2 \epsilon \varkappa_r \\ \Phi(x_0, x_s) = 2\Phi(x_s) - \Phi(x_0) \end{cases}$$

5.3.6 The explicit state space representation

The explicit model representing the complete motor is derived by substituting (5.146), (5.165), (5.170) and (5.174) in (5.124) and reads

$$\begin{cases} M\ddot{\xi}_1 + \mathcal{D}_o\dot{\xi}_1 + K_o\xi_1 = \eta V_A - [f_n\psi(x_0) + f_t G_2(x_0, x_s)]\xi_1 + f_t G_1(x_0, x_s)\xi_2 \\ M\ddot{\xi}_2 + \mathcal{D}_o\dot{\xi}_2 + K_o\xi_2 = \eta V_B - [f_n\psi(x_0) + f_t G_2(x_0, x_s)]\xi_2 - f_t G_1(x_0, x_s)\xi_1 \\ J_r\ddot{\theta} + \mathcal{D}_r\dot{\theta} = \tau_i \Phi(x_0, x_s) - \mathcal{T}_{app} \\ M_r\ddot{z} + \mathcal{D}_z\dot{z} = f_i\Phi(x_0) - F_{app} \end{cases} \tag{5.175}$$

Thereafter, by rearranging the terms the following compact explicit model is obtained

$$\begin{cases} M\ddot{\xi}_1 + \mathcal{D}_o\dot{\xi}_1 + K_v\xi_1 = \eta V_A + \mathcal{D}^*\xi_2 \\ M\ddot{\xi}_2 + \mathcal{D}_o\dot{\xi}_2 + K_v\xi_2 = \eta V_B - \mathcal{D}^*\xi_1 \\ J_r\ddot{\theta} + \mathcal{D}_r\dot{\theta} = \tau_i \Phi(x_0, x_s) - \mathcal{T}_{app} \\ M_r\ddot{z} + \mathcal{D}_z\dot{z} = f_i\Phi(x_0) - F_{app} \end{cases} \tag{5.176}$$

where the parameters of the state space model are summarized in table 5.1.

The derived model (5.176) can be expressed in state space model representation by

$$\dot{\mathbf{x}} = A_*\mathbf{x} + B_*\mathbf{u} \tag{5.177}$$

The state vector is given by

$$\mathbf{x} = \begin{bmatrix} \xi_1 & \xi_2 & \dot{\xi}_1 & \dot{\xi}_2 & \theta & \dot{\theta} & z & \dot{z} \end{bmatrix}^t \tag{5.178}$$

The transfer matrices A_*, B_* are respectively given by

$$A_* = \begin{pmatrix} 0 & 0 & 1 & 0 & 0 & 0 & 0 & 0 \\ 0 & 0 & 0 & 1 & 0 & 0 & 0 & 0 \\ \frac{-K_v}{M} & \frac{\mathcal{D}^*}{M} & -\frac{\mathcal{D}_o}{M} & 0 & 0 & 0 & 0 & 0 \\ \frac{-\mathcal{D}^*}{M} & \frac{-K_v}{M} & 0 & \frac{-\mathcal{D}_o}{M} & 0 & 0 & 0 & 0 \\ 0 & 0 & 0 & 0 & 0 & 1 & 0 & 0 \\ 0 & 0 & 0 & 0 & 0 & \frac{-\mathcal{D}_r}{J_r} & 0 & 0 \\ 0 & 0 & 0 & 0 & 0 & 0 & 0 & 1 \\ 0 & 0 & 0 & 0 & 0 & 0 & 0 & \frac{-\mathcal{D}_z}{M_r} \end{pmatrix}$$

$$B_* = \begin{pmatrix} 0 & 0 & 0 & 0 \\ 0 & 0 & 0 & 0 \\ \frac{\eta}{M} & 0 & 0 & 0 \\ 0 & \frac{\eta}{M} & 0 & 0 \\ 0 & 0 & 0 & 0 \\ 0 & 0 & \frac{1}{J_r} & 0 \\ 0 & 0 & 0 & 0 \\ 0 & 0 & 0 & \frac{1}{M_r} \end{pmatrix}$$

The input vector $\mathtt{u}$ is given by

$$\mathtt{u} = \begin{pmatrix} V_A \\ V_B \\ \tau_i \Phi(x_0, x_s) - \mathcal{T}_{app} \\ f_i \Phi(x_0) - F_{app} \end{pmatrix}$$

Finally, the explicit state space model and its parameters are recalled in table 5.1.

$M\ \ddot{\xi}_1 + \mathcal{D}_o\ \dot{\xi}_1 + K_v \xi_1 = \eta V_A + \mathcal{D}^* \xi_2$
$M\ \ddot{\xi}_2 + \mathcal{D}_o\ \dot{\xi}_2 + K_v \xi_2 = \eta V_B - \mathcal{D}^* \xi_1$
$J_r\ \ddot{\theta} + \mathcal{D}_r\ \dot{\theta} = \tau_i \Phi(x_0, x_s) - \mathcal{T}_{app}$
$M_r\ \ddot{z} + \mathcal{D}_z\ \dot{z} = f_i \Phi(x_0) - F_{app}$
$A = \sqrt{\xi_1^2 + \xi_2^2}$
$x_0 = \frac{1}{k} \arccos(\frac{h-z}{R_r A})$
$x_s = \frac{1}{k} \arccos(\frac{R_o^2 \dot{\theta}}{k h R_r A \omega})$
$K_v = K_o + K(x_0, x_s)$
$\mathcal{D}^* = f_t G_1(x_0, x_s)$
$K(x_0, x_s) = f_n \psi(x_0) + f_t G_2(x_0, x_s)$
$f_t = \mu h k R_r^2 \epsilon \varkappa_r\ ,\ f_n = R_r^2 R_0 \epsilon \varkappa_r$
$\psi(x_o) = k x_0 - \frac{\sin 2kx_0}{2}$
$G_1(x_0, x_s) = 2\,(2\Delta_1(x_s) - \Delta_1(x_0))$
$G_2(x_0, x_s) = 2\,(2\Delta_2(x_s) - \Delta_2(x_0) - 1)$
$\Delta_1(x) = \frac{kx}{2} + \frac{\sin 2kx}{4} - \cos kx_0 \sin kx$
$\Delta_2(x) = \frac{\sin^2 kx}{2} + \cos kx_0 \cos kx$
$\Phi(x_0, x_s) = 2\Phi(x_s) - \Phi(x_0)$
$\Phi(x_s) = \sin kx_s - kx_s \cos kx_o$
$\Phi(x_0) = \sin kx_0 - kx_0 \cos kx_0$
$\tau_i = 2\mu R_r A R_0^2 \epsilon \varkappa_r,\ f_i = 2 R_r A R_0 \epsilon \varkappa_r$
$K_r = \varkappa_r R_o \epsilon\ ,\ \Lambda_0^* \approx R_r A R_0^2 \epsilon$

Table 5.1: Summary of the explicit state space model and its parameters

5.4 The simplified model

Due to the symmetrical nature of the stator design the dynamics of the rotary PEM can be captured in a lower order model as stated below

5.4.1 The simplified model of the stator

It is possible to reduce the above state space model (5.176) by decoupling the modes and thereby obtain a separate model for each phase of the stator. Under the assumption that only two orthogonal temporal modes $\xi_1(t) = A\cos\omega t$ and $\xi_2(t) = A\sin\omega t$ are excited within the body of the stator the following relation can be used

$$\begin{cases} \dot{\xi}_1\ (t) = -\omega\xi_2(t) \\ \dot{\xi}_2\ (t) = \omega\xi_1(t) \end{cases} \tag{5.179}$$

after substitution of (5.179) in (5.176) and rearranging the terms the model of the stator becomes

$$\begin{cases} M\ \ddot{\xi}_1 + \mathcal{D}_v(x_0, x_s)\ \dot{\xi}_1 + K_v(x_0, x_s)\xi_1 = \eta\, V_A \\ M\ \ddot{\xi}_2 + \mathcal{D}_v(x_0, x_s)\ \dot{\xi}_2 + K_v(x_0, x_s)\xi_2 = \eta\, V_B \end{cases} \tag{5.180}$$

where

$$\begin{cases} \mathcal{D}_v(x_0, x_s) = \mathcal{D}_o + \frac{\mathcal{D}^*(x_0, x_s)}{\omega} \\ K_v(x_0, x_s) = K_o + K(x_0, x_s) \end{cases} \tag{5.181}$$

The above relation (5.180) suggests that the behavior of the complete stator can be predicted by a single second order system with varying parameters. These parameters are functions of the external conditions which are the pressure distribution at the contact surface between the stator and the rotor and the load torque at the rotating shaft of the motor. Consequently, the final model of the stator is given by

$$\boxed{M\ \ddot{\xi}_i + \mathcal{D}_v(x_0, x_s)\ \dot{\xi}_i + K_v(x_0, x_s)\xi_i = \eta\, V_i} \tag{5.182}$$

where M (constant) is the modal mass, $\mathcal{D}_v(x_0, x_s)$ (varying) is the damping of the modal amplitude in forced conditions, $K_v(x_0, x_s)$ (varying) is the resulting stiffness of the forced stator, η (constant) is the electromechanical modal force factor and finally the voltage supply V_i and the modal amplitude ξ_i are phase dependent.

5.4.2 Vertical motion model

The vertical motion of the rotor is given by the following second order system

$$M_r\ \ddot{z} + \mathcal{D}_z\ \dot{z} = F_{int} - F_{app} \tag{5.183}$$

where F_{app} is the applied force and F_{int} is the interface force at the contact surface given by

$$\begin{aligned} F_{int} &= \iint P(r,\theta,t)dS \\ &= \varkappa_r \iint (w(r,\theta,t) + h - z(t))rdrd\theta \end{aligned}$$

For simplicity reasons the following notations will be used

$$\left\| \begin{array}{c} K_r = \varkappa_r R_o \epsilon \ , \ K_r^* = 2\pi K_r \\ \mathtt{z} = z - h \\ F(x_0) = K_r \int_0^{2\pi} w(r,\theta,t)d\theta \end{array} \right.$$

which leads to the following equation of motion in vertical direction

$$\boxed{M_r \ddot{\mathtt{z}} + \mathcal{D}_{\mathtt{z}} \dot{\mathtt{z}} + K_r^* \mathtt{z} = F(x_0) - F_{app}} \tag{5.184}$$

where

$$\begin{aligned} F(x_0) &= K_r R_r A(k \int_{-x_0}^{x_0} \cos kx \ dx) \\ &= 2K_r R_r A \sin kx_0 \end{aligned} \tag{5.185}$$

Finally the slip point coordinate of the half width of the contact zone is given by

$$x_0 = \frac{1}{k} \arccos(\frac{\mathtt{z}}{R_r A}) \tag{5.186}$$

5.4.3 Spinning motion model

The spinning motion of the rotor is given by the following first order system

$$\boxed{J_r \dot{\Omega} + \mathcal{D}_r \Omega = \mathcal{T}(x_0, x_s) - \mathcal{T}_{app}} \tag{5.187}$$

where $\mathcal{T}_{app}$ is the applied torque and $\mathcal{T}(x_0, x_s)$ is the interface torque at the contact surface given by

$$\begin{aligned} \mathcal{T}(x_0, x_s) &= \mu \iint r\zeta_v P(r,\theta,t)dS \\ &= 2\mu\Lambda_0^* \varkappa_r \left(2\Phi(x_s) - \Phi(x_0)\right) \end{aligned} \tag{5.188}$$

where (5.133), (5.136), (5.150), (5.173) and (5.169) are used. The stick point condition is achieved when the following equality is fulfilled $|v_s| = |v_\theta|$, where v_s is the velocity of the particles of the stator at the interface contact given by $v_s = khR_r R_o^{-1} A\omega \cos kx$ and v_θ is the rotary velocity of the rotor given by $v_\theta = R_o\Omega$. Thereby, the stick point is given by

$$x_s = \frac{1}{k} \arccos(\frac{R_o^2 \Omega}{khR_r A\omega}) \tag{5.189}$$

5.4.4 The complete simplified model

The following table gives the simplified analytical model to be implemented in the Matlab-Simulink environment.

$$
\begin{array}{|l|}
\hline
M\,\ddot{\xi}_1 + \mathcal{D}_v(x_0,x_s)\,\dot{\xi}_1 + K_v(x_0,x_s)\xi_1 = \eta\,\hat{V}\cos\omega t \\
M\,\ddot{\xi}_2 + \mathcal{D}_v(x_0,x_s)\,\dot{\xi}_2 + K_v(x_0,x_s)\xi_2 = \eta\,\hat{V}\sin\omega t \\
M_r\,\ddot{\mathbf{z}} + \mathcal{D}_z\,\dot{\mathbf{z}} + K_r^*\mathbf{z} = F(x_0) - F_{app} \\
J_r\,\dot{\Omega} + \mathcal{D}_r\Omega = \mathcal{T}(x_0,x_s) - \mathcal{T}_{app} \\
A = \sqrt{\xi_1^2 + \xi_2^2} \\
x_0 = \frac{1}{k}\arccos\left(\frac{\mathbf{z}}{R_r A}\right) \\
x_s = \frac{1}{k}\arccos\left(\frac{R_o^2\Omega}{khR_rA\omega}\right) \\
\mathcal{D}_v(x_0,x_s) = \mathcal{D}_o + \frac{\mathcal{D}^*(x_0,x_s)}{\omega} \\
K_v(x_0,x_s) = K_o + K(x_0,x_s) \\
\mathcal{D}^*(x_0,x_s) = f_t G_1(x_0,x_s) \\
K(x_0,x_s) = f_n\psi(x_0) + f_t G_2(x_0,x_s) \\
f_t = \mu h k R_r^2 \epsilon \varkappa_r \\
f_n = R_r^2 R_0 \epsilon \varkappa_r \\
\psi(x_o) = kx_0 - \frac{\sin 2kx_0}{2} \\
G_1(x_0,x_s) = 2\left(2\Delta_1(x_s) - \Delta_1(x_0)\right) \\
G_2(x_0,x_s) = 2\left(2\Delta_2(x_s) - \Delta_2(x_0) - 1\right) \\
\Delta_1(x) = \frac{kx}{2} + \frac{\sin 2kx}{4} - \cos kx_0 \sin kx \\
\Delta_2(x) = \frac{\sin^2 kx}{2} + \cos kx_0 \cos kx \\
F(x_0) = 2K_r R_r A \sin kx_0 \\
\mathcal{T}(x_0,x_s) = 2\mu\Lambda_0^*\varkappa_r\left(2\Phi(x_s) - \Phi(x_0)\right) \\
\Phi(x) = \sin kx - kx\cos kx_0 \\
K_r = \varkappa_r R_o \epsilon \\
K_r^* = 2\pi K_r \\
\Lambda_0^* \approx R_r A R_0^2 \epsilon \\
\hline
\end{array}
$$

Table 5.2: Summary of the complete simplified analytical model

5.4.5 Prerequisites for simulation

The following table summarizes the parameters that must be known beforehand in order to perform the simulation successfully. These parameters are given in appendix C for the Shinsei motor USR60.

$s_{11}^E, s_{12}^E, s_{66}^E$: Compliances at constant electrical field
d_{31} : Dielectrical constant
ε_{33}^T : Electrical permitivity at constant stress
ρ_s : Mass density of the substrate
ρ_p : Mass density of the piezo plate
J : Young's modulus of the substrate
ν : Poisson ratio of the substrate
$\mathtt{G}$: Shear modulus of the substrate
h : Half thickness of the stator
ι_p: Thickness of the piezoelectric plate
a : Outer radius of the stator
b : Inner radius of the stator
R_r : Radial shape constant of the traveling wave
ϵ : Width of the contact surface
$\varkappa_r$: Rotor stiffness per unit area
k : Number of wave length
M_r : Rotor mass
J_r : Rotor inertia
μ : Coulomb's friction coefficients

Table 5.3: Summary of the parameters that constitute the prerequisites for simulation

5.5 Conclusion and perspectives

In this chapter the necessary theoretical background for modeling the electromechanical behavior of the rotary piezoelectric motor is first given. Thereafter, the state space model of the complete traveling wave type rotary PEM is derived by applying the basic laws of variational work and elasticity theory (Hamilton's principle). Second, a reduced state space model is derived on the basis of the special design of the motors of interest (i.e. two phase symmetrical system). Third, a further simplified model is derived within the framework of various assumptions on the behavior of the stator. Consequently, the assumed excited modes are decoupled and thereby the performance characteristics of the stator are predicted by a single second order system. Fourth, the stick-slip behavior of the driving mechanism is integrated in the time varying parameters of the model. This makes it possible to predict the essential features of the behavior and performance characteristics of the motor as a function of the external loading parameters. The derived complete simplified model is thereby a simplified model of the stator together with the model of the rotor in spinning and vertical directions.

5.5.1 Advantages and performances

The main advantage of the analytical method is that it provides a general framework model for simulating different geometries of the motor. This model is not restricted to the nine wave Shinsei motor USR60. The model can be extended to encompass any n'th wave traveling wave piezomotor provided that the electrical potential at the surface of the corresponding n'th wave piezocermics is appropriately defined. Furthermore, this model constitutes a powerful and suitable test bench for the control community for investigating the usability of the existing linear and nonlinear control methods in a simulated environment. Consequently, the existing control algorithms can be applied directly to the the simulated model and thereby their degree of usability and performance can be established without resorting to actual experiments. Moreover, this model provides the opportunity for the control community to push forward their knowledge and thereby find new methods more suitable for controlling this kind of devices.

5.5.2 Drawbacks and limitations

The main drawback of the analytical method is that the electromechanical constants of the motor are usually not known with a sufficient accuracy. This results in a large discrepancy between the theoretical model and the real system. The effect of temperature has not been considered in the model derived in this chapter, thereby only the behavior of the motor in short term operations can be predicted.

5.5.3 The alternatives

The analytical modeling of the stator of the piezoelectric motor constitutes the main source of errors. This is generally due to the uncertainties on the available electromechanical constants of the piezoceramics, and also to the many assumptions on the behavior of the stator in order to simplify the modeling task. Therefore, the modeling of the stator should be carried out with another more suitable method, such as the equivalent circuit method. Consequently, the main objective is to combine the strength of the equivalent circuit method for modeling the stator with the strength of the analytical method for modeling the remaining dynamics of the motor.

Chapter 6

Hybrid Model

In this chapter the derivation procedure of a hybrid model of a rotary traveling wave PEM is presented. This model combines the strength of the equivalent circuit method with the strength of the analytical method. For modeling the stator, Equivalent Circuit Modeling (ECM) which is a powerful alternative to the analytical approach (Ikeda (1996)), is used. However, the effect of the stick-slip behavior of the driving mechanism on the performance of the motor is carried out analytically. Therefore the analogy between the structure of the ECM and a simplified analytical model of the stator is emphasized. Consequently a hybrid model is derived. Moreover a tracking facility which will update the temperature sensitive parameters is integrated in the model presented in this chapter.

6.1 The general framework model of the forced stator

The derivation begins by applying Hamilton's principle modified for general electromechanical systems, see section 5.1

$$\delta \int_{t_1}^{t_2} L \, dt + \int_{t_1}^{t_2} \delta W \, dt = 0 \tag{6.1}$$

where L is the Lagrangian of the system and δW is the variational work due to the external forces. The equations of motion can be derived by making the appropriate substitutions for L and δW in (6.1). This leads to the following compact model of the forced stator, represented by the actuator equation (6.2) and the sensor equation (6.3)

$$\mathbf{M}\,\ddot{\xi} + \mathcal{D}\,\dot{\xi} + \mathbf{K}\xi = \Pi\mathbf{v} + \mathbf{F}_{\mathbf{n}}^{*} + \mathbf{F}_{\mathbf{t}}^{*} \tag{6.2}$$

$$\Pi^{t}\xi + \mathbf{C}_{p}\mathbf{v} = \mathbf{q} \tag{6.3}$$

where $\mathbf{v}$ is the voltage vector, applied through electrodes, explicitly defined in (5.100), $\mathbf{q}$ is the charge vector on the electrodes of the stator, $\mathbf{M}$ is the total modal mass matrix defined in (5.80), $\mathcal{D}$ is the structural modal damping matrix assumed to be diagonal, $\mathbf{K}$ is the total modal stiffness matrix defined in (5.81), II is the electromechanical coupling matrix defined in (5.82) and finally $\mathbf{C}_p$ is the piezoelectric capacitance matrix given by

$$\mathbf{C}_p = \int_{V_p} \mathbf{N}_e^t \varepsilon^S \mathbf{N}_e dV \tag{6.4}$$

where $\mathbf{N}_e$, defined in (5.119), is the electrical field shape matrix, which is derived from the electrical potential shape matrix Φ_e by using the electrical mapping operator matrix $\mathbf{L}_e$, ε^S is the clamped dielectric constant matrix, defined in (5.83), which within the framework of the made assumptions in section 2.2.2 reduces to one element, see section 5.1.2

$$\varepsilon^S = \varepsilon_{33}^S = \varepsilon_{33}^T - 2d_{31}^2 (c_{11}^E + c_{12}^E) \tag{6.5}$$

6.1.1 The explicit general model of the forced stator

In this section the explicit general model of the stator is derived from the actuator and sensor equations given in (6.2) and (6.3) respectively. The model derivation is performed within the framework of the assumptions made in section 5.2.1

6.1.2 The explicit actuator equation

For convenience some of the main results in section 5.2 are briefly recalled and appropriate references are given for each item.

- It is assumed that only two orthogonal mechanical modes can be excited within the piezoceramic plate, see section 5.2.1
- The two phase motor is powered by two high frequency voltages 90^o out of phase temporally, see section 5.2.2
- The parameters in the actuator equation $\mathbf{M}, \mathbf{K}$ and II reduce to diagonal matrices, as shown in sections 5.2.3, 5.2.4 and 5.2.5 respectively. Likewise the modal damping matrix is assumed to be diagonal. For convenience these parameters are recalled
  - The modal mass matrix $\mathbf{M}$ is expressed by the following diagonal matrix

$$\mathbf{M} = \begin{pmatrix} M & 0 \\ 0 & M \end{pmatrix} \tag{6.6}$$

    where M is the modal mass of the stator.

– The modal damping matrix $\mathcal{D}$ is expressed by the following diagonal matrix

$$\mathcal{D} = \begin{pmatrix} \mathcal{D}_o & 0 \\ 0 & \mathcal{D}_o \end{pmatrix} \tag{6.7}$$

where $\mathcal{D}_o$ is the modal damping of the stator.

– The modal stiffness matrix $\mathbf{K}$ is expressed by the following diagonal matrix

$$\mathbf{K} = \begin{pmatrix} K_o & 0 \\ 0 & K_o \end{pmatrix} \tag{6.8}$$

where K_o is the modal stiffness of the stator.

– The electromechanical coupling matrix II is expressed by the following diagonal matrix

$$\mathrm{II} = \begin{pmatrix} \eta & 0 \\ 0 & \eta \end{pmatrix} \tag{6.9}$$

where η is the modal electromechanical force factor.

- The loaded stator is subject to normal and tangential forcing at the interface contact. These forcing vectors are recalled below

– The normal forcing vector $\mathbf{F}_n^*$ is expressed by the following two dimensional vector

$$\mathbf{F}_n^* = \begin{pmatrix} F_{n1} \\ F_{n2} \end{pmatrix} \tag{6.10}$$

– The tangential forcing vector $\mathbf{F}_t^*$ is expressed by the following two dimensional vector

$$\mathbf{F}_t^* = \begin{pmatrix} F_{t1} \\ F_{t2} \end{pmatrix} \tag{6.11}$$

Consequently, by substituting (6.6), (6.7), (6.8), (6.9), (6.10) and (6.11) in (6.2) the following actuator model is obtained

$$\begin{cases} M\ddot{\xi}_1 + \mathcal{D}_o\dot{\xi}_1 + K_o\xi_1 = \eta V_A + F_{n1} + F_{t1} \\ M\ddot{\xi}_2 + \mathcal{D}_o\dot{\xi}_2 + K_o\xi_2 = \eta V_B + F_{n2} + F_{t2} \end{cases} \tag{6.12}$$

6.1.3 The explicit sensor equation

As in the case of the actuator equation, the parameters of the sensor equation will be explicitly defined within the framework of the assumption stated in section 5.2.1. It should be noticed that only $\mathbf{q}$ and $\mathbf{C}_p$ must be defined, the other parameters are already known from the previous analysis.

6.1.3.1 Calculation and diagonalization of the capacitance matrix

The piezoelectric capacitance matrix $\mathbf{C}_p$ of any piezoelectric vibrating plate, of clamped dielectric constant matrix ε^S and volume V_p, is a function of the electrical field shape matrix $\mathbf{N}_e$ and reads

$$\mathbf{C}_p = \int_{V_p} \mathbf{N}_e^t \varepsilon^S \mathbf{N}_e dV \tag{6.13}$$

where $\mathbf{N}_e$, defined in (5.119), is the electrical field shape matrix derived from the electrical potential shape matrix Φ_e by using the electrical mapping operator matrix $\mathbf{L}_e$, and where ε^S is the clamped dielectric constant matrix defined in (5.83), which within the framework of the made assumptions in section 5.2.1 reduces to one component defined in (6.5) such that

$$\varepsilon^S = \varepsilon_{33}^S \tag{6.14}$$

For convenience, the electrical shape matrix defined in (5.119) is recalled

$$\mathbf{N}_e = \mathbf{L}_e \Phi_e = \frac{1}{\iota_p} \begin{pmatrix} \phi_A & \phi_B \end{pmatrix}$$

where $\mathbf{L}_e = \frac{1}{\iota_p}$ is the electrical mapping operator, ι_p is the thickness of the piezo plate and finally ϕ_A and ϕ_B are the assumed shapes of the electric potential within the stator defined in (5.101). Moreover by using (5.119) and (6.14) the following matrix equation

$$\mathbf{N}_e^t \varepsilon^S \mathbf{N}_e = \frac{\varepsilon_{33}^S}{\iota_p^2} \begin{pmatrix} \phi_A^2 & \phi_A \phi_B \\ \phi_A \phi_B & \phi_B^2 \end{pmatrix}$$

leads to the following matrix integral equation

$$\begin{aligned} \mathbf{C}_p &= \frac{\varepsilon_{33}^S}{\iota_p^2} \int_{V_p} \begin{pmatrix} \phi_A^2 & \phi_A \phi_B \\ \phi_A \phi_B & \phi_B^2 \end{pmatrix} dV \\ &= \begin{pmatrix} C_{p11} & C_{p12} \\ C_{p21} & C_{p22} \end{pmatrix} \end{aligned} \tag{6.15}$$

where the components of the capacitance matrix read

$$\begin{cases} C_{p11} = \frac{\varepsilon_{33}^S}{t_p^2}\int_{V_p}\phi_A^2 dV \\ C_{p12} = C_{p21} = \frac{\varepsilon_{33}^S}{t_p^2}\int_{V_p}\phi_A\phi_B dV \\ C_{p22} = \frac{\varepsilon_{33}^S}{t_p^2}\int_{V_p}\phi_B^2 dV \end{cases} \tag{6.16}$$

Furthermore, by substituting (5.101) which defines the potential functions ϕ_A and ϕ_B in (6.16) and by proceeding to further calculations over the total volume of the piezoelectric plate the following is obtained

$$\begin{cases} C_{p11} = C_{p22} = C_p \\ C_{p12} = C_{p21} = 0 \end{cases}$$

Finally, the capacitance matrix is diagonalized and reads

$$\mathbf{C}_p = \begin{pmatrix} C_p & 0 \\ 0 & C_p \end{pmatrix} \tag{6.17}$$

where C_p is the modal capacitance of the stator.

6.1.3.2 The electrical charges flowing through the electrodes of the stator

The two phase stator of the PEM is powered by two high frequency voltages 90^o out of phase temporally see section 5.2.2. As there are only two effective electrodes (phase A and phase B), the charge vector $\mathbf{q}$ on the right side of the sensor equation (6.3), which represents the charge on the electrodes of the stator, reduces to two elements

$$\mathbf{q} = \begin{pmatrix} q_A \\ q_B \end{pmatrix} \tag{6.18}$$

Consequently, the sensor equation provides valuable insight into the complementary electrical dynamics of the stator subsystem. For instance, the current on the electrodes is the time derivative of the charges on the electrodes, and by taking the time derivative of the sensor equation (6.3), the following current equation is obtained

$$\mathbf{I} = \dot{\mathbf{q}} = \mathrm{II}^t\dot{\xi} + \mathbf{C}_p\dot{\mathbf{v}} \tag{6.19}$$

6.1.3.3 The model representation of the explicit sensor equation

By substituting (6.9) (6.17) and (6.18) in (6.3) the following explicit model of the sensor equation is obtained

$$\begin{cases} \eta\xi_1 + C_pV_A = q_A \\ \eta\xi_2 + C_pV_B = q_B \end{cases} \tag{6.20}$$

6.1.4 The model representation of the forced stator

The derived models in (6.12) and (6.20) together constitute the model representation of the forced stator given below

$$\begin{cases} M\ddot{\xi}_1 + \mathcal{D}_o\dot{\xi}_1 + K_o\xi_1 = \eta V_A + F_{n1} + F_{t1} \\ M\ddot{\xi}_2 + \mathcal{D}_o\dot{\xi}_2 + K_o\xi_2 = \eta V_B + F_{n2} + F_{t2} \\ \eta\xi_1 + C_p V_A = q_A \\ \eta\xi_2 + C_p V_B = q_B \end{cases} \tag{6.21}$$

6.2 Modeling of the free stator

The relation (6.21) suggests that the behavior of the free stator, (i.e. no external forcing is applied), can be predicted by the following monophase actuator and sensor equations, which constitute the reduced model

$$M\ddot{\xi} + \mathcal{D}_o\dot{\xi} + K_o\xi = \eta V \tag{6.22}$$

$$\eta\xi + C_p V = q \tag{6.23}$$

where ξ, V and q are phase dependent. The sensor equation (6.23) can be written as

$$\dot{q} = \eta\dot{\xi} + C_p\dot{V} \tag{6.24}$$

By multiplying the left and right sides of the equation (6.23) with $e^{j\omega t}$ then the complex notaion can be used. Consequently, in complex notation the modal amplitude is given by $\underline{\xi} = \xi e^{j\omega t}$, the charge and the voltage are given by $\underline{q} = qe^{j\omega t}$ and $\underline{V} = Ve^{j\omega t}$ respectively, the current is given by $\underline{I} = \dot{\underline{q}} = Ie^{j\omega t}$. This leads to rewrite the current equation (6.24) as

$$\underline{I} = j\omega\eta\underline{\xi} + j\omega C_p\underline{V} \tag{6.25}$$

which is further written in terms of electrical admittance as

$$\underline{Y} = j\omega\eta\frac{\underline{\xi}}{\underline{V}} + j\omega C_p \tag{6.26}$$

By using the actuator equation (6.22) the equation (6.26) becomes

$$\begin{aligned} \underline{Y} &= \frac{\eta^2 j\omega}{M(j\omega)^2 + \mathcal{D}_o j\omega + K_o} + j\omega C_p \\ &= \frac{\eta^2}{j\omega M + \mathcal{D}_o + \frac{K_o}{j\omega}} + j\omega C_p \\ &= \underline{Y}_m + \underline{Y}_d \end{aligned} \tag{6.27}$$

where $\underline{Y}_m$ and $\underline{Y}_d$ are the electrical motional admittance and the damped admittance, respectively. The relation (6.27) suggests that the parameters $M, \mathcal{D}_o, K_o, \eta$ and C_p can be identified by using the electrical network method as stated below.

6.2.1 Identification of the parameters $M, \mathcal{D}_o, K_o$ and η

For practical purposes it is sufficient to observe the electrical admittance of the stator around its fundamental resonance frequency see chapter 4. For convenience, the main topics of the equivalent circuit modeling will be recalled. Furthermore, for simplicity reasons and also for consistence with the notation used in section 4.1.2.1 the complex notation will be omitted.

The electrical admittance Y of any piezoelectric transducer, which is the ratio between the input current I and the input voltage V, is given by the sum of the damped Y_d and the motional Y_m admittance

$$Y = Y_d + Y_m \tag{6.28}$$

Where

$$\begin{cases} Y_d = 1/R_d + j\omega C_d \\ Y_m = 1/[R + j(\omega L - 1/\omega C)] \end{cases} \tag{6.29}$$

The motional admittance of the stator can also be provided by measuring the electromechanical admittance of the stator. The electromechanical admittance y_m is the ratio between the rate of vibration $\dot{u}$ and the input voltage V and is given by

$$y_m = 1/[r + j(\omega l - 1/\omega c)] \tag{6.30}$$

The electrical motional admittance Y_m and the electromechanical admittance y_m are related by the electromechanical transformer Π such that

$$y_m = \frac{Y_m}{\Pi^2} \tag{6.31}$$

Consequently, the electromechanical parameters seen as their electrical equivalents become

$$R = \tfrac{r}{\Pi^2}\ ,\ L = \tfrac{l}{\Pi^2}\ ,\ C = \Pi^2 c \tag{6.32}$$

The identification of the electrical admittance parameters (R_d, C_d, R, L, C) and the electromechanical admittance parameters (r, l, c) is carried out by using the electrical network method based on the Nyquist and the Bode diagrams of the admittance, see section 4.1.2.1.

It must be emphasized that for a monophase system the electromechnical transformer identifies with the modal force factor. For a polyphase system, however, an insight is needed in order to distinguish between the electromechanical transformer and the modal force factor.

The stator of the PEM under identification is a two phase symmetrical system with each phase providing a standing wave. Due to the special design of the stator these standing waves are combined and create a traveling wave within the body of the stator. The electrical admittance of each phase of the stator was measured in the same conditions and then plotted for comparison see section 4.2. From figure 4.16 it can be noticed that the two phases exhibit almost the same admittance, consequently the stator is assumed to be perfectly symmetrical and therefore only one phase needs to be identified.

The electrical admittance of the free stator is provided for one phase around the fundamental frequency. The exploitation of the Bode diagram in figure 4.18 and the Nyquist diagram in figure 4.19 by using the electrical network method leads to the following values

$$\begin{array}{lll} Q = 160 & R_d = 3.12\,10^4 & C_d = 5.4\,10^{-9} \\ R = 149.75 & L = 0.102 & C = 1.66\,10^{-10} \end{array}$$

It must be noticed that the quality factor Q which is over 100 in this case enhances the validity of the approximation made to derive the parameters of the network.

Thereafter, the parameters of the motional admittance are directly derived by measuring the electromechanical admittance y_m of the vibrating gain of the stator. The exploitation of the Bode magnitude and the Nyquist diagrams in figure 4.21, of the electromechanical admittance, and the derivation of the quality factor from the pass band at -3dB of the frequency response lead to the following values

$$Q = 159.55 \qquad r = 15.4 \qquad l = 0.0101 \qquad c = 1.68\,10^{-9}$$

The quality factor which is slightly different from the previous case enhances both the validity of the approximation and the compatibility of these two methods. The above mechanical (r, l, c) values can be seen as their electrical equivalents and thereby deduce the electromechanical transformer

$$\Pi = 0.32$$

The identified values are thereafter used in a simulated equivalent circuit model environment, and for each case an admittance is provided over a certain range of frequencies around the fundamental resonance and the results are then compared to the experimental data. From figure 4.22 it can be noticed that the simulated model predicts most of the characteristics of the electrical gain admittance, especially in the range of frequencies located above the fundamental resonance. Furthermore, from figure 4.23 it can be noticed that most of the characteristics of the vibrating gain can be predicted in a simulated

environment. However, this is only valid in a narrow range of frequencies lying above the fundamental frequency.

The identification of the $M, \mathcal{D}_o, K_o$ parameters is carried out directly, by using (6.27), (6.30), (6.31) and observing that

$$y_m = \frac{1}{j\omega M + \mathcal{D}_o + \frac{K_o}{j\omega}} = \frac{1}{j\omega l + r + \frac{1}{j\omega c}} \tag{6.33}$$

which leads to the following

$$\boxed{M = l,\ \mathcal{D}_0 = r,\ K_0 = 1/c} \tag{6.34}$$

whereas the identification of the modal force factor requires an insight into the physical behavior of the stator under identification. The relation between the modal force factor η and the electromechanical transformer Π of the traveling wave piezoelectric motor USR60, see section 4.2.1.2, is given by

$$\boxed{\eta = R_r\, \Pi} \tag{6.35}$$

where R_r is a radial function depending on the design of the stator and the modal shape of the traveling wave in the radial direction given by equation (5.95). By assuming that the contact interface between the stator and the rotor is mainly concentrated around the middle radius of the annular plate R_o given by equation (5.97) then R_r becomes a constant depending only on the amplitude of the radial mode at the point of contact.

6.3 The explicit model of the complete motor

The model of the complete motor is identical to the modal derived in chapter 5, where the parameters of the unforced stator are identified by the equivalent circuit method. For convenience, the main topics of the modeling process will be recalled.

- The pressure distribution at the stator-rotor interface contact is explicitly defined in the moving coordinate system, see section 5.3.1, where
  - The stator is assumed to be a rigid body along the contact interface
  - The rotor is modeled as a linear spring
- The normal modal forcing vector is explicitly defined in section 5.3.2
- The tangential modal forcing vector is explicitly defined in section 5.3.3
- The interface force is explicitly defined in section 5.3.4

- The interface torque is explicitly defined in section 5.3.5

Finally, the explicit state space model representation is recalled for convenience. By substituting (5.146), (5.165), (5.170) and (5.174) in (5.124) and in the spining and vertical motion model and thereafter rearranging the terms, see section 5.3.6, the following explicit model is obtained

$$\begin{cases} M\ \ddot{\xi}_1 + \mathcal{D}_o\ \dot{\xi}_1 + [K_o + K(x_0, x_s)]\xi_1 = \eta V_A + \mathcal{D}^* \xi_2 \\ M\ \ddot{\xi}_2 + \mathcal{D}_o\ \dot{\xi}_2 + [K_o + K(x_0, x_s)]\xi_2 = \eta V_B - \mathcal{D}^* \xi_1 \\ J_r\ \ddot{\theta} + \mathcal{D}_r\ \dot{\theta} = \tau_i \Phi(x_0, x_s) - \mathcal{T}_{app} \\ M_r\ \ddot{z} + \mathcal{D}_z\ \dot{z} = f_i \Phi(x_0) - F_{app} \end{cases} \tag{6.36}$$

6.4 The complete hybrid model

The simplified model derived in section 5.4 is valid only for short term operation. For long term operation the effect of temperature must be integrated in the model.

6.4.1 The simplified model

For convenience, the simplified model will first be recalled.

- The model of the stator is predicted by a single second order system, with varying parameters, see section 5.4.1, given by

$$\boxed{M\ \ddot{\xi}_i + \mathcal{D}_v(x_0, x_s)\ \dot{\xi}_i + K_v(x_0, x_s)\xi_i = \eta\, V_i} \tag{6.37}$$

  where the varying parameters are given by

$$\begin{array}{c} \mathcal{D}_v(x_0, x_s) = \mathcal{D}_o + \frac{\mathcal{D}^*(x_0, x_s)}{\omega} \\ K_v(x_0, x_s) = K_o + K(x_0, x_s) \end{array} \tag{6.38}$$

- The vertical motion model of the rotor, see section 5.4.2, is given by

$$\boxed{M_r\ \ddot{\mathbf{z}} + \mathcal{D}_z\ \dot{\mathbf{z}} + K_r^* \mathbf{z} = F(x_0) - F_{app}} \tag{6.39}$$

  where

$$F(x_0) \quad = \quad 2K_r R_r A \sin k x_0 \tag{6.40}$$

  and the slip point expression of the half width of the contact zone is given by

$$x_0 \quad = \quad \frac{1}{k} \arccos\left(\frac{\mathbf{z}}{R_r A}\right) \tag{6.41}$$

- The spinning motion model of the rotor, see section 5.4.3, is given by

$$\boxed{J_r\ \dot{\Omega} + \mathcal{D}_r\Omega = \mathcal{T}(x_0, x_s) - \mathcal{T}_{app}} \tag{6.42}$$

where $\mathcal{T}(x_0, x_s)$ is the interface torque at the contact surface given by

$$\mathcal{T}(x_0, x_s) = 2\mu\Lambda_0^*\varkappa_r\ (2\Phi(x_s) - \Phi(x_0)) \tag{6.43}$$

and the stick point is given by

$$x_s = \frac{1}{k}\arccos(\frac{R_o^2\Omega}{khR_rA\omega}) \tag{6.44}$$

6.4.2 Temperature integration in the hybrid model

The resonance and antiresonance frequencies of the PEM change with the temperature which in terms of hybrid modeling can be represented by the same model as before but with temperature sensitive parameters. The effect of the heating process that takes place within the body of the stator on the performance of the PEM can be monitored by the feedback signal. Consequently, it is possible to integrate a tracking capability of the mechanical resonance frequency in the model in order to maintain the output performance characteristics of the motor despite the temperature changes.

By sensing the feedback signal as a function of the temperature of the PEM the characteristic shown in figure 3.12 is obtained when operating under nominal conditions. It should be noticed from figure 3.12 that the resonance frequency of the feedback signal shifts towards lower frequencies as the temperature of the PEM increases during the operation process. Consequently, given the fact that the modal mass is a mechanical constant then the only parameters subject to variation under temperature changes are the damping and the stiffness/elasticity of the motional part whereas the changes of the piezoelectric capacitance exist but are overlooked in the modeling process. Moreover, the influence of the damping changes are assumed to be negligible. The following relation represents the resonance behavior of the motional impedance as a function of temperature

$$\begin{cases} M(2\pi f_r)^2 = K_v \\ M(2\pi f_{r_o})^2 = K_v^o \\ f_r = f_{r_o} - \ell\,\Delta\Theta \end{cases} \tag{6.45}$$

where f_{r_o} and f_r are resonance frequencies at the ambient and working temperature respectively, $\Delta\Theta$ is the temperature gradient during operation and ℓ is the slope of the resonance-temperature characteristic. In terms of hybrid modeling information the stiffness should be updated during the temperature changes as follows

$$\begin{aligned} K_v &= M(2\pi f_r)^2 = M[2\pi(f_{r_o} - \ell\,\Delta\Theta)]^2 \\ &\approx K_v^o(1 - 2\frac{\ell}{f_{r_o}}\,\Delta\Theta) \end{aligned}$$

where

$$\begin{cases} K_v^o = M(2\pi f_{r_o})^2 \\ K_v = K_v^o(1 - 2\frac{\ell}{f_{r_o}}\,\Delta\Theta) \end{cases} \tag{6.46}$$

For USR60: $\ell = 5\ Hz.\deg^{-1}$ and $2\frac{\ell}{f_{r_o}} \approx 2.5\ 10^{-4}$.

6.5 Summary of the complete hybrid model

The following table summarizes the simplified hybrid model to be implemented in the Matlab-Simulink environment

$M\ \ddot{\xi}_1 + \mathcal{D}_v(x_0, x_s)\ \dot{\xi}_1 + K_v(x_0, x_s)\xi_1 = \eta\hat{V}\cos\omega t$
$M\ \ddot{\xi}_2 + \mathcal{D}_v(x_0, x_s)\ \dot{\xi}_2 + K_v(x_0, x_s)\xi_2 = \eta\hat{V}\sin\omega t$
$M_r\ \ddot{\mathbf{z}} + \mathcal{D}_z\ \dot{\mathbf{z}} + K_r^*\mathbf{z} = F(x_0) - F_{app}$
$J_r\ \dot{\Omega} + \mathcal{D}_r\Omega = \mathcal{T}(x_0, x_s) - \mathcal{T}_{app}$
$A = \sqrt{\xi_1^2 + \xi_2^2}$
$x_0 = \frac{1}{k}\arccos(\frac{\mathbf{z}}{R_r A})$
$x_s = \frac{1}{k}\arccos(\frac{R_o^2\Omega}{khR_r A\omega})$
$\mathcal{D}_v(x_0, x_s) = \mathcal{D}_o + \frac{\mathcal{D}^*(x_0, x_s)}{\omega}$
$K_v^o(x_0, x_s) = K_o + K(x_0, x_s)$
$f_{r_o} = \frac{1}{2\pi}\sqrt{\frac{K_v^o(x_0, x_s)}{M}}$
$K_v(x_0, x_s) = K_v^o(x_0, x_s)(1 - 2\frac{\ell}{f_{r_o}}\,\Delta\Theta)$
$\mathcal{D}^*(x_0, x_s) = f_t G_1(x_0, x_s)$
$K(x_0, x_s) = f_n\psi(x_0) + f_t G_2(x_0, x_s)$
$f_t = \mu hk R_r^2\epsilon\varkappa_r$
$f_n = R_r^2 R_0\epsilon\varkappa_r$
$\psi(x_o) = kx_0 - \frac{\sin 2kx_0}{2}$
$G_1(x_0, x_s) = 2\,(2\Delta_1(x_s) - \Delta_1(x_0))$
$G_2(x_0, x_s) = 2\,(2\Delta_2(x_s) - \Delta_2(x_0) - 1)$
$\Delta_1(x) = \frac{kx}{2} + \frac{\sin 2kx}{4} - \cos kx_0 \sin kx$
$\Delta_2(x) = \frac{\sin^2 kx}{2} + \cos kx_0 \cos kx$
$F(x_0) = 2K_r R_r A\sin(kx_0)$
$\mathcal{T}(x_0, x_s) = 2\mu\Lambda_0^*\varkappa_r\,(2\Phi(x_s) - \Phi(x_0))$
$\Phi(x) = \sin kx - kx\cos kx_0$
$K_r = \varkappa_r R_o\epsilon\ ,\ K_r^* = 2\pi K_r\ ,\ \Lambda_0^* \approx R_r A R_0^2\epsilon$

Table 6.1: Summary of the complete hybrid model

6.6 Simulation and model validation

The derived hybrid model of the RPEM is implemented in a Matlab-Simulink environment. The results achieved by the simulated model are then compared to the measured characteristics in order to establish the validity of the model.

6.6.1 The effect of the driving frequency on the motor

The performance of the simulated model is given in terms of the output speed performance under varying frequency. The range of frequencies between 40 kHz and 42 kHz is explored and the achieved results are given in figure 6.1

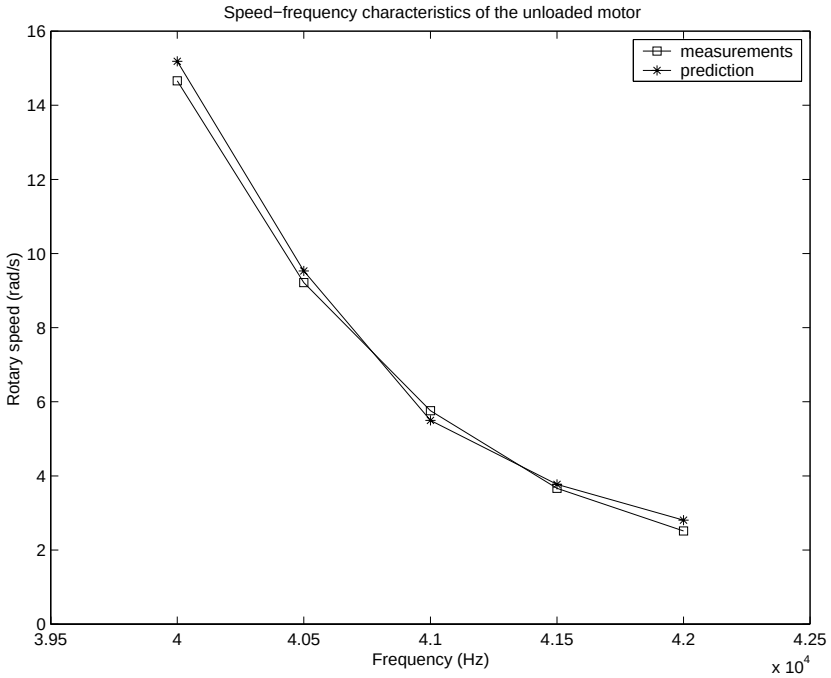

Figure 6.1: Comparison of the speed-frequency characteristics for the unloaded motor: simulation and measurements

It must be emphasized that the results reported in this figure are obtained for the free motor (i.e. no load) operating under its nominal conditions. In the same figure 6.1 are reported the results of the real speed measured directly on the motor. It can be noticed that there is agreement between the simulated model and the measured data, which validates the hybrid modeling of the free motor.

6.6.2 The effect of varying torque on the motor

The speed-torque relationship is the most important characteristic of any electromechanical motor and therefore model validation should respect this criterion. Figure 6.2 represents speed-frequency characteristics under different load torques obtained from the simulated hybrid model.

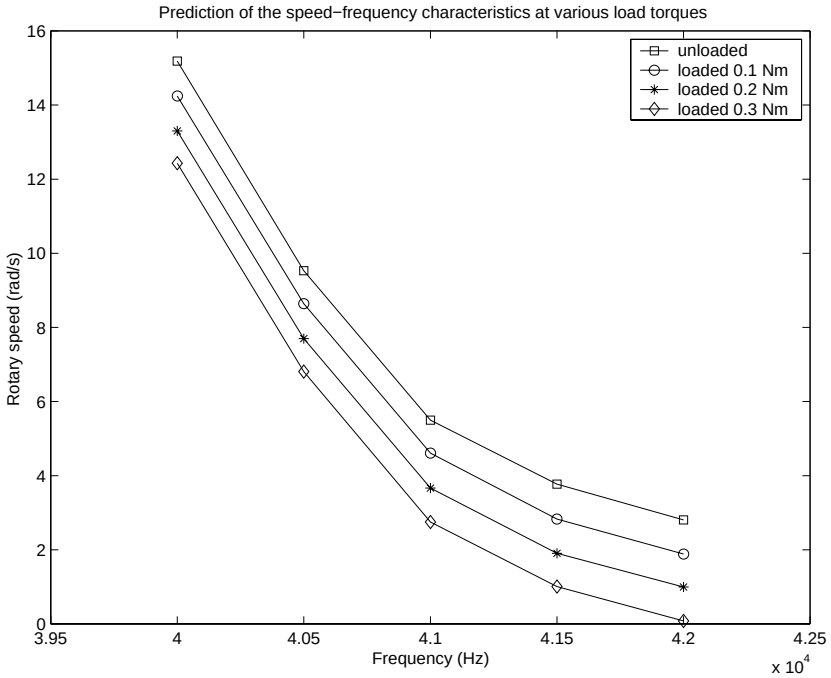

Figure 6.2: Prediction of the speed-frequency characteristics at various load torques

The range of torques between 0 Nm and 0.32 Nm is explored and the results achieved by the simulated model when compared to the real measurements are reported in figure 6.3 for the load torques 0.1 Nm, 0.2 Nm and 0.3 Nm respectively.

It can be noticed from the compared results that there is agreement between the simulated results and the measured results, which validates the model in the range of torques $[0\ Nm, 0.32\ Nm]$ and frequencies of interest i.e. in the neighborhood above the fundamental resonance frequency.

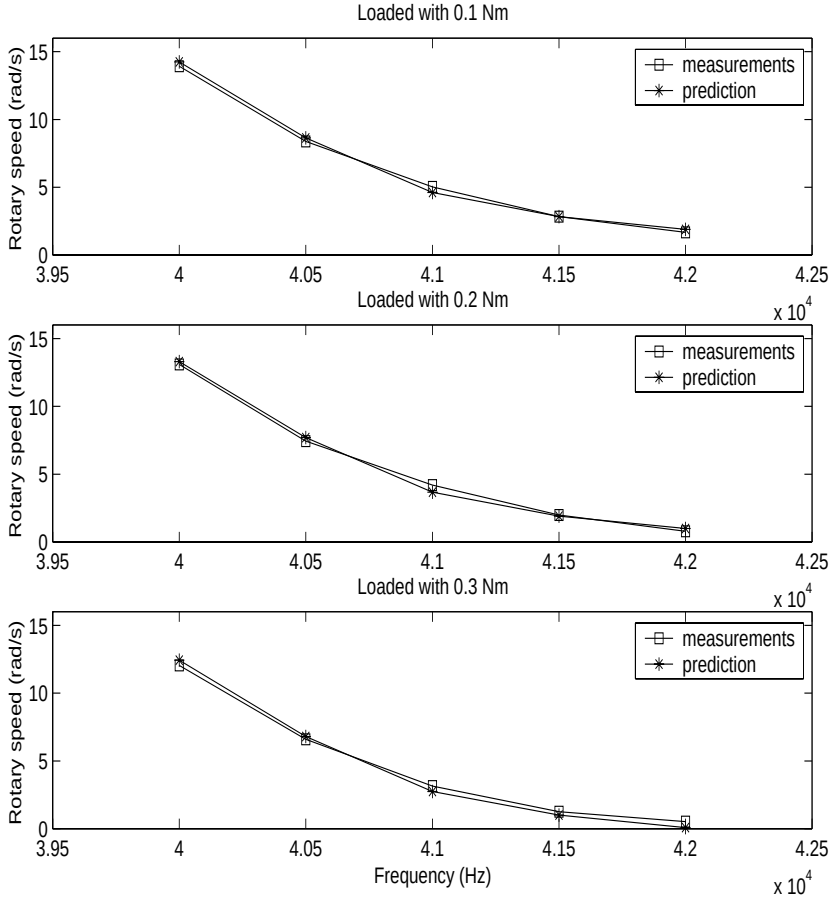

Figure 6.3: Comparison of the speed-frequency characteristics for the loaded motor: simulation and measurements, at load torques 0.1 Nm , 0.2 Nm and 0.3 Nm respectively

6.6.3 The effect of varying temperature on the motor

The mechanical resonance frequency of the motor shifts towards lower frequencies during the operation of the motor due to the temperature increase within the body of the stator. In order to overcome this problem in a simulated environment and therefore predict the performance characteristics of the motor despite the changes in its temperature, a tracking facility which updates the temperature sensitive parameters is introduced in the hybrid model. Figure 6.4 shows the prediction results achieved for the speed of the unloaded motor subjected to temperature variation.

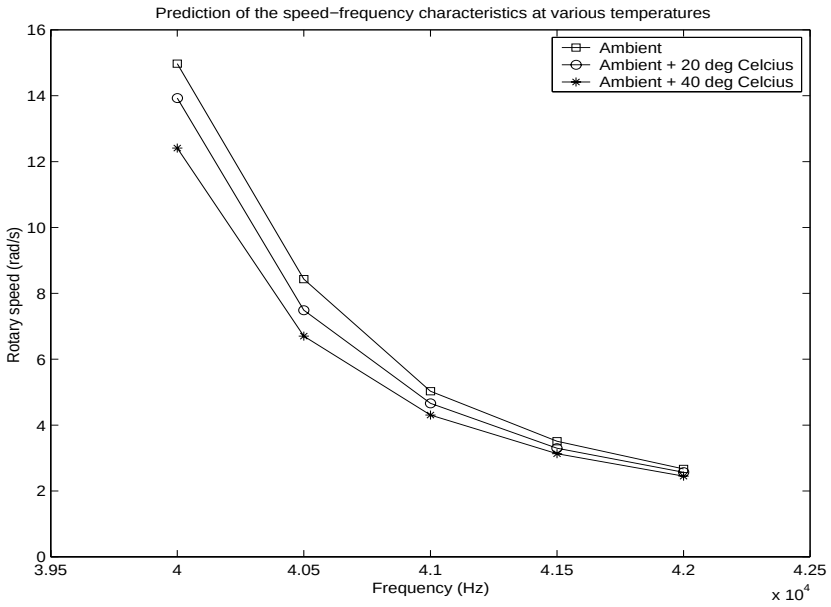

Figure 6.4: Prediction of the speed-frequency characteristics at various temperatures

From figure 6.4 it can be noticed that the resonance frequency is a decreasing function of temperature and consequently for a fixed frequency above the resonance frequency the performance of the motor, in terms of speed, deteriorates. The main conclusion to be drawn is that for speed control purposes the influence of temperature changes must be integrated in the model prediction for long term operations.

6.7 Conclusion and Perspectives

In this chapter the general framework model of the traveling wave type annular forced stator is first recalled. This model is derived by applying the basic laws of variational work and elasticity theory (Hamilton's principle). Second, a reduced model is derived on the basis of the special design of the stator of interest (i.e. two phase symmetrical systems) and various assumptions on its behavior. Third, the analogy between the equivalent circuit model and the derived analytically reduced model of the unforced stator, which models the behavior of one phase of the stator, is highlighted. This makes it possible to substitute the parameters of the equivalent circuit model in the framework of the simplified analytical model. Consequently, the large uncertainties on the dielectrical and electromechanical constants are avoided. Fourth, the simplified hybrid model of the complete motor is thereby derived in terms of the forced stator model, the spinning motion model and the vertical motion model. Finally the effect of temperature on the mechanical resonance frequency is considered and thereby integrated in the final model for long term operations. The derived model has been simulated in a Matlab-Simulink environment. The achieved results have shown an agreement between the simulated results and the experimental results. The experiments have been conducted on a case study: Shinsei motor "type USR60", in the range of torques $[0 - 0.32Nm]$ and frequencies of interest (i.e. in the neighborhood above the fundamental resonance frequency). Thereby the validity of the model has been established.

6.7.1 Advantages and performances

The main advantage of the hybrid method is that it provides a general framework model for simulating a wide variety of traveling wave motors. Many different geometries of the motor can be used provided that they fulfill the symmetry requirements of a perfect traveling wave generation at the surface of the stator. This model is not restricted to the nine wave Shinsei motor USR60. This model encompasses any n'th wave traveling wave piezomotor provided that the electromechanical parameters of the free stator can be identified by using the equivalent circuit method. The strength of this method makes it possible to avoid the large source of errors due to the uncertainties on the available electromechanical constants of the piezoceramics and the required simplifying assumptions on the behavior of the stator. Moreover, the use of the laws of physics for modeling the contact mechanism and the dynamics of the rotor makes it possible to capture the nonlinear behavior of the motor and thereby constitute a better alternative to the equivalent circuit method.

6.7.2 Drawbacks and limitations

The main drawback of the hybrid method is that it provides a solution oriented problem, in the sense that an identification of the parameters is required at each time a new motor has to be modeled. Consequently, this process is time consuming and requieres a fully operational test bench.

6.7.3 Perspectives

The hybrid model constitutes a powerful and suitable test bench for the control community for investigating the usability of the existing linear and nonlinear control methods in a simulated environment. Consequently, the existing control algorithms can be applied directly to the the simulated model and thereby their degree of usability and performance can be established without resorting to actual experiments. Moreover, this model provides the opportunity for the control community to push forward their knowledge and thereby find new methods more suitable for controlling this kind of devices.

Chapter 7

Conclusion and Perspectives

This thesis considers the modeling of a rotary traveling wave piezoelectric motor, with the emphasis on the procedure of deriving a simplified model with low computational demands. The objective of the modeling task is to fulfill the requirements of a flexible test bench model suitable for control investigation purposes. This final chapter provides an overview of the content of this thesis and thereafter summarizes the major achievements of the work and suggests some directions and perspectives for future use of this work.

7.1 Overview of the content of this thesis

A brief summary of the content and utility of each part of this thesis is given in the following items.

- **The piezoelectric field and its applications**: is addressed in order to stress the state of the art in this field. The emphasis is put on the degree of innovation in this field and its contribution to the industry and science by presenting an overview of the piezoelectric materials and their use as actuators, for solving some engineering problems, together with their limitations and advantages compared to the traditional and well-established electromagnetic devices. Finally the trends of these new devices are discussed in the framework of the more general class of smart structures. Furthermore, some of the theoretical background that lays the foundations of piezoelectricity is recalled. The emphasis is put on the interaction processes that take place within the piezoelectric media and the necessary definitions of their different constitutive relations in tensor notation. Consequently, the fundamental relations that represent the behavior of any piezoelectric media for in-

dependent variable sets are presented within the framework of the thermodynamic field. Thereafter the matrix notation for the constitutive relation is addressed in order to stress that, in contrast to the tensor algebra, formulae and constants are easily transformed using matrix algebra. Moreover, the particular case of the PZT ceramics used in piezomotors is addressed in order to stress that the symmetrical nature of the crystal structure induces some simplification. Consequently, the electromechanical coupling in the piezoelectric PZT ceramics is achieved through three principal modes of vibrations. These modes are the longitudinal mode, the transversal mode and finally the shear mode. Finally, the electromechanical coupling factor which is the parameter that guarantees the effective energy conversion in a linear interaction system is addressed. The emphasis is put on the different ways of defining this coupling factor and thereby make it ready for use in the subsequent chapter of this thesis.

- **The experimental investigations**: of the Shinsei ultrasonic motor USR60, which is used as a case study in this thesis, is addressed. The different parts that constitute the motor and how they are connected besides the working principle and the specifications of this motor are introduced in order to make the reader familiar with this piezoelectric device. Thereafter, the results of the investigations, which consist of the establishment of the operating characteristics of the motor under various working conditions, are reported. The objectives of the experimental approach are to establish the physical understanding of the behavior of the motor in particular its nonlinearities and also identify some of the parameters of the motor which are necessary for the modeling task.

  Consequently, the influence of the excitation parameters, which are the relative phase shift, frequency and the common amplitude voltage of the power supply, on the output speed of the motor under various working conditions is investigated and the corresponding characteristics are reported. Furthermore, the speed-torque characteristic is measured under nominal conditions. Thereafter, the influence of several parameters, such as the excitation frequency, the normal forcing, the load torque and the output speed on the feedback signal is investigated and the corresponding characteristics are reported. Furthermore, the influence of temperature changes on the motor is investigated by monitoring the shift of the resonance frequency of the feedback signal versus temperature under nominal conditions of operation. Moreover, the measurement of the electrical admittance of the stator over a large span of frequencies is provided for the purpose of making some comparisons with other approaches predicting the behavior of the transducer by applying the basic laws of physics. Then, the measurement of the electrical admittance of the stator in sweep up and sweep down frequency conditions around the fundamental resonance is addressed in order to highlight the nonlinearities of this device. Finally, the influence of the common amplitude voltage and the load torque on the admittance of the loaded motor is investigated and the correspond-

ing characteristics are reported. The outcome of this experimental approach is that the influence of the excitation and load parameters on the behavior of the motor is explored within the range of their limits. This provides the necessary knowledge for achieving the objective of this thesis.

- **The equivalent circuit modeling**: is addressed by first recalling the theoretical background of the equivalent circuit method. Thereafter, equivalent circuit modeling of a ring type stator, regarded as a straight beam with infinite length undergoing bending deformations of transverse type (T-effect) is addressed. Consequently, Mason's equivalent circuit model for a T-effect bar transducer is derived by applying the basic laws of physics. This leads to a set of equations representing the electromechanical coupling in the piezoceramic beam. This set of equations are represented by Mason in the form of a six terminal equivalent circuit information. This circuit is further reduced to a four terminal network which represents the closed shape ring. Furthermore, it is shown mathematically that the output terminal of this circuit, which represents the electromechanical motional branch of the admittance, can be expressed by an infinite number of resonant serie circuits in parallel. Thereafter, the electromechanical coupling factor is expressed as a function of the force factor and the admittance parameters. Furthermore, by only considering the behavior of the ideal stator (i.e. no losses) around the fundamental resonance frequency and assuming that the output branch behaves like a short circuit the two terminal representation is obtained. Finally, the equivalent circuit model for one phase of the real stator integrating the losses around the fundamental resonance frequency where the mechanical parameters are seen as their electrical equivalent is emphasized. The identification method, which uses the electrical network method to establish the parameters in the equivalent circuit model, is addressed. Consequently, the definitions of the characteristic parameters obtained from the different diagrams of the admittance are recalled and a final set of equations that gives the evaluation formula for each parameter in the two-terminal equivalent circuit model is emphasized. Thereafter, the analysis in terms of equivalent circuit information provides the final representation of the complete motor by two four-terminal equivalent circuits connected by a wave mixer and ends by a load box that represents all the phenomena that intervene, beyond the stator, at the interface contact with the rotor. Furthermore, it is stressed that due to the symmetrical nature of the stator the final equivalent circuit model of the complete motor can be reduced to a mono-phase four terminal circuit. Moreover, it is shown that, according to the piezoelectric direct effect, valuable information about the traveling wave characteristics within the stator can be obtained by sensing the feedback electrode. Consequently, the proportionality between the amplitude of the feedback voltage and the ideal rotary speed of the motor is highlighted, and also the proportionality to the amplitude of the traveling wave is stressed. These results suggests that the feedback voltage can be used for predicting and controlling the motor.

The equivalent circuit modeling of the traveling wave motor USR60 is done stepwise by first considering the free stator then the unloaded motor and finally the loaded motor. It is shown by admittance measurement of the free stator that this device can be assumed to be perfectly symmetrical and thereby only one phase needs identification. The identification of parameters of the two terminal equivalent circuit model is carried out by using the electrical network method. Consequently, the extraction of respectively the parameters of the electrical and electromechanical admittance of the stator makes it possible to derive the electromechanical force factor. Thereafter, the equivalent circuit model prediction of the stator is validated by simulation and comparison to the real data. Furthermore, the prediction of the behavior of the stator over a large span of frequencies by using the equivalent circuit model is stressed. Moreover, a thorough analysis of the electromechanical force factor is carried out in which the emphasis is put on the difference between the effective force factor and the modal force factor. Consequently, the relationship between the modal force factor and the motional current is emphasized and an explicit relationship between the modal force factor and the effective force factor is highlighted. The unloaded motor is addressed by integrating the losses due to the pressure and the friction in the equivalent circuit model. The losses of power due to pressure conditions are represented by an extra resistance at the input terminal. The frictional losses are integrated by adjusting the motional resistance by simulation and by subtracting from the ideal motional current an amount image of the speed drop seen as its electrical equivalent. Furthermore, the capacitance of the motional admittance is adjusted by monitoring the resonance frequency of the feedback signal of the unloaded motor under operation. The loaded motor is addressed by integrating the speed drop due to the load torque in the equivalent circuit model. It must be emphasized that the changes in damping and the capacitance of the motional admittance caused by the load torque can be neglected in the simulation process.

Thereafter, it is emphasized that in terms of equivalent circuit modeling the effect of temperature can be represented by the same equivalent circuit model but with varying parameters. Consequently, it is pointed out that for practical reasons only the changes of the motional admittance with temperature must be integrated in the final model. Thereby, a tracking facility which updates the temperature sensitive parameters is derived and thereafter simulated. The results achieved by simulations are then reported and commented. These results suggest that for speed control purposes the influence of temperature changes must be integrated in model prediction for long term operations. Finally, the derived equivalent circuit model of the motor is simulated and thereby the effects of the excitation frequency and the load torque are investigated. Consequently, the different results achieved by the simulated model and the feedback predictions are compared to the measured characteristics. Thereby the validity of these two methods is established in the range of torques and frequencies of interest.

- **The analytical modeling**: is addressed by first recalling the necessary theoretical background of the energy method which uses Hamilton's principle modified for general electromechanical systems. The appropriate definitions of the constitutive relations describing the behavior of any vibrating elastic substrate are recalled and the relevant piezoelectric relation describing the stator in transverse mode of vibrations is stressed. Thereafter, the Lagrangian of the system and the variational work done by the external forces are explicitly defined as a function of the parameters of the vibrating stator. Consequently, the general actuator and sensor equations representing the behavior of the stator are derived. The dynamic of the rotor is addressed and thereby the equations of motion of the rotor in vertical and spinning direction together with the interface force and the interface torque are stressed.

  The general framework model of the motor is derived by using only the actuator equation of the stator together with the vertical and spinning motion models of the rotor. Thereafter, the different parameters of the model are addressed in the framework of some necessary assumptions on the behavior of the stator in order to simplify the modeling task. Consequently, the applied voltage is explicitly defined for the nine wave motor and the parameters of the actuator equation, which are the modal mass matrix, the modal stiffness matrix and the electromechanical coupling matrix, are calculated and diagonalized. Thereby, a state space representation is obtained.

  The pressure distribution at the stator-rotor interface contact is addressed by introducing a wave oriented coordinate system rotating with the traveling wave, in which to write the equations describing the mutual interaction between the stator and the rotor. Thereafter, the nonlinear elements in the state space model are addressed. Consequently, the normal modal forcing vector, the tangential modal forcing vector, the interface force and interface torque are derived explicitly as functions of the excited modes and the stick-slip behavior of the contact mechanism. Finally, an explicit state space representation of the complete motor is derived.

  Moreover, the complexity of the obtained model is addressed by considering the symmetrical nature of the design of the stator. Thereby, a simplified model of the motor is derived within the framework of various assumptions on the behavior of the stator. This makes it possible to predict the performance of the stator by a single second order system with varying parameters. These parameters are mainly functions of the stick-slip coordinates of the contact mechanism and reflect the external conditions, which are the pressure distribution at the interface contact and the torque load on the motor. The derived complete and final simplified model is thereby a simplified actuator model of the stator together with the model of the rotor in spinning and vertical directions. Consequently, the complexity of the model is reduced.

Finally, a summarizing table reports the final simplified analytical model derived in this chapter. Thereafter, in order to implement this model in a simulated environment, a table summarizing the parameters that must be known beforehand in order to perform the simulation successfully is given. Finally, a conclusion is drawn, and thereafter the advantages and performance together with the drawbacks and limitations of this modeling method are stressed and finally the alternative solution and its perspective is emphasized.

- **The hybrid modeling**: is addressed by first recalling the general framework analytical model of the stator. It is emphasized that both the actuator and the sensor equations must be used for deriving the hybrid model. Thereby, the piezoelectric capacitance matrix is defined. The different diagonal matrices representing the parameters of the actuator model are recalled and thereafter the piezoelectric capacitance matrix is calculated and diagonalized and the charge vector on the electrodes of the stator is defined. Consequently, an explicit actuator model and sensor model representing the dynamic of the stator are derived.

  Moreover, a reduced model of the stator representing only one phase of the stator is highlighted. From the sensor equation the electrical admittance of one phase of the stator is derived. Thereby, the analogy between the equivalent circuit method and the analytical method is emphasized. The actuator equation of the free stator is used to derive the analytical electromechanical admittance of the stator, which is the ratio between the temporal amplitude of vibration and the input voltage. Thereafter, the substitution of this ratio in the analytical electrical admittance suggests that the parameters of the actuator equation of the free stator can be identified by using the electrical network method. Consequently, the identification of the parameters of the analytical model is provided by the equivalent circuit method and thereby a hybrid model of the stator is obtained. Thereafter, the remaining parts of the simplified analytical model are recalled and thereby the simplified hybrid model of the complete motor is given for short term operations. For long term operation the temperature effect is considered and thereby integrated in the complete and final simplified hybrid model of the motor for long term operations.

  Finally, a summarizing table reports the final simplified hybrid model derived in this chapter, and a reference to the appropriate appendix containing the data of the motor used in simulation is given.

  Different experiments are done in order to establish the validity of the model. For instance, the influence of the excitation frequency and the influence of the load torque on the speed performance of the motor are tested. The results of the simulations are compared to the real characteristics of the motor and thereby the validity of the model is established. Finally, a conclusion is drawn.

7.2 Final conclusion

Theoretical and experimental methods are used in this thesis. The main achievement of this work is the combination of the strength of the equivalent circuit method and the analytical method in a hybrid simplified model providing the ability to predict most of the performance characteristics of the motor under various working conditions.

The following conclusions are drawn on the accomplishments and contributions of the thesis

- The theoretical background of the equivalent circuit modeling method is addressed when applied to the ring-type stator. Thereafter, the electrical network method is used to establish the parameters of the equivalent circuit model experimentally. A special attention is paid to the integration of the appropriate electromechanical force factor in the equivalent circuit model. The emphasis is put on the difference between the effective force factor and the modal force factor. The final equivalent circuit model for short term operations is derived stepwise, by first considering the free stator, then the unloaded motor and finally the loaded motor. For long term operations, a tracking facility which updates the temperature sensitive parameters is integrated in the final model.

- The theoretical background of the analytical model of the rotary piezoelectric motor is addressed. Thereafter a general state space model is derived. By making some assumptions on the behavior of the stator a simplified model is obtained. Consequently, the excited modes are decoupled and the dynamic of the stator is captured in a single second order model. The stick-slip behavior is integrated in the time varying parameters of the model. The final model is derived in terms of the simplified stator model, the vertical motion model and finally the spinning motion model.

- The equivalent circuit model suffers from its inability to cope with the frictional behavior of the motor, whereas the electrical network method provides relatively more accurate values of the parameters used in the equivalent circuit model. Besides, the available electromechanical constants, of the piezoceramics used in this kind of motors, are not accurate values. These uncertainties combined with the calculus approximation generally result in a large discrepancy from the real parameters of the motor. Therefore, the analogy between the equivalent circuit model and the derived analytically reduced model of the free stator, which both represents the behavior of one phase of the stator, is highlighted. This makes it possible to substitute the parameters of the equivalent circuit model in the framework of the simplified analytical model. Consequently, the large uncertainty on the dielectrical and electromechanical constants is avoided. The simplified hybrid model of the complete motor is thereby derived in terms of the forced stator

model, the spinning motion model and the vertical motion model. Finally, for long term operations a tracking facility of the temperature sensitive parameters is integrated in the final hybrid model.

7.3 Perspectives and recommendations

The modeling procedure presented in this thesis lays the foundations for a general framework test bench for simulating a large variety of traveling wave motors, i.e. different sizes, shapes and number of waves provided that the symmetry requirement for a perfect traveling wave generation is fulfilled. The procedure of the equivalent circuit method can easily be applied to any kind of piezoelectric motor, in particular the rotary standing wave motors. The analytical modeling procedure and thereby the hybrid case can also be pushed further to encompass the rotary standing wave motors if an appropriate model of the contact mechanism is defined. The contributions of this work can be used with benefit at different levels of utility. The following items state some suggestions for future use of the different achievements of this work.

- **The power supply**: of the motor is the cornerstone of this kind of device. Therefore, the investigation of the new appropriate power supply strategies can be carried out in a simulated environment by only using the equivalent circuit model due to its simplicity.

- **The design**: of the motor is responsible for most of the output power performance of the motor. Therefore, the investigation of the influence of the different geometrical parameters of the motor on the output performance can be carried out in a simulated environment by using the analytical model. Furthermore, the analytical model can be used to investigate the performance of various types of piezoelectric materials and also the influence of the materials used in the frictional layer of the contact mechanism.

- **The control**: of the motor is the most important part in the final operational motor. Therefore, the investigation of suitable control strategies can be carried out in a simulated environment by using either of the models derived in this thesis. However, it must be emphasized that the hybrid model is the most appropriate model for achieving realistic results. With this model many control strategies can be investigated including linear and nonlinear control methods.

Perspectives and recommendations for solving the control problem

The hybrid model of the PEM no matter how much simplified is still highly nonlinear, time varying and has load and temperature dependent parameters. Moreover, it must be

emphasized that developing mathematical models for real systems is always problematic; the models developed never completely describe the real system. This mismatch between the behavior of the real system and that expected from the model is called uncertainty. The quality ascribed to a particular model depends on the amount of uncertainty in the model relative to the expected objective for using the model. Furthermore, the control characteristic of the PEM is complicated, highly nonlinear, and the control characteristic and motor parameters are time-varying due to temperature rise and changes in motor drive operating conditions, such as drive frequency, source voltage, and load. The control strategies have not yet been investigated thoroughly regarding the complexity of the strongly nonlinear behaviour of the PEM. The objective of solving the control problem is to design a suitable control system to ensure that the proper response to the given inputs occurs despite the influences of temperature fluctuations and external loading on the motor. Therefore, an appropriate use of the PEM requires that a high-precision control system must be used.

It must be emphasized that, in light of the experimental investigations, frequency control is the most appropriate method for controlling the PEM. Therefore, a simple model representing the frequency-output relationship must be derived from the hybrid model in order to design the control system for the simulated model. The following items constitute some suggestions/directions for solving the control problem in a simulated environment, without resorting to actual experiments on the real PEM.

- **Adaptive and nonlinear robust control**

  Due to the time varying nature of the hybrid model representing the PEM, it is believed that adaptive control constitutes an appropriate solution to the control problem. Moreover, when using a model-based controller it is known that often the parameters in the model do not match the parameters of the real plant so servo errors will result. These servo errors could be used to drive some adaptation schemes which attempt to update the values of the model parameters until the errors disappear.

  An alternative solution to adaptive control is to use a robust controller. For instance, a nonlinear robust control strategy combined with an appropriate model of the friction mechanism driving the real system is believed to be the most appropriate solution to the control problem.

  Robust control attempts to deliver controllers that make the very best use of available information about the system (i.e. given a linear model, a specified amount of undermodeling uncertainty, assumptions on external forces, "noise", impact behavior, a precise description of the performance objective, etc...). Nonlinear robust control, on the other hand, is a label that describes the development of robust controllers for systems with nonlinear models.

  The nonlinear behavior of the PEM cannot be linearly undermodeled in a way that will meet the performance objective. Therefore, the objective behind the deriva-

tion of a nonlinear robust controller to the PEM is to find a good set of constant gains that despite the "motion" of the poles will guarantee that they remain in reasonably favorable locations. Furthermore, the main problem in deriving a robust controller to the PEM is to design the feedback loop and the feedforward model so that the stability and performance are maintained in spite of process variations. Finally, the objective of this method is to design a controller for the PEM which is robust against its nonlinearities and adaptive to its environmental conditions.

- **Fuzzy and neurofuzzy adaptive control**

  The fuzzy logic-based approach to solving problems in control has been found to excel in systems which are very complex, highly nonlinear and with parameter uncertainty. Fuzzy logic can be applied to the PEM if the previously mentioned conventional model-based approache are difficult or not cost-effective to implement. However, as the complexity of the PEM is high, reliable fuzzy rules and membership functions necessary to describe the behavior of the PEM could be difficult to determine. Furthermore, due to the complexity and the dynamic nature of the PEM, rules and membership functions must be adaptive to the changing environment in order to continue to be useful. Therefore neurofuzzy, which is the combination of fuzzy logic and neural networks, may be used in order to overcome the drawbacks of either. Neural network learning provides a good way to adjust the expert's knowledge and automatically generates additional fuzzy rules and membership functions in order to meet certain specifications and reduce design time and costs. On the other hand, fuzzy logic enhances the generalization capability of a neural network system by providing more reliable output when extrapolation is needed beyond the limits of the training data. The neurofuzzy system consists of the various components of a traditional fuzzy system, except that each stage is performed by a layer of hidden neurons, and neural network learning capability is provided to enhance the system knowledge. Neurofuzzy systems offer the precision and learning capability of neural networks, and yet they are easy to understand like fuzzy systems. Explicit knowledge acquired from experts can be easily incorporated into such a system, and implicit knowledge can be learned from training samples to enhance the accuracy of the output. Furthermore, the modified and new rules can be extracted from a properly trained neurofuzzy system to explain how the results are derived. Finally, the objective of this method is to design an adaptive neurofuzzy controller for the PEM which is simple to implement, adaptive to its environmental conditions and fulfills the stability requirement of an adaptive robust controller.

Finally, the applications of the findings of this work should lead to an assessment of the tools developed for the PEM, identify gaps in the understanding of the modeling/control process, and ask new questions based on the peculiarities of the real PEM system.

Bibliography

Berg, M., P. Hagedorn and T. Sattel (1998). Comparison of Experimental and Simulation Data of Ultrasonic Traveling Wave Motors. In proc.: *Actuator 98*. pp. 253–255.

Ferreira, A., P. Cusin, P. Minotti and P. Le Moal (1996). Traveling Wave Ultrasonic Motors: III. Validity Limits of 2-D Models and Current Prospects. *J. of Physic III France* **6**, 1363–1388.

Flynn, A. M. (1995). Piezoelectric Ultrasonic Micromotors. PhD thesis. Department of Electrical Engineering and Computer Science, MIT.

Friend, J. R. (1994). Analysis of the performance and contact behavior of the piezo lectric traveling-wave motor. Master's thesis. University of Missouri Rolla.

Friend, J. R. and D. S. Stutts (1997). The Dynamics of an Annular Piezoelectric Motor Stator. *Journal of sound and vibration*.

Furuya, S., T. Maruhashi, Y. Izuno and M. Nakaoka (1990). Load-Adaptive Frequency Tracking Control Implementation of Two-Phase Resonant Inverter for Ultrasonic Motor. *IEEE PESC'90* pp. 17–24.

Hagedorn, P. and J. Wallashek (1992). Traveling Wave Ultrasonic Motors, Part I: Working principles and Mathematical Modeling of The Stator. *Journal of Sound and Vibration* **155**, 31–46.

Hagedorn, P., J. Wallashek and W. Konrad (1993). Traveling Wave Ultrasonic Motors, Part II: A Numerical Method for the Flexural Vibrations of the Stator. *Journal of Sound and Vibration* **168**, 115–122.

Hagedorn, P., T. Sattel, D. Speziari, J. Schmidt and G. Diana (1998). The Importance of Rotor Flexibility in Ultrasonic Traveling Wave Motors. *Smart Mater. Struct.* **7**, 352–368.

Hagood, N. and J. Andrew (1995). Modeling of a Piezoelectric Rotary Ultrasonic Motor. *IEEE Trans. Ultrason. Ferroelectr. Frequency Control* **42**(2), 210–224.

Hagood, N., W. Chung and A. Flotow (1990). Modeling of a Piezoelectric Actuator Dynamics for Active Structural Control. *J. of Intell. Mat. Syst. and Struct.* **1**, 327–354.

Hirata, H. and S. Ueha (1991). Revolution Speed Characteristics of an Ultrasonic Motor Estimated from the pressure Distribution of the Rotor. *Japanese Journal of Applied Physics* **31**(1), 248–250.

Hirata, H. and S. Ueha (1993). Characteristics Estimation of a Traveling Wave Type Ultrasonic Motor. *IEEE Trans. Ultraso. Ferroelec. and Freq. Control* **40**(4), 402–406.

Hirata, H. and S. Ueha (1995). Design of a Traveling Wave Type Ultrasonic Motor. *IEEE Trans. Ultraso. Ferroelec. and Freq. Control* **42**(2), 225–231.

Holland, R. and E. EerNisse (1969). *Design of Resonant Piezoelectric Devices*. M.I.T. Press.

Ikeda, T. (1996). *Fundamentals of Piezoelectricity*. Oxford University Press.

Izuno, Y. and M. Nakaoka (1994). High Performance and High Precision Ultrasonic Motor-Actuated Positioning Servo Drive System using Improved Fuzzy-Reasoning Controller. *IEEE PESC'94*.

Kumada, A. (1987). Ultrasonic motor using bending, longitudinal and torsional vibrations. US Patent No. 4 642 509. 10 Claims, 14 Drawing Sheets.

Kumada, A. (1989). Piezoelectric revolving resonator and ultrasonic motor. US Patent No. 4 868 446. 10 Claims, 17 Drawing Sheets.

Kumada, A., T. Iochi and M. Okada (1991). Piezoelectric revolving resonator and single phase ultrasonic motors. US Patent No. 5 008 581. 6 Claims, 6 Drawing Sheets.

Lin, F. (1997). Fuzzy Adaptive Model-Following Position Control for Ultrasonic Motor. *IEEE Trans. on Power Electronics* **12**(2), 261–268.

Lin, F. and L. Kuo (1997). Driving Circuit for Ultrasonic Motor Servo Drive with Variable-Structure Adaptive Model-Following Control. *IEE Proceedings online*.

Lin, F., R. Wai and H. Lin (1999). An Adaptive Fuzzy-Neural-Network Controller for Ultrasonic Motor Drive Using the LLCC Resonant Technique. *IEEE Trans. Ultrason. Ferroelec. and Freq. Control* **46**(3), 715–727.

Maas, J. and H. Grotstollen (1996*a*). Cascaded Control Scheme for Speed Variable Ultrasonic Drives. *IEEE IAS'96* **1**, 440–447.

Maas, J. and H. Grotstollen (1996*b*). Dynamic Analysis of Inverter-Fed Ultrasonic Motors. *IEEE PESC'96* pp. 1780–1786.

Maas, J., N. Fröhleke, P. Krafka and H. Grotstollen (1995*a*). Prototype Drive and Modulation Concepts for DSP-Controlled Ultrasonic Motors Powered by resonant Converters. In proc.: *EPE'95*. Sevilla (Spain). pp. 1777–1782.

Maas, J., P. Ide and H. Grotstollen (1996). Characteristics of Inverter-Fed Ultrasonic Motors - Optimization of Stator-Rotor Interface. *IAS'95* pp. 241–244.

Maas, J., P. Ide, N. Fröhleke and H. Grotstollen (1995*b*). Simulation Model for Ultrasonic Motors Powered by resonant Converters. *IEEE IAS'95* **1**, 111–120.

Maas, J., T. Schulte and H. Grotstollen (1997). Optimized Drive Control for Inverter-Fed Ultrasonic Motors. *IEEE IAS'97* **1**, 690–698.

Maas, J., T. Schulte and H. Grotstollen (1998). High Performance Speed Control for Inverter-Fed Ultrasonic Motors Optimized by a Neural Network. In proc.: *Actuator 98*. pp. 260–263.

Maeno, T. and D. Bogy (1992). Effect of the Hydrodynamic Bearing on Rotor/stator Contact in a Ring-type Ultrasonic Motor. *IEEE Trans. on Ultraso. Ferroelec. and Freq. Control* **39**(6), 675–681.

Maeno, T., T. Tsukimoto and A. Miyake (1990). The Contact Mechanism of an Ultrasonic Motor. In proc.: *7th IEEE International Symposium on Application of Ferroelectrics*. In Kanagawa, Japan. pp. 535–538.

Maeno, T., T. Tsukimoto and A. Miyake (1992). Finite-Element Analysis of the Rotor/stator Contact in a Ring-type Ultrasonic Motor. *IEEE Trans. on Ultraso. Ferroelec. Freq. Control* **39**(6), 668–674.

Mason, W. (1964). *Physical Acoustics*. Harcourt Brace Jovanovich, Academic Press.

Mass, J. and H. Grotstollen (1997). Averaged Model of Inverter-Fed Ultrasononic Motors. *IEEE PESC'97* **1**, 740–746.

Minotti, P., P. Le Moal, L. Buchaillot and A. Ferreira (1996). Traveling Wave Ultrasonic Motors: I. Modeling of the Mechanical Energy Transduction of Stator/Rotor Interface. *J. of Physic III France* **6**, 1315–1337.

Moal, P. Le, P. Minotti, A. Ferreira and J. Duffaud (1996). Traveling Wave Ultrasonic Motors: II. Bidimensional Analytical Modeling of the Stator/Rotor Contact. *J. of Physic III France* **6**, 1339–1361.

Nakamura, K., M. Kurosawa and S. Ueha (1993). Design of a Hybrid Transducer Type Ultrasonic Motor. *IEEE Trans. on Ultrasonics, Ferroelectrics and Frequency Control* **40**(4), 395–401.

Nakamura, K., M. Kurosawa, H. Kurebayashi and S. Ueha (1991). An Estimation of Load Characteristics of an Ultrasonic Motor By measuring Transient Responses. *IEEE Trans. on Ultrasonics, Ferroelectrics and Frequency Control* **38**(5), 481–485.

Nogarede, B. and E. Piecourt (1994). Modelisation of a Traveling Wave Piezoelectric Motor by Equivalent Electromechanical Circuit. In proc.: *IECM'94*.

Ragulskis, K., R. Bansevicius, R. Barauskas and G. Kulvietis (1988). *Vibromotors for Precision Microrobots*. Hemisphere Publishing Corporation.

Sashida, T. (1985). Motor device utilizing ultrasonic oscillation. US Patent No. 4 562 374. 29 Claims, 22 Drawing Sheets.

Sashida, T. and T. Kenjo (1993). *An Introduction to Ultrasonic Motors*. Oxford Science Publications.

Sattel, P., P. Hagedorn and M. Berg (1998). Simulation Model Used as Design Tool for Traveling Wave Ultrasonic Motors. In proc.: *Actuator 98*. pp. 249–252.

Schmidt, J., P. Hagedorn and M. Bingqi (1996). A Note on the Contact Problem in an Ultrasonic Traveling Wave Motor TMO. *J. Non-Linear Mechanics* **31**(6), 915–924.

Senjyu, T., S. Yokoda, H. Miyazato and K. Uezato (1997). Speed Control of Ultrasonic Motors by Adaptive Control with a Simplified Mathematical Model. *IEE Proceedings online*.

Takano, T., H. Hirata and Y. Tomikawa (1990). Analysis of Nonaxisymmetric Vibration Mode Piezoelectric Annular Plate and its Application to an Ultrasonic Motor. *IEEE Trans. on Ultrasonics, Ferroelectrics and Frequency Control* **37**(6), 558–565.

Takano, T., Y. Tomikawa and C. Kusakabe (1992). Same Phase Drive-Type Ultrasonic Motors Using Two Degenerate Bending Vibration Modes of a Disk. *IEEE Trans. on Ultrasonics, Ferroelectrics and Frequency Control* **39**(5), 180–186.

Uchino, K. (1997). *Piezoelectric Actuators and Ultrasonic Motors*. Kluwer Academic Publishers.

Ueha, S. and Y. Tomikawa (1993). *Ultrasonic Motors: Theory and Applications*. Oxford Science Publications.

Wallaschek, J. (1998). Contact Mechanics of Piezoelectric Ultrasonic Motors. *Smart Material and Structure* **7**, 369–381.

Xisheng, C. and J. Wallaschek (1995). Estimation of the Tangential Stress in the Stator/Rotor Contact of Traveling Wave Ultrasonic Motors Using Visco-elastic Foundation Models. In proc.: *CM'95*. Ferrara (Italy).

Appendix A

Test Bench

This appendix presents the test bench used for conducting the experiments on the Shinsei motor USR60 used as a case study in this thesis. The experiments have been carried out during my four months stay, in the spring of 1999, at the LEEI, ENSEEIHT, Toulouse in France under the supervision of Professor Bertrand Nogarede.

A.1 The experimental test bench

For conducting the experiments a test bench comprising two different but complementary test setups is used. These two setups referred to by the manual test setup and the automatic test setup will be presented and discussed in the following sections.

A.1.1 The manual test setup

The a priori determination of the intrinsic characteristics of the motor, requires a suitable and well defined power supply. The power supply should provide two orthogonal sinusoidal waves in order to avoid simultaneous excitation of several modes of vibrations of the stator. Furthermore, It should provide the ability of varying freely the amplitude, frequency and phase of the excitation waves.

For that purpose, a manual test setup have been developed at the LEEI, ENSEEIHT, Toulouse in France. A sketch of the experimental setup, which contain the different elements that constitute the electromechanical system and the measurment tools, is shown in figure A.1. The two electrodes of the motor are then connected to the two phase power supply. It should be noticed that the two phase generator (HP 3326A) and the linear power amplifier constitute the power supply. The linear power amplifier, which

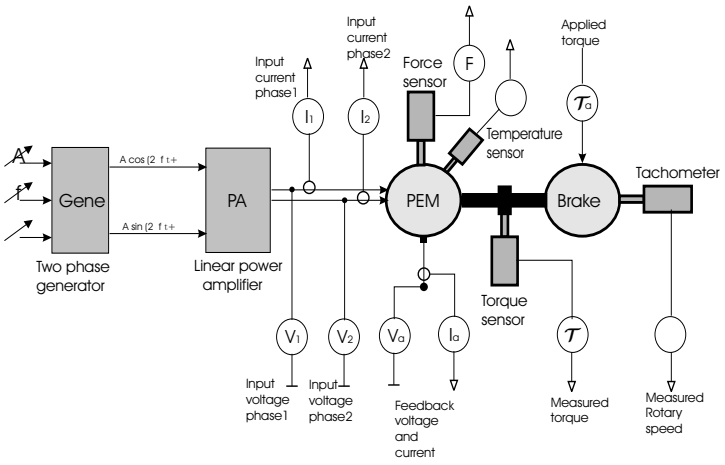

Figure A.1: The manual test setup

was designed and manifactured at the LEEI is able to provide sinusoidal voltages at up to 300 Vpp under 1 App between 3 and 100 kHz.

Voltage and current probes together with a gain-phasemeter (HP 3575A) allow the measurments of the electrical variables at different terminals of the motor

- Two inputs of the voltage supply (V_1, V_2)
- Two inputs of the absorbed current (I_1, I_2)
- Relative phase $\Delta\phi$ between the inputs of the voltage supply
- Voltage V_a and current I_a of the feedback signal

The mechanichal part of the setup shows the motor loaded by a brake and an axial loading. The brake device (Merobel EFAS 10) provides torques between 0 and 1 Nm and the ability of varying the magnitude of the torques independently from the rotary speed. The axial load can be adjusted by spring-knob regulator. This unit permits the analysis of the influence of the axial force on the torque speed characteristics.

The resisting torque and the applied axial load are measured by constraint Gauge, (respectively Sedeme XF 2daN and 20daN). The rotary speed Ω is obtained by measuring the frequency (Philips PM6665) of a triangular signal, image of the position, provided by multi-round potentiometer. The temperature of the motor is measured by a thermocouple sensor.

A.1.2 The automatic test setup

The main objective of the automatic test setup is to provide a mechanical and electrical characterization of the electromechanical motor. Consequently, the main functions that the setup should fulfill are stated below

- Generate polyphase signal over a large pass band, with the possibility of amplitude and frequency calibration
- Measurement of the electrical quantities: current, voltage and phase
- Measurement of the mechanical quantities: displacement and vibration velocity
- Frequency analysis and data collection

For that purpose, an automatic test setup have been developed at the LEEI, ENSEEIHT, Toulouse in France. A sketch of the experimental setup, which contain the different elements that constitute the electromechanical system and the measurment tools, is shown in the figure A.2

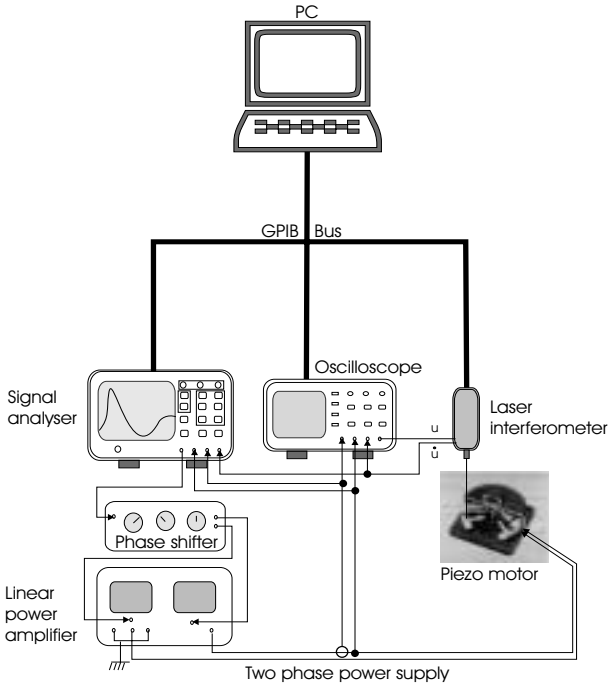

Figure A.2: The automatic test setup

The automatic method is based principally on the Dynamic Signal Analyzer type (HP 3562A) which is a dual channel, fast Fourier network, spectrum, and wave form analyzer. The Signal Analyzer combined with the phase shifter and the linear power amplifier serves as the power supply for the electromechanical system under analysis. The Signal Analyser provides an automatically controlled varying frequency. The main function of the Analyser is to perform data collection and identification of the admittance of the electromechanical system.

Beside the Signal Analyser an other important measurment tool is the laser interferometer, which is shown on the same figure A.2. The laser interferometer, which is controlled by the computer, measures the displacement and the rate of vibration at the surface of the stator. The main advantage of this measurement tool is its high precision which is less than the wave length of the laser beam. Furthermore, the measurments which are performed without contact, by using a reflecting beam, avoids the perturbation of the system under characterization.

- **Operating principle of the laser interferometer**: The operting principle of this tool is based on the interference phenomenon between two beams provided by the same source. The Polytec interferometer used in this setup is based on the Mach-zehnder configuration, see figure A.3.

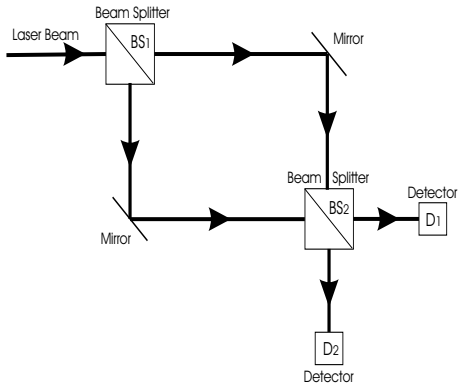

Figure A.3: Operating principle of the Mach-Zehnder interferometer

The original laser beam is diveded by a beam splitter BS1 into two beams with equal light intensity. Then, each beam is again splitted by the beam splitter BS2. The beams obtained at the end of this operation are then the supperposition of two beams each, with their light intensity $\mathcal{I}_1$ and $\mathcal{I}_2$ collected respectively on the

photodetector D1 and D2 are given by the following equations

$$\mathcal{I}_1 = \frac{\mathcal{I}^2}{2}[1 + \cos(\varphi_2 - \varphi_1)] \tag{A.1}$$

$$\mathcal{I}_2 = \frac{\mathcal{I}^2}{2}[1 + \cos(\varphi_2 - \varphi_1)] \tag{A.2}$$

where $\mathcal{I}$ is the light intensity and φ_i is the phase of the beam i given by

$$\varphi_i = \frac{2\pi \mathtt{d}_i}{\lambda} \text{ for } i = 1, 2 \tag{A.3}$$

where $\mathtt{d}_i$ is the path lenght taken by the beam i and finally λ is the wave lenght of the light source.

It can be noticed from (A.1), (A.2) and (A.3) that the knowledge of the light intensity received by D_1 and D_2 alow the determination of the relative phase between the beams. Consequently, it is possible to determine the lenght difference between the paths taken by these two beams of light.

However, this design doesn't allow the measurements of the displacement of external surfaces. The modified version shown in figure A.4, provide the possibility for a beam to escape from the previous circuit. Consequently, one of the mirrors in this case becomes a polarized beam splitter PBS, and the unit QWP introduce a quarter of wave lenght phase shift. Hence, the incident beam from BS1 can completely pass through PBS, whereas the reflected beam (in quadratic with the original beam) is deviated towards BS2.

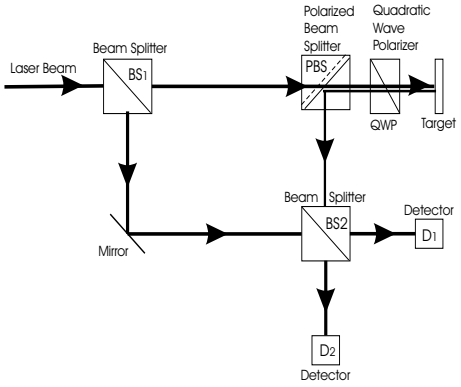

Figure A.4: The modified Mach-Zehnder interferometer for external measures

Finally, the latest improvement must be added in order for the system to be effectively operational. For that reason the Bragg cell is used in order to introduce

a controled frequncy shift f_B by a reference RF, see figure A.5. When the frequencies detected on D_1 and D_2 are centered arround f_B then the detection of the direction of the displacement is possible (heterodyne interferometer).

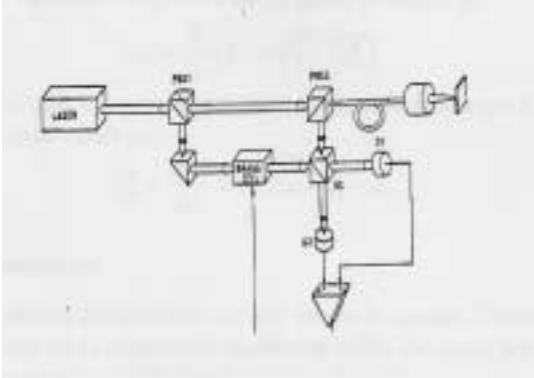

Figure A.5: Operating principle of the Polytec laser interferometer

The electrical measurements and their visualisations are obtained by an oscilloscope. The current measurements are obtained by using a shunt, because in practice, the available currents are very low, which alter the precision when using the current probe. However, the use of shunt must be taken into account in order to avoid errors when sorting through the measurments.

Finally, the use of a PC equipped by a GPIB interface, allows the development of a certain number of programs in Labview software environment, dedicated to the automation of the acquisition sequences and data manipulation.

With this method, different admittance characteristics of the system can be obtained by on the one hand programing different amplitude voltage of the power supply and different spans of frequencies to be analyzed, and on the other hand by varying manually the values of the external input parameters such as the normal forcing F and/or the load torque $\mathcal{T}$.

The admittance of the electromechanical system identified by the signal analyzer is obtained in the forms of Bode diagram and Nyquist diagram, which provides many valuable information on the electromechanical behavior of the system over the range of excited frequencies.

Appendix B

Vibration of an Annular Plate

The equation of transverse motion of an annular forced plate neglecting shear deformation and rotary inertia is given by

$$\frac{J\mathtt{h}^3}{12(1-\nu^2)} \bigtriangledown^4 u(s,t) + \rho\mathtt{h}\frac{\partial^2 u(s,t)}{\partial t^2} = F(s,t) \tag{B.1}$$

where J, ν, ρ and $\mathtt{h}$ are respectively the young modulus, the Poison ratio, the mass density of the plate and finally the thickness of the plate. The term $u(s,t)$ denotes the displacement of the plate, $F(s,t)$ denotes the general forcing acting on the plate and the $\bigtriangledown^4$ symbol is the biharmonic operator which in polar coordinates ($s = (r,\theta)$) takes the form

$$\bigtriangledown^4 = (\frac{\partial^2}{\partial r^2} + \frac{1}{r}\frac{\partial}{\partial r} + \frac{1}{r^2}\frac{\partial^2}{\partial \theta^2})^2 \tag{B.2}$$

For the case of the free vibrating plate (i.e. the unforced case: $F(s,t) = 0$) and assuming that the vibration of the plate is harmonic in time (i.e. periodic behavior providing resonant and antiresonance frequencies under certain conditions), the solution can be obtained as a product of one time dependent function and one space dependent function

$$u(s,t) = U(s)e^{j\omega t} \tag{B.3}$$

The unforced plate solution provides a set of mutually orthogonal modes that describe all possible motions of the plate. The forced plate's solution is then obtained as a particular case of the unforced one in the sense that only one or some of the modes are allowed to take place. For the free plate the equation B.1 can after simplification be reduced to

$$\frac{J\mathtt{h}^3}{12(1-\nu^2)} \bigtriangledown^4 U(s) - \rho\mathtt{h}\omega^2 U(s) = 0 \tag{B.4}$$

which can be further manipulated to become

$$(\bigtriangledown^4 - \lambda^4)U(s) = 0 \tag{B.5}$$

where

$$\lambda^4 = \frac{12(1-\nu^2)\rho\omega^2}{J\mathrm{h}^2} \tag{B.6}$$

The solution of B.5 can be provided by separating the spatial variables in a form

$$U(s) = R(r)\Psi(\theta) \tag{B.7}$$

after substitution and grouping the r dependent and θ dependent terms the following equations are obtained

$$\frac{d^2\Psi(\theta)}{d\theta^2} + n^2\Psi(\theta) = 0 \tag{B.8}$$

$$\frac{d^2R(r)}{dr^2} + \frac{1}{r}\frac{dR(r)}{dr} + (-\frac{n^2}{r^2} \pm \lambda^2)R(r) = 0 \tag{B.9}$$

The general solution to the transverse vibration of the annular plate is a summation of the plate's vibration over all the possible modes of vibration given by

$$u(s,t) = \sum_{n=1}^{\infty}\sum_{m=1}^{\infty} \xi_{nm}(t)U_{nm}(s) \tag{B.10}$$

where the indexes m and n denote respectively the m 'th radial and n 'th circumferential modes. The resonant frequency ω_{nm} of the plate for the (n,m) 'th mode is obtained by solving the eigenvalue problem for λ, see (Friend and Stutts (1997)), and reads

$$\omega_{nm} = \lambda_{nm}^2\sqrt{\frac{\mathcal{G}}{\rho\mathrm{h}}} \tag{B.11}$$

where

$$\mathcal{G} = \frac{J\mathrm{h}^3}{12(1-\nu^2)}$$

If only the circumferential modes are considered then the resonant frequency ω_n of the plate for the n 'th mode is given by

$$\omega_n = \lambda_n^2\sqrt{\frac{\mathcal{G}}{\rho\mathrm{h}}} \tag{B.12}$$

where

$$\lambda_n = \frac{n}{r}$$

Appendix C

Motor Data

The following tables summarize the parameters that are required by the analytical model and the hybrid model for the Shinsei motor USR60.

- The mechanical constants of the motor

Mass density of the substrate, (kg.m^{-3})	$\rho_s =$ 8780
Mass density of the piezo plate, (kg.m^{-3})	$\rho_p =$ 7650
Young's modulus of the substrate, (GPa)	$J =$ 120
Poisson ratio of the substrate	$\nu =$ 0.3
Shear modulus of the substrate, (GPa)	$\mathtt{G} =$ 44
Half thickness of the stator, (m)	$h =$ $1.5\ 10^{-3}$
Outer radius of the stator, (m)	$a =$ $23.5\ 10^{-3}$
Inner radius of the stator, (m)	$b =$ $30\ 10^{-3}$
Radial shape constant of the travelling wave	$R_r =$ 0.7
Middle radius of the contact surface, (m)	$R_o =$ $26.75\ 10^{-3}$
Width of the contact surface, (m)	$\epsilon =$ $4.41\ 10^{-3}$
Rotor stiffness per unit area, (N.m^{-3})	$\varkappa_r =$ $5.4\ 10^{11}$
Number of wave length	$k =$ 9
Rotor mass, (kg)	$M_r =$ $30\ 10^{-3}$
Rotor inertia, (kg.m^{-2})	$J_r =$ $7.2\ 10^{-6}$
Coulomb's friction coefficients.	$\mu =$ 0.3

- The electromechanical constantes of the piezo ceramic

Compliances at constant electrical field, ($m^2.N^{-1}$)	$s_{11}^E =$ 10.66 10^{-12} $s_{12}^E =$ -3.34 10^{-12} $s_{66}^E =$ 28.07 10^{-12}
Dielectrical constant, ($C.N^{-1}$)	$d_{31} =$ -108 10^{-12}
Electrical permitivity at constant stress, ($F.m^{-1}$)	$\varepsilon_{33}^T =$ 1.02 10^{-8}

- The remaining parameters

Rotor damping in spining direction	$D_r = 5\%$
Rotor damping in vertical direction	$D_z = 5\%$
The applied axial load, (N)	$F_{app} = 160$
The applied external torque, (Nm)	$\mathcal{T}_{app} = [0, 0.32]$

- The identified parameters for the hybrid model

Modal mass of the stator (kg)	$M =$ 10.1 10^{-3}
Modal damping of the stator, ($Ns.m^{-1}$)	$\mathcal{D}_o = 15.4$
Modal stiffness of the stator, ($N.m^{-1}$)	$K_o =$ 5.9524 10^8
Modal coupling factor of the stator, ($N.V^{-1}$)	$\eta = 0.2263$